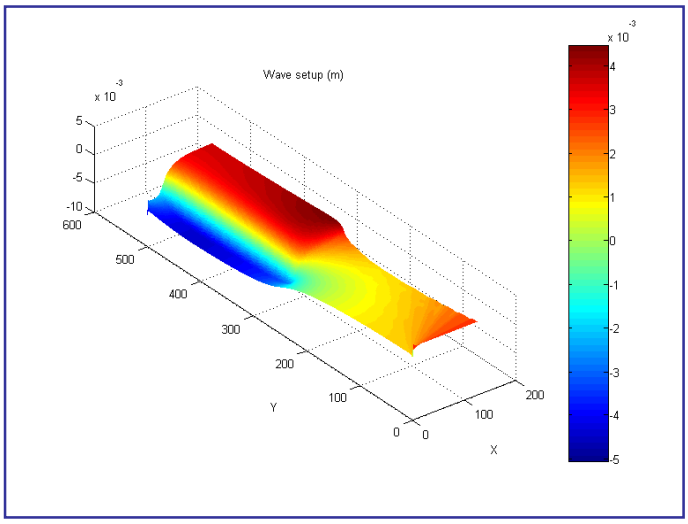
Wave attenuation over salt marsh vegetation

A numerical implementation of vegetation in SWAN





M.Sc. Thesis

M.C. Meijer, September 2005
Delft University of Technology
Faculty of Civil Engineering and Geosciences
Section of Hydraulic Engineering

Thesis committee:

Prof. dr. ir. M.J.F. Stive
ir. H.J. Verhagen
dr. ir. M.J. Baptist
drs. M.B. de Vries

Preface

This thesis is submitted in partial fulfilment of the requirements for a Dutch Master of Science Degree in Hydraulic engineering at the Faculty of Civil Engineering and Geosciences of Delft University of Technology. This report is titled Wave attenuation over Salt Marsh Vegetation, and it describes a numerical modeling study to implement vegetation in SWAN.

First of all, I would like to thank the members of the graduation committy, Prof. dr. ir. M.J.F. Stive, ir. H.J. Verhagen and dr. ir. M.J. Baptist for their contributions to this report and especially drs. M.B. de Vries for all his time and effort to intoduce me into the world of Biogeomorphology. I would also like to specially thank Marcel Zijlema for all his help with programming in SWAN and dr.ir. Uijttewaal for the lectures on turbulence in vegetation.

Furthermore I'd like to thank the people at Wetterskip Frieslan and Rijkswaterstaat Directie Noord Nederland for the possibility they accomodated for a field trip to a Friesian Salt Marsh.

Finally I'd like to specially thank Bastiaan Burger for our splendid cooperation during the implementation and validation of the model, for the numerous late night pizzas and all the rides to the central station.

Martijn Meijer
Delft, September 2005

Abstract

Salt marshes are transitional areas between soil and water. Until recently these areas were usually diked and drained in order to create new agricultural land, but nowadays fortunately more awareness exists about the importance of these inter tidal areas as nature reserves and as natural coastal protections.

Although awareness on the coastal protection value of salt marshes has increased in recent years, it is still uncertain how and to what extent waves are reduced by these vegetated intertidal areas. Usually, when applying coastal protection, the wave attenuating properties of the foreshore system are being disregarded. This can lead to an over-dimensioned structure and hence to a relatively expensive solution.
The difficulty in quantifying the wave attenuating properties of salt marshes is that the interaction of the water waves with vegetation is a dynamic process; the plants are being moved by the interaction with water waves. At the same time, the short wave characteristics are being altered by the interaction with the vegetation.

These uncertainties in the wave attenuating qualities of vegetation has led to an increasing demand for a numerical model in which wave attenuation over vegetated foreshores can be simulated.
The objective of this study is to make a numerical wave model to predict the changes in wave characteristics over foreshores with vegetation.
With these predictions, the wave attack on the underlying coastline can be computed. Indirectly it can be used to determine potential differences in required height of a dike or to determine a potential decrease in flooding frequency of unprotected coasts due to the presence of vegetation.

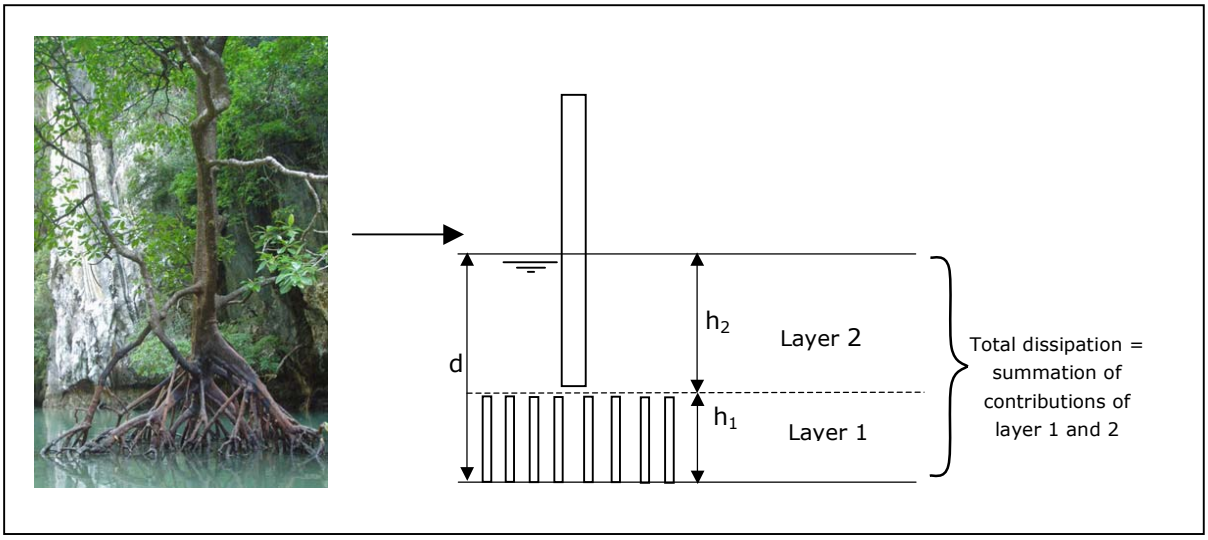
It was decided to implement vegetation in the existing numerical model SWAN in order to make it suitable for modelling situations with vegetated foreshores.
Parallel to this Msc. study, Bastiaan Burger wrote his Msc. thesis on the wave attenuating properties of Mangrove forests. Because of these common interests, it has been concluded to partially work together on creating a model that is capable of modelling wave attenuation by any type of foreshore vegetation.

The best available numerical description of the effect of vegetation on waves is based on the representation of vegetation by vertical, ridged cylinders and was derived by Dalrymple et al.(1984). This method gives a reasonable physical representation of the vegetation and implementing it in SWAN is feasable. The physical vegetation properties that are considered in this formulation are the relative vegetation height, vegetation diameter and density, and the drag coefficient.

The calibration parameter in the Dalrymple et al.(1984) formulation, which is of significant importance for determining the wave dissipation due to vegetation, is the drag coefficient (C_d). By varying the drag coefficient different types of vegetation (both stiff and flexible) can be modelled. The value of the drag coefficient is dependent on the Reynolds number and on the shape and orientation of the object. Another important factor is the water level above the vegetation. A study of the drag coefficient, first for a single cylinder in flow, subsequently for a multi cylinder array, gave insight in the relation with both wave and vegetation characteristics. In a multi cylinder array the drag coefficient is dependent on the shape and orientation of the objects and the relative spacing between them. The dependency of the drag coefficient on waves was found in the relation with the Keulegan-Carpenter number, which contains the wave parameters u_c (horizontal orbital

velocity) and T_p (peak period). A number of processes that are not accounted for in the Dalrymple formulation are discounted in the drag coefficient. Therefore it is not physically correct to refer to the "drag coefficient" in the model.

After a first analyses of the Dalrymple formulation it was found valid to vertically divide the vegetation into different segments, to calculate the dissipation in each segment and to add these contributions up to find the total energy dissipation by one vegetation stem. In the figure below a mangrove tree with different vegetation characteristics per layer is schematized in this manner.



First homogeneous vegetation was implemented in SWAN, subsequently the model was adjusted to accommodate horizontally varying vegetation fields (patchy vegetation) and finally the model was expanded to vertically variable vegetation.

The adjusted SWAN model was validated on the results of a physical model test and the implementation was found successful.
A sensitivity analyses was performed in order to determine the response of the model to changes in parameters. As a final validation the model was applied on field measurement results from the Paulina Marsh in the Westerschelde. In this case all parameters were known except for the drag coefficient, which was calibrated. The results were satisfactory, the value for the drag coefficient ranged between 0.5 and 3.0 and the relation with the vegetation height was as expected.

In vegetation fields wave energy is dissipated leading to wave setup. An important phenomenon, especially in mangrove forests, is sediment transport due to secondary flows that are induced by differences in wave setup. In SWAN this vegetation induced setup was successfully visualized. These results can be used as input for flow and morphological models.

The implementation of vegetation in SWAN was found successful for all types of vegetation.
However, due to the dependency of the drag coefficient on wave and vegetation characteristics, the model can only be applied on specific situations where wave and vegetation measurements have been taken.
In order to make the model generally applicable, more research needs to be done on the dependency of the drag coefficient on wave and vegetation characteristics. When more is known about these relations, a first prediction can be made on the value of the drag coefficient in a specific situation. This can be accomplished by doing physical modelling tests and taking wave measurements over vegetated foreshores.

Index

Preface i

Abstract ii

1. Introduction 1

1.1 Problem introduction 1
1.2 Problem analyses 1
1.2.1 Problem definition 1
1.2.2 Research objective 1

2. Background information on Salt Marshes 2

3. Previous research 4

3.1 Introduction 4
3.2 Field measurements 4
3.3 Numerical modelling studies 4
3.3.1 Increase of the Collins bed friction factor in D3dSWAN 5
3.3.2 Modelling plants as vertical cylinders 6
3.3.3 Implementation criteria 8

4. Physical properties of the Drag Coefficient in a Vegetation Field 9

4.1 Introduction 9
4.2 Dependence of drag on vegetation characteristics 10
4.2.1 Single cylinder approach 10
4.2.2 Multi cylinder array approach 11
4.3 Dependence of the drag on wave characteristics 14
4.4 Conclusions 15

5. Numerical modelling in SWAN 16

5.1 General description of SWAN 16
5.2 Modelling wave attenuation by vegetation 18
5.2.1 Implementation of the Dalrymple formulation in SWAN 18
5.2.2 Homogeneous vegetation 18
5.2.3 Horizontal variation of vegetation 20
5.2.4 Vertical variation of vegetation 20
5.2.5 Implementation in source code 23
5.3 Validation of the SWAN model 23

6. Sensitivity analyses 25

6.1 Model setup 25
6.2 Sensitivity to changes in water level 26
6.3 Influence of change in vegetation characteristics on wave attenuation 28
6.4 Influence of change in wave characteristics on wave attenuation 30

6.4.1 Influence of wave height to the amount of wave attenuation 30
6.4.2 Influence of change in wave frequency on wave attenuation 32

7. Paulina Marsh case 34

7.1 Field measurements 34
7.2 Model results 36
7.2.1 Homogeneous vegetation 36

8. Wave induced setup and secondary flows 44

9. Conclusions and recommendations 47

9.1 Conclusions 47
9.2 Recommendations 49
9.3 Recommended flume experiments 50

List of references 51

Appendices 54

Appendix A: Salt marshes 55

A.1 Introduction 55
A.2 Salt marsh vegetation 56
A.3 Dynamics of salt marshes 58
A.3.1 General sediment transport 58
A.3.2 Effects of vegetation 59
A.3.3 Seasonal influences on salt marshes 60
A.3.4 Effects of sea level rise 60
A.3.5 Gas mining 61
A.3.6 Salt marsh vegetation 62

Appendix B. Edge influences in SWAN 64

Appendix C Results of first indication Dalrymple formulation 66

Appendix D SWAN Source Code 67

D.1 General description SWAN source code 67
D.2 Working with SWAN 67
D.3 Input of vegetation parameters 67
D.4 Scource code Subroutine INPVEG 68
D.5 Vertical averaging of parameters 69
D.6 Subroutine SVEG 71

Appendix E Validation on physical model results 75

Appendix F Sensitivity analyses 77

F.1 Change in H_s 77

F.2 Change in N 78
F.3 Change in relative vegetation height 80
F.4 Change in Tp 82

Appendix G: Energy density spectra 84

Appendix H Model results Paulina Marsh 85

H.1 Results for various values of C_d 85
H.2 Appendix X Constant drag coefficient assumed 87

Appendix I Wave setup 89

Appendix J List of coefficients 95

List of figures

Figure 1: Overview of salt marsh locations along the Dutch coast (from:www.kweldervisie.nl) 2
Figure 2: "De schorren" Marsh at Texel *(from:www.waddenzee.nl)* 3
Figure 3: Different zones of energy dissipation in a submerged vegetation. 9
Figure 4: Flow around a cylinder, a. theoretical and b. experimental (for Re = 2300) (from Battjes 1999) 10
Figure 5: Relation between Reynolds number and drag coefficient for a single circular cylinder in flow. from: Battjes (1999 11
Figure 6: Single cylinder in a turbulent flow regime 11
Figure 7 Staggered configuration of cylinders with wake 12
Figure 8: Dependency of C_d on the population density ad (Nepf 1999) 13
Figure 9: Relation between Keulegan-Carpenter number and C_d for different values of α 14
Figure 10: Example horizontal variation 20
Figure 11: Vertical distribution of horizontal orbital velocity for a. shallow water and b. transitional water depth 20
Figure 12: Schematized velocity profile in homogeneous vegetation, where 21
Figure 13: Horizontal orbital velocity profiles 21
Figure 14: Linear relation between energy dissipation and the vegetation height 22
Figure 15: Schematization of a mangrove tree in the SWAN model 22
Figure 16: SWAN implementation validation 24
Figure 17: Model setup of sensitivity analyses 25
Figure 18: significant wave height over vegetation at varying water levels 26
Figure 19: Relation between K_T and water level 27
Figure 20: Wave attenuation with different densities 28
Figure 21: Relation between the amount of energy dissipation and stem density. 29
Figure 22: Decrease in significant wave height over vegetation 30
Figure 23: Energy dissipation at different incoming significant wave height. 31
Figure 24: Relation between the transmission coefficient and the incoming significant wave height 31
Figure 25: The difference between the incoming spectral energy and the spectral energy behind the vegetation, which are given in Appendix G. 32
Figure 26: Change in Hs for different wave spectra 33
Figure 27 Location of the pressure sensors at the salt marsh. P0 is the landward side. 34
Figure 28: Bathymetry of the transect at the Paulina Marsh 35
Figure 29: Model setup Paulina Marsh 36
Figure 30: First results Paulina Marsh 37
Figure 31: Wave damping over Paulina Marsh with h=1.28 m 38
Figure 32: Wave damping over Paulina Marsh with h=2.57 m 38
Figure 33: Calibrated drag coefficient at Paulina Marsh 39
Figure 34: Drag coefficient boundaries 39
Figure 35: Modelled situation 41
Figure 36: Wave attenuation over zoned and homogeneous vegetation at Paulina Marsh 42
Figure 37: Wave attenuation over zoned and homogeneous vegetation at hypothetical marsh 43
Figure 38: Schematization of wave set down and setup 44
Figure 39: Model layout for wave setup cases 45
Figure 40: Wave setup in case B. 46
Figure 41: Top view wave setup and possible setup induced flow 46
Figure 42 Overview of salt marsh locations along the Dutch coast 55
Figure 43: "De schorren" Marsh at Texel (from:www.waddenzee.nl) 56
Figure 44: typical zonation of a Wadden Sea marsh after: Erchinger, (1985) 57
Figure 45: Salt marsh generation (A), and degeneration and re-growth (B) 59
Figure 46 marsh in winter (left) and in summer (right). 60

Figure 47: Possible responses of salt marshes to sea- level rise (Janssen-Stelder after Orson et al. 1985)..... 61
Figure 48: wave energy losses over the model edges..... 64

List of Tables

Table 1 Summary of Reynolds number and array configuration (Nepf 1999) 13
Table 2: Swan model input..... 26
Table 3: Swan input parameters 28
Table 4: Swan input parameters 30
Table 5: SWAN model input..... 32
Table 6: Plant characteristics of Spartina Anglica vegetation at Paulina schor. 35
Table 7: Wave measurements used in SWAN model 35
Table 8: Modeled case..... 41
Table 9: Zoned situation 42
Table 10: Homogeneous vegetation (averaged values of table 9)..... 42
Table 11: SWAN model input 44

1. Introduction

1.1 Problem introduction

Beds, banks and shores are the borders between soil and water. Until some decades ago, hydraulic engineers were only interested in shaping these boundaries to fight erosion or to create transhipment possibilities, but growing attention in society to environmental aspects has lead to another approach. The transition between land and water plays an important role in nature and landscape and this awareness also has consequences for hydraulic engineers. Nature friendly protections have become an important issue in the hydraulic engineering practice worldwide.
Vegetation, present at a foreshore, can both reduce loads and increase strength. It has a relatively large resistance to waves and currents, thus reducing the loads, and roots can increase strength by protecting the grains on a micro scale. Decision-makers often undervalue the shoreline protection services afforded by natural landscapes and do not give this service appropriate weight when evaluating development options. The most important reason for this oversight is the difficulty in quantifying these services.

1.2 Problem analyses

1.2.1 Problem definition

When applying coastal protection at a location where the foreshore is vegetated by halophytes (vegetation that can thrive in a salt water environment), a lot of uncertainty exists about the attribution of the natural foreshore to wave reduction. Usually the wave attenuating properties of the foreshore system are being disregarded, often leading to an over-dimensioned construction and hence to a relatively expensive solution.
Some research has been done in the past on the wave reduction by vegetation, but there is no unambiguous way to model wave transmission over and through vegetation yet.
The problem definition therefore states:

> It is known that vegetation influences wave transmission, but to what extent is yet unclear.
> Further more, there is no unambiguous way to model the vegetation's effect on wave reduction.

1.2.2 Research objective

The difficulty in this research is *how* to model the vegetation present at the foreshore. When one looks at the vegetation present on a marsh or mangrove coast, it can be seen that a wide variety of plants and trees are present that vary in height, plant density and stiffness of the stems. Therefore the objective of this thesis is stated as:

> The objective of this thesis is to make SWAN suitable to model situations with vegetated foreshores. The model has to be applicable on all types of halophytic vegetation.

The desired outcome of this study is a wave model that is suited to predict the changes in wave characteristics over foreshores with halophytic vegetation.
With these predictions, the wave attack on the underlying coastline can be computed. Indirectly it could be used to determine potential differences in required height of a dike or to determine a potential decrease in flooding frequency of unprotected coasts due to the presence of vegetation.

2. Background information on Salt Marshes

When looking at the distribution of foreshore ecosystems over the world, it roughly can be said that salt marshes inhabit the areas above 25 degrees Northern latitude and below 25 degrees southern latitude and that the (sub) tropical area between these latitudes is inhabited by Mangroves (Mitsch and Gosselink, *2000*). All these foreshore systems are rather complex and are in a state of dynamic equilibrium with the surrounding environment. As can be seen in practice all around the world, a disruption of this equilibrium can have huge consequences, especially in developing countries where large areas of mangrove vegetation disappear each day to make place for farmland, shrimp ponds and salt mining. The natural protection against flooding is being replaced by small soil dams that hardly offer any protection against wave attacks, leading to flooding hazards at storm conditions.

In the Netherlands salt marshes can be found around the Wadden Sea coast in the north, and along the south west coast, in the province of Zeeland. The locations are indicated red in Figure 42. Salt marshes are part of the inter-tidal flats and are situated at the upper part of these flats. They are bordered by mudflats at the seaside and are backed mostly by dykes. The vegetation on salt marshes is typically zoned, meaning different species thrive at different parts of the marsh. A top view of a salt marsh (see *Figure 2*) reveals a typical branched pattern of channels, which are important because of their drainage function. At the seaside edge a cliff can appear, indicating the edge of the marsh. More information about salt marshes and salt marsh vegetation is given in Appendix A.

Until recently the Dutch salt marshes have been extensively diked and drained in order to create additional agricultural land. Nowadays, fortunately, it is clear that estuarine wetlands are particularly important in shoreline stabilization and protection against storm surges. It is therefore of great importance that natural systems remain in tact and that, where possible, new formation or recovery of mangrove and marsh vegetation is stimulated.

Because salt marshes are in a state of dynamic equilibrium with the surrounding environment, it is important to get insight into the most important processes that attribute to the altering shape of the marsh. This way, future marsh developments and the altering wave attenuating skills of the marsh vegetation can be predicted.

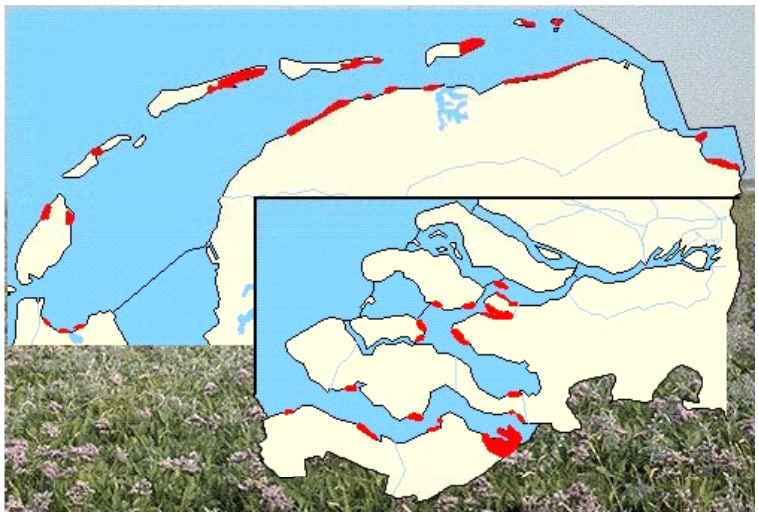


Figure 1: Overview of salt marsh locations along the Dutch coast (from:www.kweldervisie.nl)



Figure 2: "De schorren" Marsh at Texel *(from:www.waddenzee.nl)*

The shape of a salt marsh is continuously altering. On the one hand sand settles on or erodes from the marsh, leading to an increase or decrease of the seaward marsh extent. On the other hand land subsidence and rise can occur due to the presence of vegetation and due to human interference (for instance gas mining). An extensive description on the dynamics of salt marshes and the most important processes that influence the marsh shape is given in Appendix A.

3. Previous research

3.1 Introduction

Some research has been done in the past on wave attenuation over vegetation; however the results sometimes were rather contradictorily.
A study carried out by Mőller et al. (*1999*) reveals that wave attenuation does not vary linearly with distance across the salt marshes, but that most wave energy is dissipated or reflected over the first 10 to 50 meters of the salt marsh surface. On the other hand, extensive field measurements carried out seaward and leeward of a very robust *M. perifera* kelp bed along the Californian coast assure that wave energy is practically unaffected by these plants (Elwany et al.,*1995*, Seymour, *1996*). These contradictory research results make clear that a lot of uncertainty still exists and that a model that can predict wave attenuation over different types of vegetation is highly desirable. From previous research on the wave attenuating skills of foreshores with halophytic vegetation, important information can be obtained which can be used for the development and validation of a numerical model. In the next paragraphs a description is given of a field study and a numerical study that will be used to develop the new SWAN implementation.

3.2 Field measurements

In order to validate the results from a numerical model, field measurements or physical model tests are desirable. When the model results agree with the measured values it can be stated that the model gives a good approximation of the reality. In the validation section (section 4.3) a description is given on the physical model test results that were used to validate the model. Not many field measurements have been done in the past over salt marshes. There is a lack of real time wave measurements where the wave attenuation over vegetation has accurately been measured. The only available field measurements over a salt marsh where taken at the Paulinaschor in the Westerschelde by WL Delft Hydraulics in association with NIOO. In chapter 6 some results from the Paulina Marsh measurements are given and used as input for the adjusted SWAN model.

3.3 Numerical modelling studies

There are generally two different approaches for implementing the effect of vegetation on waves. In the first approach the effect of the vegetation on wave dissipation is imbedded into the bed friction factor. In a wave simulation program this means raising the bottom friction factor to take vegetation into account.
The second method is based on modelling the plants physical properties by representing them by cylinders of varying diameter and length and with a certain relative spacing.

3.3.1 Increase of the Collins bed friction factor in D3dSWAN

De Vries and Roelvink (2004) implemented the vegetation influence into SWAN by replacing the Collins friction factor for bottom roughness by a factor that contains marsh vegetation characteristics such as plant length, stiffness and number of plants per square meter. They defined the 'vegetation friction factor parameter' by using the energy dissipation formula of Van Rijn.
The dissipation is equal to the time-averaged work done by the friction force at the bottom. The energy dissipation per unit area, integrated over the vegetation height dz, assuming constant density, becomes:

$$D_v = \frac{4}{3\pi} \rho \cdot U_{orb}^3 \cdot f_w^* \cdot D \cdot n \cdot dz \qquad (3.1)$$

where:

D_v - Dissipation of energy per unit area of vegetation [$Nm^{-1}s^{-1}$]

In this approach four characteristics of the vegetation field are included,

f_w^* = friction factor [-]
D = stem diameter [m]
n = vegetation density [m^{-2}]
dz = vegetation height [m]

The friction factor f_w^* is still dependent on other species-specific characteristics such as the stiffness and the roughness of the plant surface.

In a simplified case, with shallow water wave conditions and constant plant density in height, the total vegetation friction factor c_v equals:

$$c_v = f_w^* \cdot D \cdot n \cdot dz \qquad (3.2)$$

where:

c_v = vegetation friction factor [-]

This factor was successfully used to replace the Collins friction factor used in SWAN. The method was validated for the Paulina Marsh case, where the dominant vegetation is *Spartina anglica*.

3.3.2 Modelling plants as vertical cylinders

When initially the plant stems are considered stiff, and swaying motion and vortex-induced vibrations are neglected, the plants can be modelled as ridged vertical cylinders.
It should be noted that the validity of this model depends on the geometrical and biomechanical characteristics of the plant. If the plants are subsurface, short and the stems are rather stiff, the plants can be considered cylindrical and a drag force model can be considered valid (f.i. *L. hyperborea* kelp beds, *P. oceanica* seagrass meadows, *Spartina* marshes). If the plants have a large number of degrees of freedom, the buoyancy of the vegetation is large and the cylindrical approach is invalid (f.i. *M. pyrifera* kelp beds).
The method can be applied here because the typical salt marsh vegetation in the cases described here is short, subsurface and rather stiff.

The total force per unit length on a slender cylinder is assumed to be the sum of a drag force and an inertia force.

$$f(t) = C_m \frac{1}{4}\pi D^2 \rho \frac{\mathrm{d}U}{\mathrm{d}t} + C_d D \frac{1}{2}\rho U |U| \qquad [\mathrm{Nm^{-1}}] \qquad (3.3)$$

In which the coefficients C_m (inertia coefficient) and C_d (drag coefficient) are functions of *Re* and κ for a given structure shape and orientation (assuming a sinusoidal variation in time of the velocity *U*).
Furthermore:
D = plant diameter [m]

This is the so-called Morison equation.

Dalrymple et al. (1984) derived an energy dissipation factor based on the Morison equation. Mendez and Losada (2004) used the method of Dalrymple et al. for their physical model to estimate the propagation of random breaking and non-breaking waves over vegetation fields. Their approximation was based on the assumption that the linear wave theory for waves propagating over an impermeable bottom is valid to calculate *u* not only for the water region but also within the vegetation area, and considering regular waves normally incident on a coastline with straight and parallel contours. The conservation of energy equation is then reduced to

$$\frac{\partial E c_g}{\partial x} = -\varepsilon_v \qquad (3.4)$$

in which:
E = energy density [$\mathrm{Nm^{-1}}$]
c_g = wave group velocity [$\mathrm{ms^{-1}}$]
∂x = distance over vegetation field in propagation direction [m]
ε_v = time-averaged rate of energy dissipation [$\mathrm{Nm^{-1}s^{-1}}$]

For a given vegetation field, the conventional definition for the depth-integrated and time-averaged energy dissipation per horizontal area unit is given by:

$$\varepsilon_v = \overline{\int_{-h}^{-h+\alpha h} \mathrm{Fu}\,\mathrm{dz}} \qquad (3.5)$$

where the over-bar stands for time average in a wave period, $F=(F_x, 0, F_z)$ is the force acting on the vegetation per unit volume and $u=(u, 0, w)$ is the velocity for the 2D case, ah is the vegetation height and h is the water depth.
Substituting into equation 3.5 yields

$$\varepsilon_v = \overline{\int_{-h}^{-h+\alpha h} (F_x u + F_z w)\, dz} \tag{3.6}$$

It is usually assumed (e.g. Asano et al., *1993*, Mendez et al., *2004*) that in a dissipative medium such as a vegetation field, the term $F_z w$ is negligible in comparison with $F_x u$. Therefore, the time-averaged rate of energy dissipation per unit horizontal area ε_v can be expressed as:

$$\varepsilon_v = \overline{\int_{-h}^{-h+\alpha h} F_x u\, dz} \tag{3.7}$$

The force F_x acting on the plants should include the relative motion between the fluid and the plant, but in the work of Mendez et al. the plant motion has been neglected.
For this reason plant-induced forces acting on the fluid can be expressed in terms of a Morison-type equation neglecting swaying motion and inertial force. The horizontal force per unit volume is therefore given by:

$$F_x = \frac{1}{2}\rho C_D b_v N u |u| \tag{3.8}$$

Equation (3.8) is taken to be valid not only for rigid plants, but also for flexible ones considering a different value of a bulk drag coefficient C_D to cover our ignorance of the plant motion (Dalrymple et al., 1984).
Dalrymple assumes that the linear wave theory is valid to calculate u not only for the water region, but also within the vegetation area.
This leads to the following expression of the energy dissipation for waves propagating through a vegetation field:

$$\varepsilon_v = \frac{1}{2\sqrt{\pi}}\rho \tilde{C}_D b_v N \left(\frac{gk}{2\sigma}\right)^3 \frac{\sinh^3 k\alpha h + 3\sinh k\alpha h}{3k\cosh^3 kh} H_{rms}^3 \tag{3.9}$$

Herein:

ε_v	= the time-averaged rate of energy dissipation per unit horizontal area	[$Nm^{-1}s^{-1}$]
C_D	= drag coefficient	[-]
b_v	= plant stem diameter	[m]
N	= number of plants per square meter	[m^{-2}]
k	= wave number	[m^{-1}]
σ	= wave frequency	[s^{-1}]
αh	= vegetation height	[m]
h	= water depth	[m]
H_{rms}	= root mean square wave height	[m]

In this approximation, reflection induced by the plants has not been considered. However, the importance of this factor is very limited in terms of wave energy. For example, if we consider a reflection of $|R| = 20\%$, this represents an energy reflection of 4% since energy is proportional to $|R|^2$. Therefore the reflection can indeed be neglected.

3.3.3 Implementation criteria

The interaction of the water waves with submerged vegetation is a dynamic process; the plants are being moved by the interaction with water waves. At the same time, the short wave characteristics are being altered by the interaction with the vegetation; both the wave length and wave height decrease.
The implementation of vegetation in SWAN needs to fulfil the following three criteria:

1. Good schematization of the most important physical vegetation characteristics.
2. The applicability to all types of halophytic vegetation.
3. The extra dissipation term can easily be implemented in SWAN.

Representing the vegetation influence by raising the bottom friction doesn't account for criterion 1. The vegetation is represented as an extra bed roughness instead of real obstacles exposed to fluid action. A good schematization of the most important physical vegetation characteristics is fulfilled by Dalrymple by the fact that the formulation contains input parameters as plant height, stem thickness, number of stems per unit surface and a drag coefficient. The only parameter that cannot be determined fundamentally is the drag coefficient C_d, which has to be specified by comparison with experimental and field measurements. However, this coefficient has a physical meaning. By studying the physical properties of the drag coefficient a more founded first estimate of this coefficient can be made. Different types of vegetation species can be modelled by varying this parameter (See section 3). The
Asano et al. (*1993*) propose an adaptation to the Dalrymple formulation in order to include the swaying motion of the plants and thereby expand the range of the application from only stiff to both stiff and flexible vegetation. The conclusions of their physical modelling studies showed that varying the drag coefficient is sufficient to model flexible vegetation.
Finally, the Dalrymple formulation is expressed in terms of energy density, which makes it easy to implement in SWAN.
It is concluded that the Dalrymple equation fulfils best with the criteria and will be implemented in SWAN.

In order to get a first impression, the Dalrymple et al. (1984) formulation was tested on the previously described measurements done at the Paulina Marsh. This was done using Excel, the results can be found in Appendix C. As input a C_d value of 0.5 was used and for the density, height and diameter average values of the Paulina Marsh measurements were applied. These first rough estimations showed that the general trend in wave damping corresponded very well with the field measurement results.

4. Physical properties of the Drag Coefficient in a Vegetation Field

4.1 Introduction

The calibration parameter in the Dalrymple et al.(1984) formulation, which is of significant importance for determining the wave dissipation due to vegetation, is the drag coefficient C_d. It is known that the value of the drag coefficient is dependent on the Reynolds number and on the shape and orientation of the object (Mendez and Losada, *2004*). However there are numerous processes, which also can significantly contribute to the value of the drag coefficient. The numerical model results will be reflected on these physical processes in the sensitivity analyses, in order to determine in which way the model approaches or flaws the reality.

A vegetation field as a whole is an obstacle to wave motion, which is partly reflected from the field, partly attenuated and partly transmitted by interaction with the plants.
In case of a submerged vegetation field, four areas in relation to wave energy dissipation can be distinguished:
area 1: the bottom vegetation interface
area 2: in the vegetation field
area 3: the turbulent boundary layer above the vegetation and
area 4: the water layer above the vegetation.

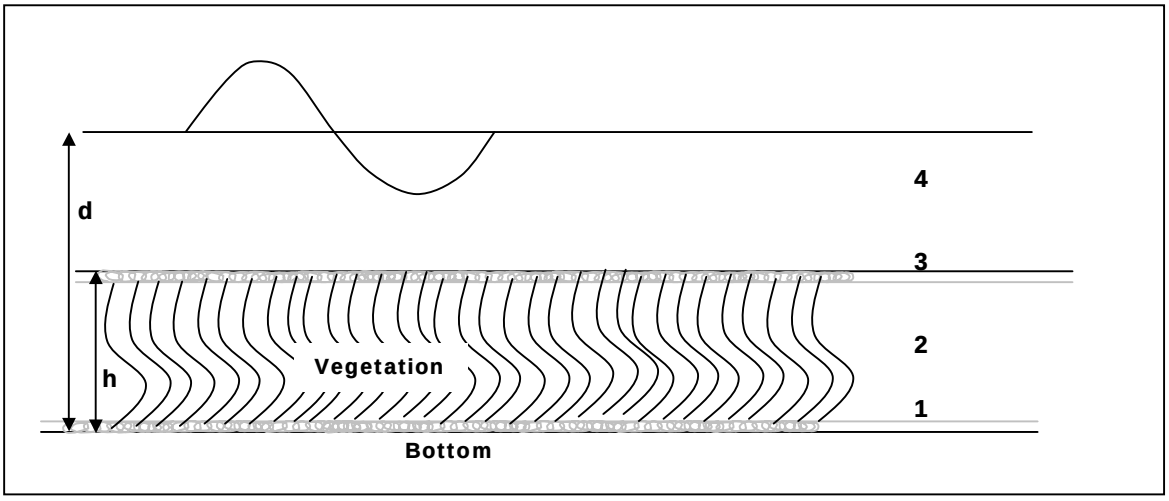


Figure 3: Different zones of energy dissipation in a submerged vegetation.

In layers 1, 2 and 3 energy is dissipated respectively due to the bed friction, wave-vegetation interaction and turbulence in the boundary layer. In layer 4 no energy is dissipated (in case no other processes that can dissipate energy are considered). In case of emerged vegetation only areas 1 and 2 dissipate energy.
In a vegetation field the dissipation due to bed friction is of an order smaller than the contribution of vegetation friction (Mendez and Losada *2004*, Mazda et al., *1997*), even in sparse vegetation (Nepf *1999*). In the Dalrymple formulation only vegetative drag is considered and the turbulence in the boundary layer and bed friction are neglected. Therefore only dissipation in area 2 will be considered.

4.2 Dependence of drag on vegetation characteristics

4.2.1 Single cylinder approach

On the scale of a particular trunk, the interaction between the trunk body and the (oscillating) flow induces vortices and a wake further downstream. Considering the flow around one cylinder, both surface friction and pressure gradients impose drag forces. The surface friction is dependent on the surface roughness. Considering vegetation as smooth cylinders, friction drag is much smaller than the drag force as result of pressure differences (Massel et al. *1999*). Therefore only the pressure drag will be considered in this approach.

The pressure drag around a cylinder in oscillating flow induces a drag force and a lift force. The cases considered in this study assume a shallow water approximation in which vertical orbital velocities are much smaller than horizontal orbital velocities, therefore lift forces are not considered dominant here and will be disregarded.

Water flowing around a cylinder causes the streamlines to contract, resulting in an increasing water velocity and hence a decrease in pressure. Behind the point of separation a wake occurs, where the pressure is much lower than at the upstream side of the object (seeFigure 4).

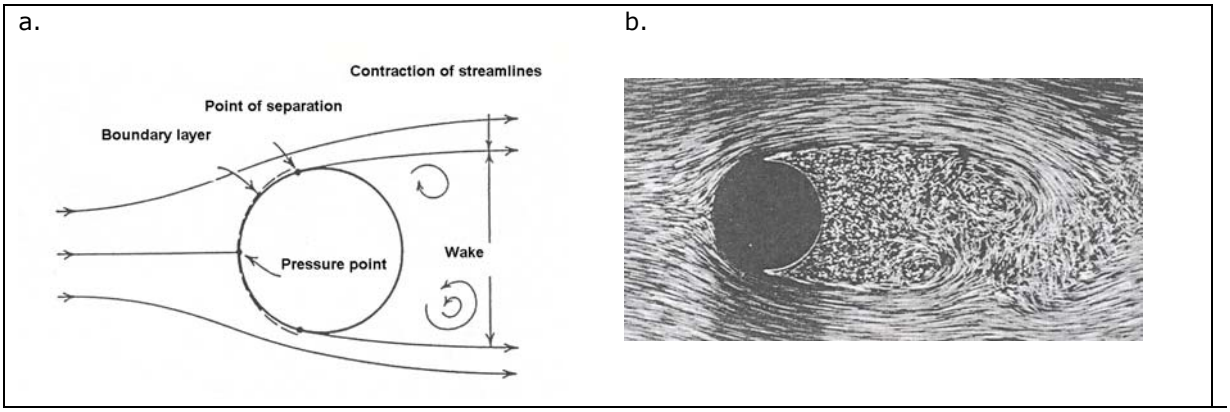


Figure 4: Flow around a cylinder, a. theoretical and b. experimental (for Re = 2300) (from Battjes 1999)

The total pressure gradient in the direction of the flow forms the largest contribution to the drag force. In practice, in a vegetation field the flow regime is turbulent (*Re*>2300). Calculations of the Reynolds number for one single stem in case of cylinders with a diameter equal to respectively a mangrove tree and a *Spartina* plant (used in the SWAN model), show that the Reynolds number is in the range of area B shown in figure 5. This implies that the drag coefficient for one rigid cylinder has a value of around 1.

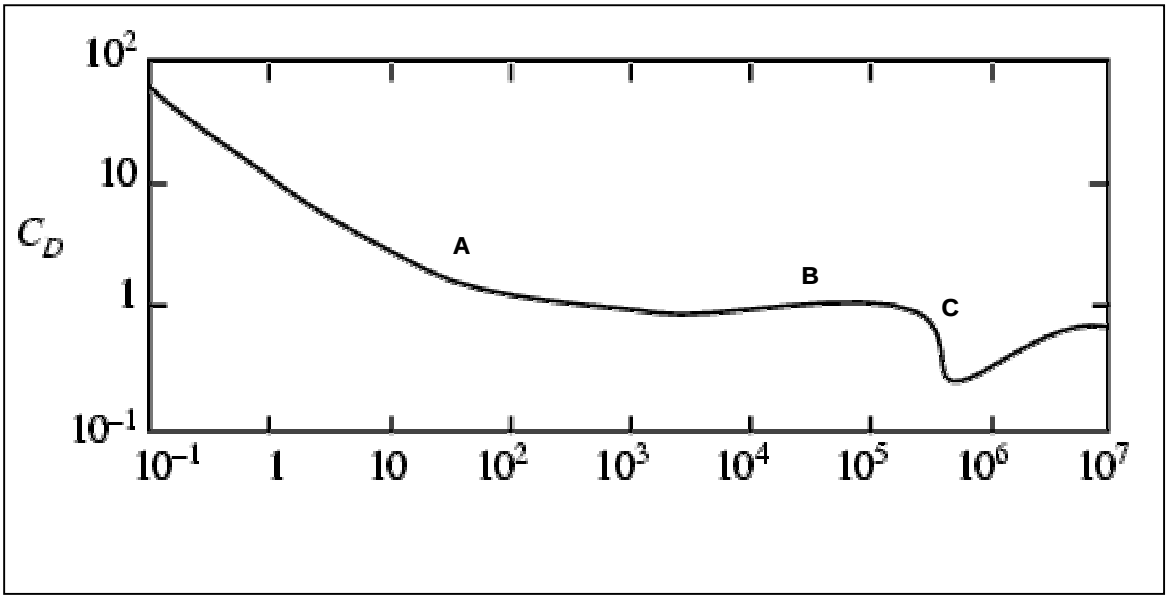


Figure 5: Relation between Reynolds number and drag coefficient for a single circular cylinder in flow. from: Battjes (1999

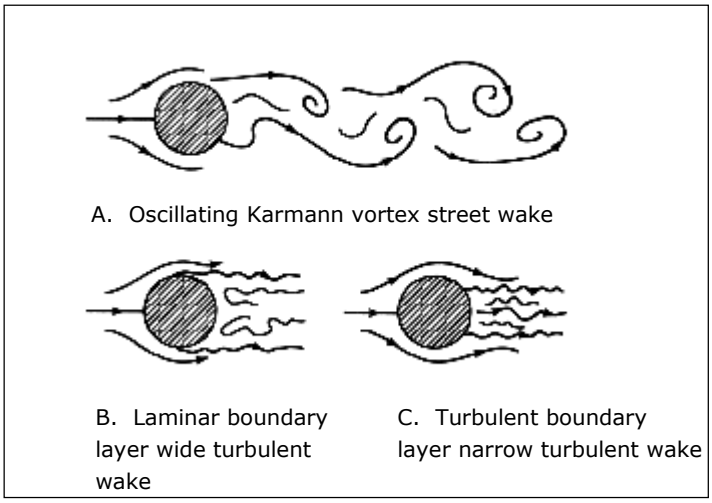


Figure 6: *Single cylinder in a turbulent flow regime*

4.2.2 Multi cylinder array approach

When considering an array of cylinders, numerous other processes influence the drag coefficient. A convenient way to approach a multi cylinder array, is defining a relative spacing (S/D), in which S represents the distance between the cylinders and D the diameter. In vegetation the configuration of the stems is irregular and at random, however for simplification purposes the configuration is considered staggered. For each flow regime a different drag coefficient has to be applied, as was seen for a single cylinder in figures 5 and 6. In a multi-cylinder array, the limits of these different regimes are different because of wake interference, sheltering, and tortuosity (Nepf *1999*).
For large relative spacing between the cylinders, larger than the wake length, the influence of the cylinders on each other is negligible, and a coefficient for one cylinder can be applied. This was confirmed for a uniform flow situation by Nepf (*1999*).

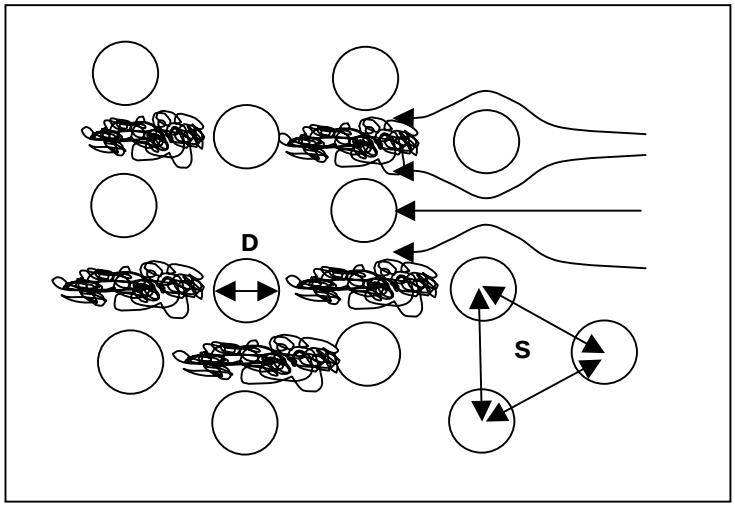


Figure 7 Staggered configuration of cylinders with wake interference and contraction of streamlines

For a decrease in relative spacing, experimental studies by Heideman and Sarpkaya (*1985*) concluded that the bulk drag coefficient for an array of cylinders is smaller than the drag coefficient for a single cylinder in oscillatory flow. An explanation can be found in the fact that the upstream cylinders influence the flow field around the down stream cylinders as shown in figure 7. Some downstream cylinders may lay in the wake of upstream cylinders and therefore be subjected to reduced flow velocities, but increased turbulence, while others may be subjected to increased fluid velocities because of fluid acceleration through spaces between upstream cylinders (Heideman and Sarpkaya, *1999*). The intensity, the length scale and diffusion of turbulence in the water body control the drag forces induced by flow on the cylinders (Massel et al., *1999*).

Another important phenomenon related to turbulence, is eddy viscosity. The turbulent transfer of momentum by eddies gives rise to an internal fluid friction, in a manner analogous to the action of molecular viscosity in laminar flow, but taking place on a much larger scale. The consequence is a decrease in the Reynolds number, resulting in a more viscous behavior of the water. Hence the contribution of the pressure drag decreases and friction drag could become of significance.

When the proximity of the plants increases even further, another change in the value of Cd can be seen. According to Massel et al.(*1999*) (after Chakrabarti, *1991*) the C_d values increase as the relative spacing *(S/D)* approaches to 1.1, where *S* is the distance between the cylinder axes. This could be explained by vegetation acting as a "blunt" object, leading to an increase in drag coefficient. At some point the vegetation can be so dense, that the water prefers the way of least resistance and flows primarily over the vegetation field instead of through it. The waves might experience the vegetation as a "raised (semi) impermeable bottom". This causes the flow lines to contract and the velocity to increase. Turbulence is still induced by the interface between vegetation and the water above.

Another important factor that can attribute to this phenomenon is the relative vegetation height. If the vegetation length is small and subsurface, the water can choose the way of minimum resistance and for the larger part flow over the vegetation. On the other hand, when the relative vegetation is large or the vegetation is emerged, the water will be more or less obliged to flow through the vegetation, leading to a different value of the drag coefficient.

Nepf (1999) studied the influence of the relative spacing on the drag coefficient in flow, defining the vegetation density as:

$$a = n \cdot d = \frac{d}{S^2} \qquad (4.1)$$

where *n* is the number of cylinders per square meter, *S* is the relative spacing and *d* is the cylinder diameter. For this cylinder model *ad* represents the fractional volume of the flow domain occupied by the plants.

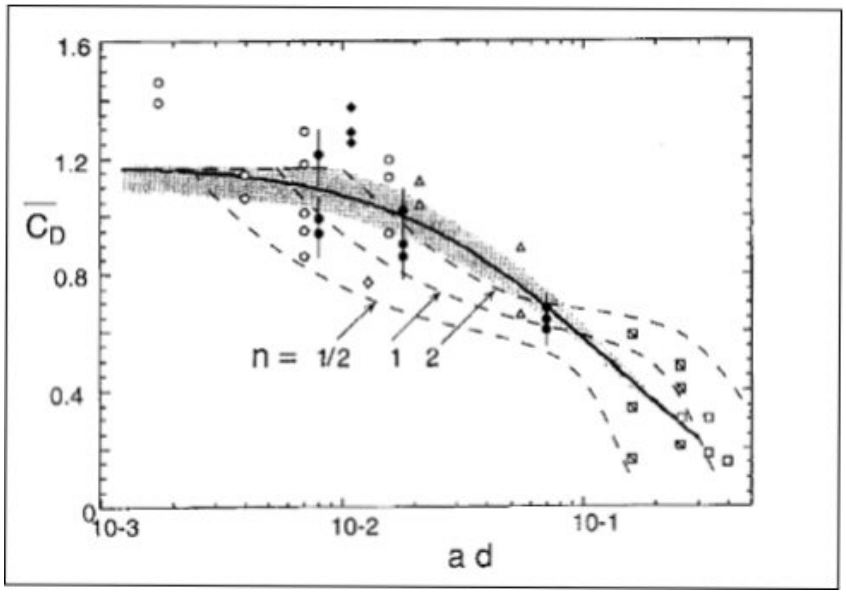


Figure 8: Dependency of C_d on the population density ad (Nepf 1999)

Nepf combined results of several numerical and physical modeling studies (table 1), with several different cylinder spacings and configurations in *Figure 8*, in which *n* represents the ratio of longitudinal to lateral row spacing, *n* = 1 means a square staggered array. A decrease in relative spacing (increase in population density ad) in this case, leads to a decrease in the drag coefficient, due to an increase in wake interference.

Source	Re_d	Configuration	Symbol in Figure 6
Dunn et al. [1996]	1,000–4,000	staggered, n = 1/2	open circle
Seginer et al. [1976]	1,000	staggered, n = 1	open diamond
Kays and London [1956]	1,000	staggered, n = 1–3	square
Petryk [1969]	10,000	random	solid diamond
		staggered, n = 1, 2	triangle
Zdravkovich [1993]	1,000	staggered, n = 1*	square with slash
Present study	4,000–10,000	random	solid circle
Model	>≈200	random	solid line
		staggered, n = 1/2–2	dashed lines

Here, n is ratio of longitudinal to lateral row spacing within staggered array.
*One third, 2/3, and fully staggered.

Table 1 Summary of Reynolds number and array configuration (Nepf 1999)

4.3 Dependence of the drag on wave characteristics

The drag coefficient is also dependent on the wave characteristics. In case of an oscillating flow in waves the value of the Keulegan-Carpenter number can be used to describe the relation between the drag coefficient and the wave characteristics. This relation is also dependent on the relative vegetation height $\alpha \left(= \frac{plant\ height}{water\ depth}\right)$

The Keulegan-Carpenter number is defined as:

$$K = \frac{u_c T_p}{b_v} \tag{4.2}$$

In which:

u_c = horizontal orbital velocity [ms^{-1}]
T_p = wave peak period [s]
b_v = plant stem diameter [m]

Mendez and Losada (*2004*) found the following relations between the drag coefficient and the Keulegan-Carpenter number for different values of relative vegetation height α (Figure 9). These are the results of 154 runs of a physical model in a flume with artificial vegetation, where the calibration parameter is C_d and where the vegetation density and diameter were kept constant. It is noted that the cylinders used in this model had a diameter of 0.025 m and a density of 1200 units per square meter. These thick stems in combination with extremely high density results in low values for the "drag coefficient" $\tilde{C}_d$ (as explained in section 4.2.2) in figure 9. It is pointed out that in this modelled case 60% of the space is occupied by mass (vegetation) and only 40% by water (solidity = 0.6). Results of these physical model tests were used to validate the SWAN model in section 5.3.

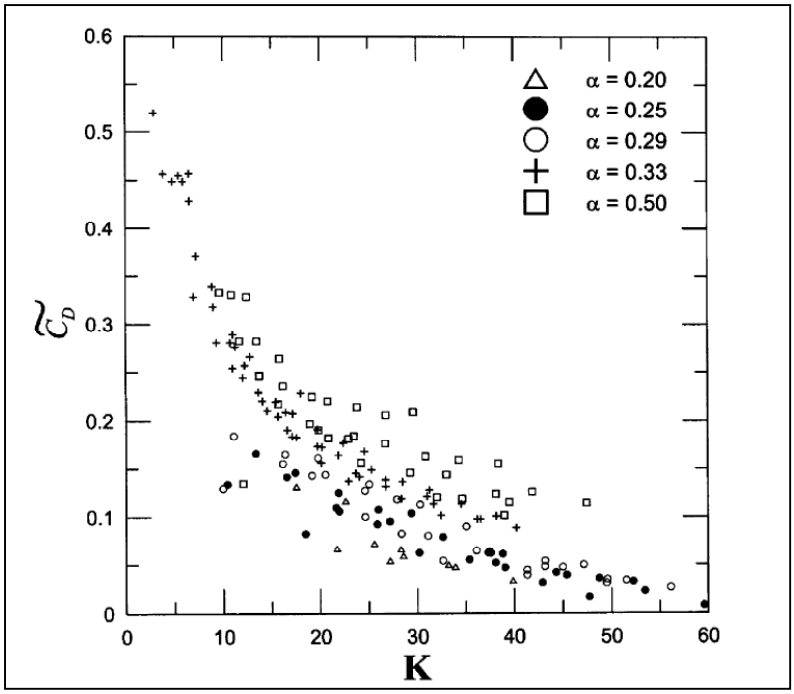


Figure 9: Relation between Keulegan-Carpenter number and C_d for different values of α (from: Mendez and Losada, 2004).

Mendez and Losada give no interpretation of these results. Some presumed processes that could explain the relations between the drag coefficient and the Keulegan-Carpenter number are described here.

A large peak period T_p, or a larger wavelength, suggests that in a certain time frame there are less flow accelerations and decelerations than in a short wave. Because in a decelerating flow more energy (due to more turbulence (Schiereck *2001* after: Booij *1992*)) is dissipated than in an accelerating flow, this energy is not available for the next acceleration. This means that in a certain time frame, more short waves dissipate more energy then a longer wave. In the *K-Cd* relation according to Mendez and Losada: A shorter period causes the *K* number to decrease resulting in a larger drag coefficient.

A wave with a high horizontal orbital velocity will induce more turbulence behind the vegetation stem, resulting in a larger wake. This results in a decrease in bulk drag coefficient due to smaller pressure differences.

4.4 Conclusions

Following from the above described processes and considerations; it becomes clear that for every situation the most important processes need to be taken into account when determining the drag coefficient. It is clear however that the value of the drag coefficient depends on the Reynolds number (and hence the flow regime) and the shape and orientation of the objects. The flow regime mainly depends on the wave characteristics and the relative spacing, position and diameter of the cylinders.

A relation between the drag coefficient and wave characteristics has been defined by Mendez and Losada (*2004*). They express this relation for different relative vegetation heights by introducing the Keulegan-Carpenter number (eq. (4.2)).
The dependency of the drag coefficient on the relative spacing was studied by Nepf (*1999*), who concludes a decline in the drag coefficient when the relative spacing decreases due to wake interference (see figure 8). An important additional parameter that arises in wake interference and that has to be taken into account is turbulent eddy viscosity. This parameter is imbedded in the calibrated drag coefficient $\tilde{C}_d$.

What has to be kept in mind is that some non-drag related and initially neglected processes such as bed friction, vegetation motion and inertia (added mass) can be present in a real time situation, whereas the Dalrymple formulation does not account for these processes. This can result in a deviant value of the drag coefficient, because the contributions of these neglected processes are discounted in the drag coefficient. Therefore it is not physically correct to refer to this parameter as the drag coefficient.

5. Numerical modelling in SWAN

This chapter describes the numerical modelling done in SWAN. A general description of the working and principles of SWAN is presented. Next important considerations with regard to the implementation of Dalrymple's (1984) formulation in SWAN are discussed, followed by a description of the validation of the implementation on the Mendez and Losada (*2004*) experimental results.

5.1 General description of SWAN

The SWAN (Simulating WAves Near shore) model is a third generation spectral model developed by a team at Delft University of Technology. The SWAN model was created in an effort to extend the success of deep ocean wave models (e.g. WAM, Komen et al. *1994*) into coastal areas. The SWAN model was designed to fill in the modelling gap in the dynamic area between 20-30m depth and the coastline. SWAN is a Eulerian model and is based on the action balance equation (Booij et al. 1999). The spectrum that is considered in SWAN is the action density spectrum $N(\sigma,\theta)$ rather than the energy density spectrum $E(\sigma,\theta)$ since in the presence of currents, action density is conserved whereas energy density is not (e.g.,Whitham, 1974). The independent variables are the relative frequency σ (as observed in a frame of reference moving with current velocity) and the wave direction θ (the direction normal to the wave crest of each spectral component). The action density is equal to the energy density divided by the relative frequency:

$$N(\sigma,\theta)=\frac{E(\sigma,\theta)}{\sigma} \qquad (5.1)$$

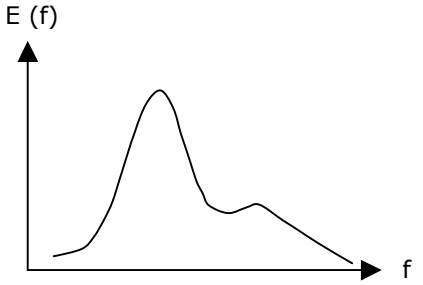


Figure 10: *energy density spectrum*

with *E* (energy density) representing the area under the spectral curve.
This spectrum may vary in time and space.
The evolution of the wave spectrum is described by the spectral action balance equation, which for Cartesian coordinates is (e.g., Hasselmann et al., 1973):

$$\frac{\partial}{\partial t}N+\frac{\partial}{\partial x}c_x N+\frac{\partial}{\partial y}c_y N+\frac{\partial}{\partial \sigma}c_\sigma N+\frac{\partial}{\partial \theta}c_\theta N=\frac{S}{\sigma} \qquad (5.2)$$

The first term represents local rate of change of *N* (action density) in time, the second and third terms represent the propagation in *x* and *y* (geographical space) with c_x and c_y (the propagation velocities in space). The fourth term represents the shifting of relative frequency due to variations in water depth and currents while the fifth term represents depth-induced refraction. The right hand term is the energy source term, which accounts for generation, dissipation and non-linear interactions between waves. Details can be found in (Booij et al., *1999*) and the User manual (*2004*).

The wave model accounts for the following effects:
• wave propagation in space: shoaling and refraction
• dissipation by bottom friction
• wave growth due to wind input
• transfer of energy within the spectrum by non-linear wave-wave interactions (both quadruplets and triads)
• dissipation by white capping
• dissipation by depth-induced breaking

The aim of this project was to extend the use of SWAN into shallow inter tidal zones, such as salt marshes and mangrove forests, and to add additional wave energy dissipation from wave-vegetation interaction. The dissipation term was added to term on the right hand side of equation((5.2).

5.2 Modelling wave attenuation by vegetation

5.2.1 Implementation of the Dalrymple formulation in SWAN

In the previous section the action density balance equation has been discussed. Implementing dissipation due to vegetation implies adding an extra source term to this equation. The subroutine of SWAN that handles these source terms is *swancom2*. Therefore the new subroutine, called *SVEG,* is implemented in *swancom2*. The result will be a model that describes wave attenuation by vegetation, in which vegetation can be varied both horizontally, to account for the zonation of vegetation, and vertically, to account for different vegetation species by vertically varying vegetation characteristics. For a general description of the SWAN Source code and the code of the implementation, see Appendix D.

The approach of the implementation of the Dalrymple formulation will be discussed here in three sections. First homogeneous vegetation was implemented in SWAN. This was subsequently expanded with horizontal variation and finally with vertical variation of the vegetation. The final result is a model in which vegetation can be varied both horizontally and vertically.

5.2.2 Homogeneous vegetation

As was described in section (3.3.2), the formulation to be implemented reads:

$$S_{veg} = \langle \varepsilon_v \rangle = \frac{1}{2\sqrt{\pi}} \rho \tilde{C}_D b_v N \left(\frac{gk}{2\sigma} \right)^3 \cdot \frac{\sinh^3 k\alpha h + 3\sinh k\alpha h}{3k \cosh^3 kh} H_{rms}^3 \qquad (5.3)$$

Since the dependent variable in SWAN is the spectral energy *E*, the formulation of Dalrymple (1984) needs to be revised.

The quantity H_{rms} can be written in terms of spectral wave energy as follows:

$$H_s = 4\sqrt{E} \qquad (5.4)$$

so that

$$H_{rms} = \frac{H_s}{\sqrt{2}} = 2\sqrt{2}\sqrt{E} \qquad (5.5)$$

Equation (5.5) substituted in equation (5.3) results in:

$$S_{veg} = \frac{8\sqrt{2}}{\sqrt{\pi}} \rho \tilde{C}_D b_v N \left(\frac{gk}{2\sigma} \right)^3 \cdot \frac{\sinh^3 k\alpha h + 3\sinh k\alpha h}{3k \cosh^3 kh} E\sqrt{E} \qquad (5.6)$$

Because S_{veg} is a dissipation term it needs to be treated implicitly. Since SWAN can only work with (quasi) linear terms, equation (5.6) needs to be linearized in *E*. The simplest approach is a linearization by a Picard iteration. In general:

$$S^n \cong \Phi^{n-1} E^n \tag{5.7}$$

This results for Sveg in:

$$S_{Veg}^n \cong \gamma E^n \text{ with } \gamma = \gamma(H_s, T_p, ..., E^{n\text{-}1}) \tag{5.8}$$

In this case:

$$\gamma = \frac{8\sqrt{2}}{\sqrt{\pi}} \rho \widetilde{C}_d b_v N \left(\frac{kg}{2\sigma} \right)^3 \cdot \frac{\sinh^3 k\alpha h + 3\sinh k\alpha h}{3k \cosh^3 kh} \sqrt{E^{n-1}} \tag{5.9}$$

where E^n is the energy density in the current iteration level and E^{n-1} is the energy density in the previous iteration level.

The vegetation parameters are the drag coefficient C_d, the vegetation density N_V, the diameter b_v and the plant height αh. These parameters are constant over the entire grid, resulting in homogeneous vegetation.
This formulation (equation 5.6) is implemented in the subroutine *swancom2,* the source code of this subroutine *SVEG* can be found in Appendix D.

Both bed friction and vegetation interaction can simultaneously be activated. Nevertheless, Mazda et al. (*1997*) and Nepf (*1999*) concludes from physical modelling tests that the contributions of bed friction to the wave dissipation is an order smaller than the vegetation interaction, thus can be neglected, as mentioned in section 4.1. SWAN is a depth-averaged model, which implies a vertically uniform horizontal orbital velocity profile.

5.2.3 Horizontal variation of vegetation

In addition to the homogeneous formulation the vegetation can easily be varied horizontally in the following manner.

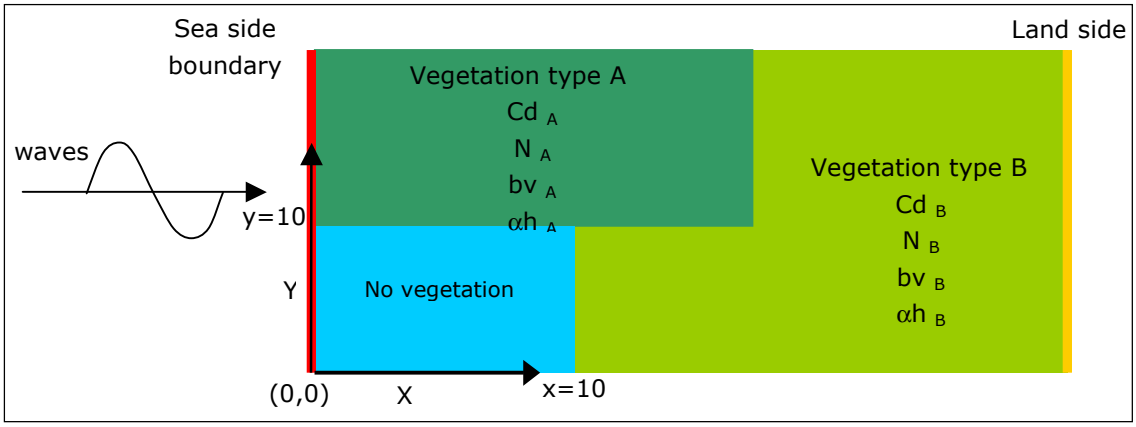


Figure 10: Example horizontal variation

For values of $x \leq 10$ and $y \leq 10$, the user defines the situation with the following vegetation characteristics: C_d=0 ; N_V=0 ; b_v=0 ; αh=0, implying that no vegetation is present. For the other areas shown in Figure 10, where vegetation type A and B are present, this works in a similar way. (For the implemented source code of this horizontal variation procedure, see Appendix D).

5.2.4 Vertical variation of vegetation

Next, vertical variation of vegetation is added. For the implementation of vertical variation of vegetation characteristics an important simplification on the vertical distribution of horizontal orbital velocity was made. Inter tidal wetlands (mangroves and salt marshes) are characterized by shallow foreshores which implies that a shallow water approximation of the waves can be assumed. In case of small wave heights a transitional situation can occur. (Figure 11)

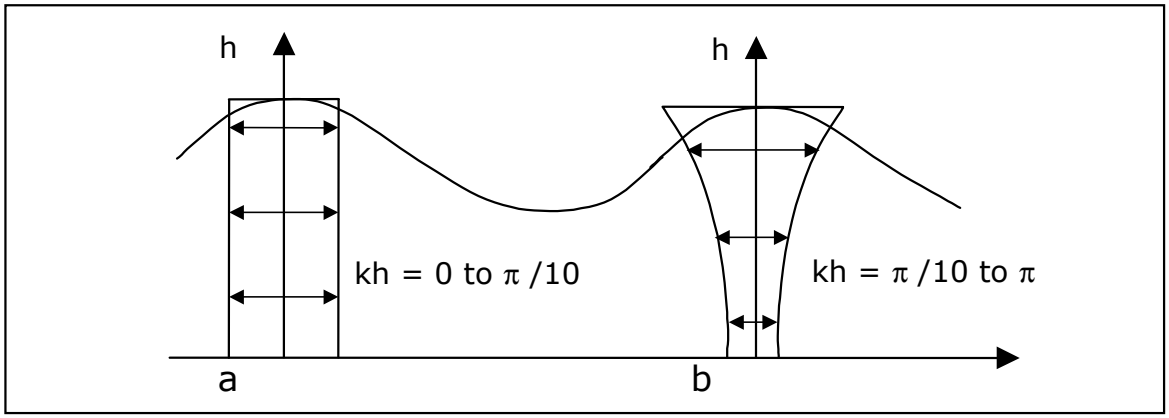


Figure 11: Vertical distribution of horizontal orbital velocity for a. shallow water and b. transitional water depth

Little is known about the orbital velocity profile inside the vegetation field, however, some research has been done on the interaction between flow and vegetation (Mazda and Wolanski, *1995)*, (Nepf, *1999*). According to Baptist (*2005*), the following flow pattern is found in submerged vegetation, when only a current is present:

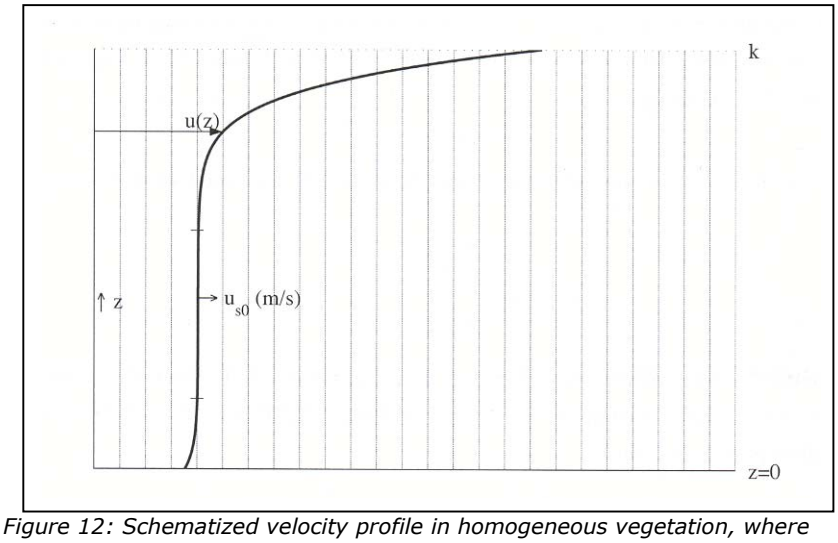


Figure 12: Schematized velocity profile in homogeneous vegetation, where k is the vegetation height (Baptist 2005)

It can be seen that the velocity profile inside the vegetation field (u_{s0}) is for the largest part uniform over the vegetation height. It is assumed that the vertical distribution of horizontal orbital velocity in a homogeneous vegetation field follows a similar profile. Because of the uniformity of the velocity profile in the vegetation, it is assumed that the amount of energy dissipation per unit vegetation height is uniformly distributed over the vertical as well, as the energy dissipation formula contains the orbital velocity in the third power.
SWAN is a depth-averaged model; therefore the true horizontal orbital velocity distribution over the vertical is represented as a uniform profile, shown in Figure 13.

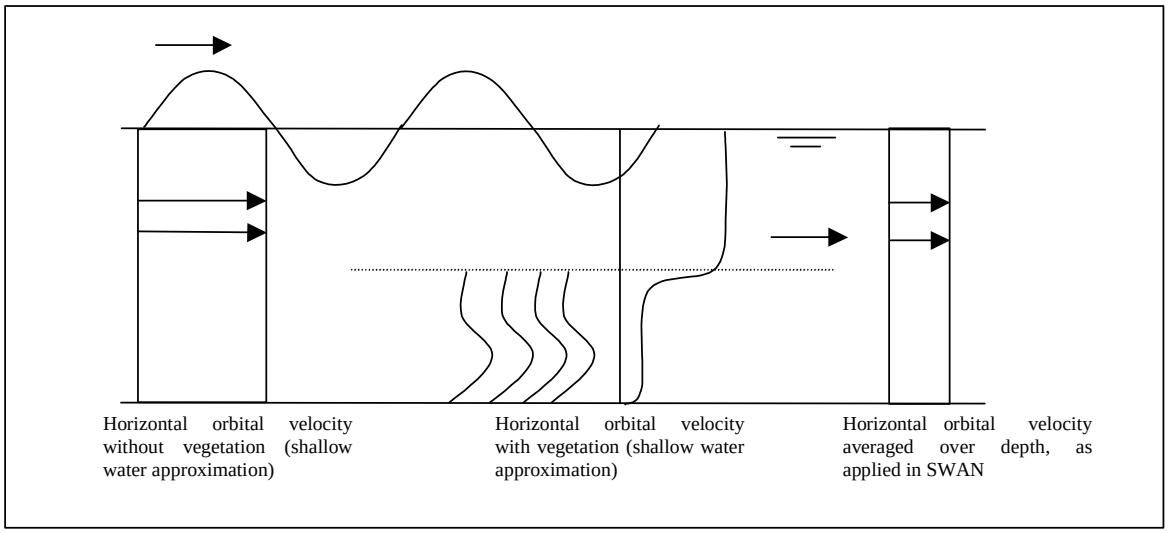


Figure 13: Horizontal orbital velocity profiles

Next it is verified if this assumption of the linear relation between the vegetation height and the amount of energy dissipation can be found when using the Dalrymple et al.(1984) formulation. The result for homogeneous vegetation is shown in Figure 14.

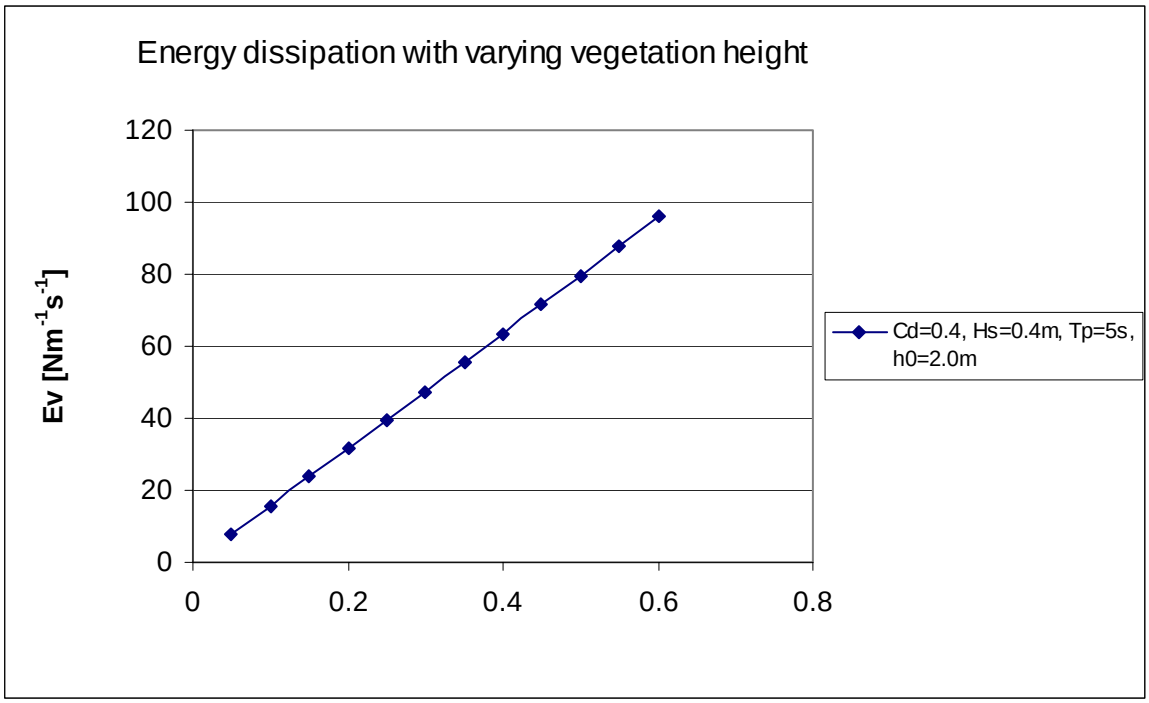


Figure 14: Linear relation between energy dissipation and the vegetation height

As can be seen, the relation between the amount of energy dissipation and vegetation height is linear. Because in this non-breaking situation bottom friction is not considered and no other external processes that could be responsible for wave energy dissipation are present, the dissipation is solely caused by the wave vegetation interaction. The conclusion that can be drawn is that, when the vegetation is being vertically sub divided into several segments, the dissipation of each segment can be added to form the total dissipation. This conclusion makes it conveniently possible to implement vertically varying vegetation, by imposing different vegetation characteristics per layer (see Figure 15).

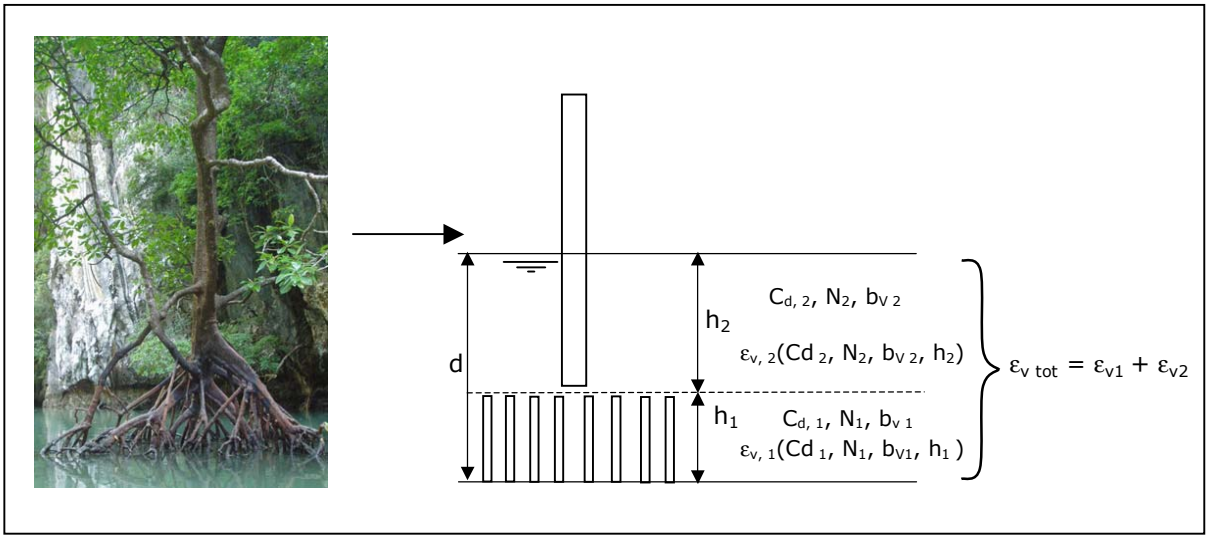


Figure 15: Schematization of a mangrove tree in the SWAN model

However, we need to realize that with applying non-homogeneous vertical vegetation characteristics, the horizontal orbital velocity profile is actually not homogeneous anymore. In SWAN as mentioned before, the total energy dissipation is a depth averaged value, therefore it can be concluded that the assumed approach of adding up the contribution of each segment (see Figure 15) to form the total amount of depth averaged energy dissipation can be considered valid.

5.2.5 Implementation in source code

In the source code this summation is done in the following manner. First the program checks whether the vegetation is submerged or emerged, by comparing the water depth with the vegetation height. If the vegetation is submerged, the energy contributions of each layer are added up. If the vegetation is emerged, only the contributions of the vegetation below the water level are taken into account. For the implemented source code of this vertical variation procedure, see Appendix D.5.

5.3 Validation of the SWAN model

The adjusted SWAN model was validated on the results of a physical model test in order to determine if the implementation of the Dalrymple formulation was successful.
Mendez and Losada (*2004*) used a physical model for the validation of their expanded version of the Dalrymple formula. The experiment was carried out in a wave flume of 33 meters long, 1 meter wide and 1.6 meter high. In the flume on a horizontal bottom a 9.3m long strip of artificial kelp (*L. Hyperborea*) vegetation was present over the entire flume width. The vegetation had the following characteristics: b_v=0.025m, αh=0.2m, N=1200 m^{-2} (respectively diameter, relative vegetation height and density). Mendez and Losada carried out a total of 154 runs with varying water depth (d=0.4-1.0m), wave peak periods (T_p=1.26-4.42s), and root mean square wave heights (Hrms=0.045-0.17m). This means that the drag coefficient Cd was the calibration parameter in the Dalrymple formulation. The input for irregular waves was the JOint North Sea WAve Project (JONSWAP) spectrum with shape parameter γ_j = 3.3, which is default in SWAN.
The results of these studies were used to validate the new SWAN model with vegetation implementation.
The same line up was used as input in the SWAN model and the results were compared with the measurements. As can be seen in

Figure *16* and appendix E, the results of the model correspond very well with the physical model tests. Thus, it can be concluded that the Dalrymple et al. (1984) formulation was implemented in SWAN successfully.

In the remaining chapters marsh vegetation is considered with vertically homogeneous vegetation and only horizontal variation of vegetation characteristics will be considered.
For the application of the model on vertically varying vegetation, the reader is being referred to the M.Sc. thesis of Burger (2005), who applied the SWAN model on (vertically varying) mangrove vegetation.

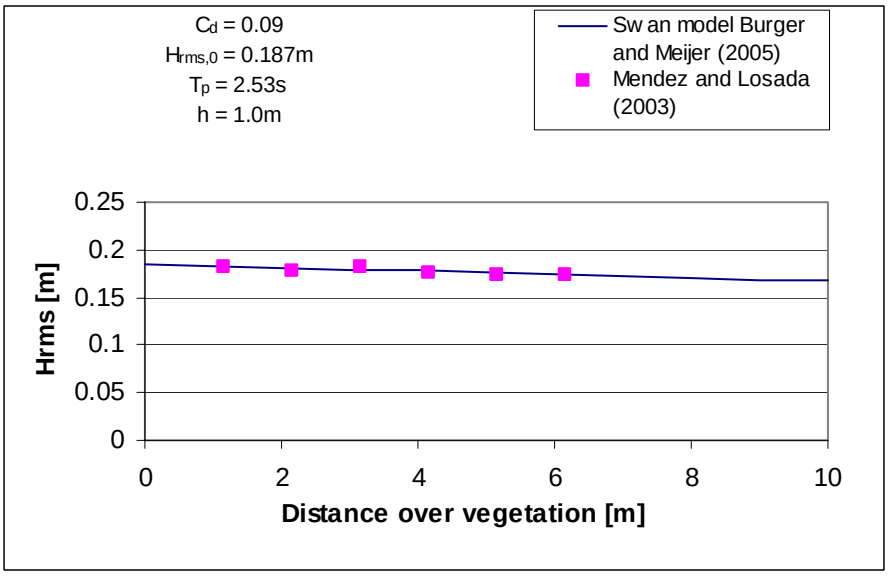


Figure 16: SWAN implementation validation

6. Sensitivity analyses

6.1 Model setup

A sensitivity analyses was performed in order to determine the response of the model to changes in parameters. In all model runs the dependency of the drag coefficient on changes in wave and vegetation characteristics, as was found in section 4, were not considered. The reaction of the model to a change in each single parameter is analyzed to determine the dominant processes present in the model, and to reflect these conclusions to observations in a real time situation. A number of model runs was performed with parameters varied in the following three areas.

- Water level
- Vegetation characteristics
- Wave characteristics

A rectangular 2D grid was used to prevent interference of the model edges with the results (see Appendix B). The results are considered at the transect line where no edge influences are present. To rule out effects of shoaling, the bottom was set horizontal. A grid was used with dimensions as given in Figure 17. Vegetation was present from x=5 to x=50 meters. In x and y direction a grid spacing of respectively 1m and 2m was used. (Figure 17)

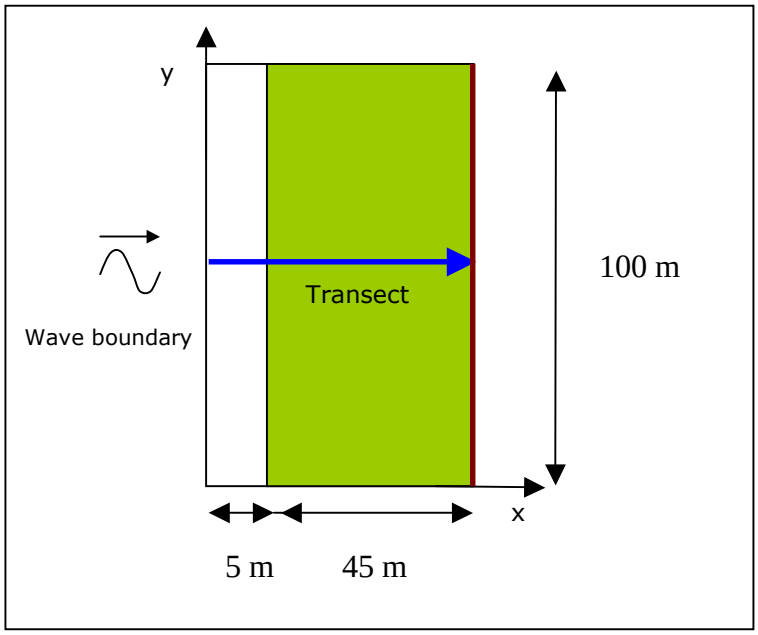


Figure 17: Model setup of sensitivity analyses

6.2 Sensitivity to changes in water level

A change in relative vegetation height influences the amount of wave damping, as was stated in section 3. For a vegetation height of 1.0 meters model runs were carried out with water levels varying from 5 to 0.4 meters, in order to include the transition area from emerged to submerged vegetation. The input parameters are given in Table 1 and the results are presented in Figure 18 and Appendix F.

Vegetation characteristics			Wave characteristics		Water level
bv (m)	N (-/m)	hveg (m)	Hs (m)	Tp (s)	h (s)
0.004	1000	1.0	0.2	4.0	0.4-4.0

Table 2: Swan model input

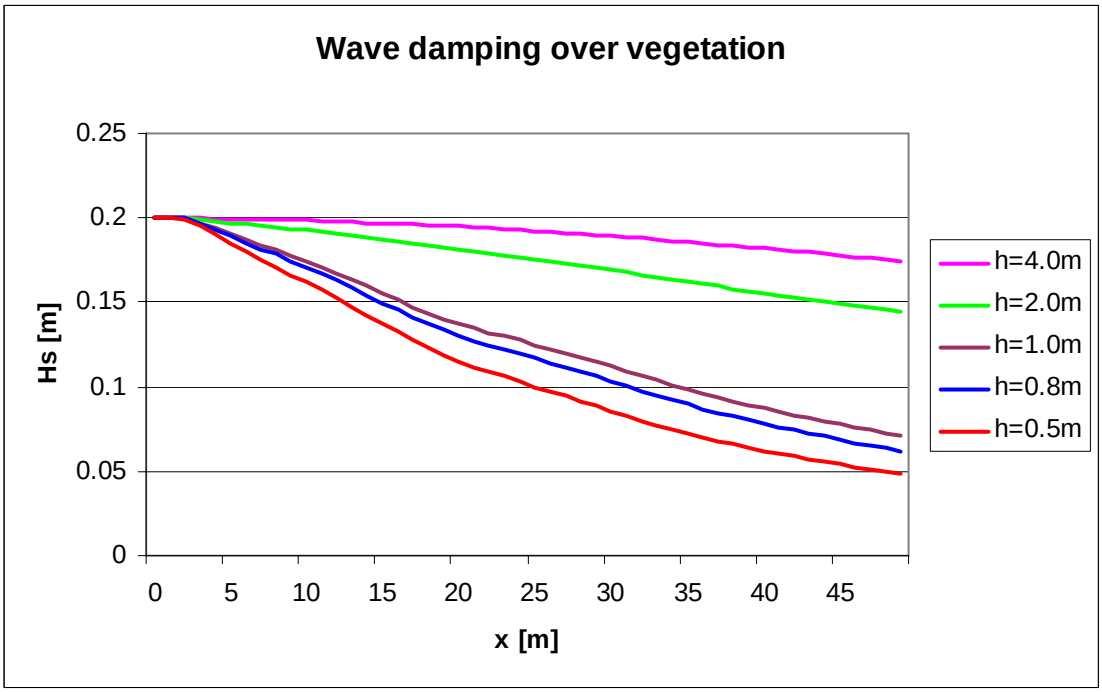


Figure 18: significant wave height over vegetation at varying water levels

This figure shows a clear increase in wave damping at decreasing water levels. In order to get a clear view of the actual amount of decrease in significant wave height, a transmission coefficient, defined as the ratio between the transmitted and the incoming significant wave height ($K_T = \frac{H_T}{H_I}$), is defined and plotted against the water level, resulting in Figure 19.

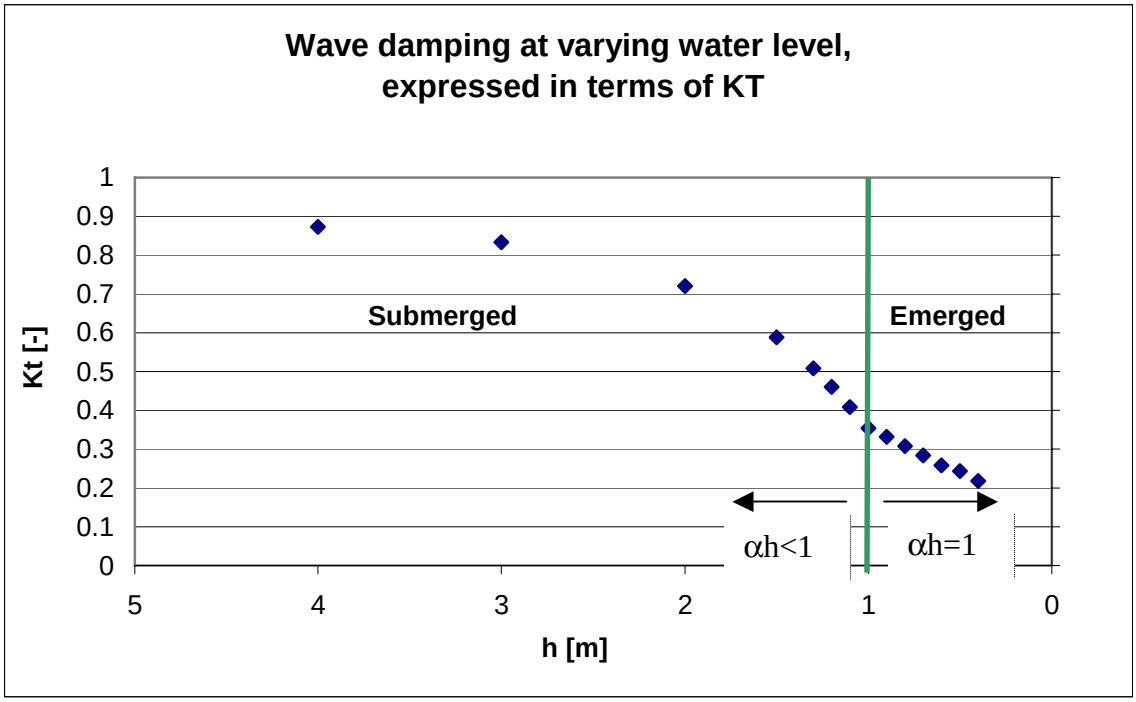


Figure 19: Relation between K_T and water level

For submerged vegetation, a decrease in water level (water level approaching top of vegetation) increases the vegetation influence on the waves, leading to a non-linear decrease in significant wave height. When the water level protrudes the vegetation and an emerged situation occurs, a linear decrease in wave height is noticed.

6.3 Influence of change in vegetation characteristics on wave attenuation

A change in vegetation characteristics influences the wave transmission through the vegetation field, as was explained in chapter 4. Especially the configuration of the stems, the relative distance and the diameter influence the flow pattern around the stems and hence the amount of energy dissipation and the wave height. In Dalrymple's energy dissipation formula (eq. 4.10) the vegetation characteristics C_d, N and b_v are linearly multiplied. Therefore a change in any one of these parameters influences the model to the same extent. An increase in density of 100% has the same result as an increase in diameter by 100%. Therefore it is sufficient to determine the reaction of the model to a change in one of these parameters; hence the model reacts in a similar manner to a change in the other plant characteristics. The parameter that was varied was the density N.

Vegetation characteristics				Wave characteristics		Water level
bv	N	Cd (-)	hveg (m)	Hs (m)	Tp (s)	h (m)
0.004	500-4000	1	0.75	0.2	4.0	1

Table 3: Swan input parameters

With increasing density, a rapid decrease in wave height in the first part of the marsh is seen (Figure 20). At some distance, the wave height has diminished and the vegetation has less influence on it. In Figure 21 this can be seen by a relative decrease in the amount of energy dissipation with increasing density.

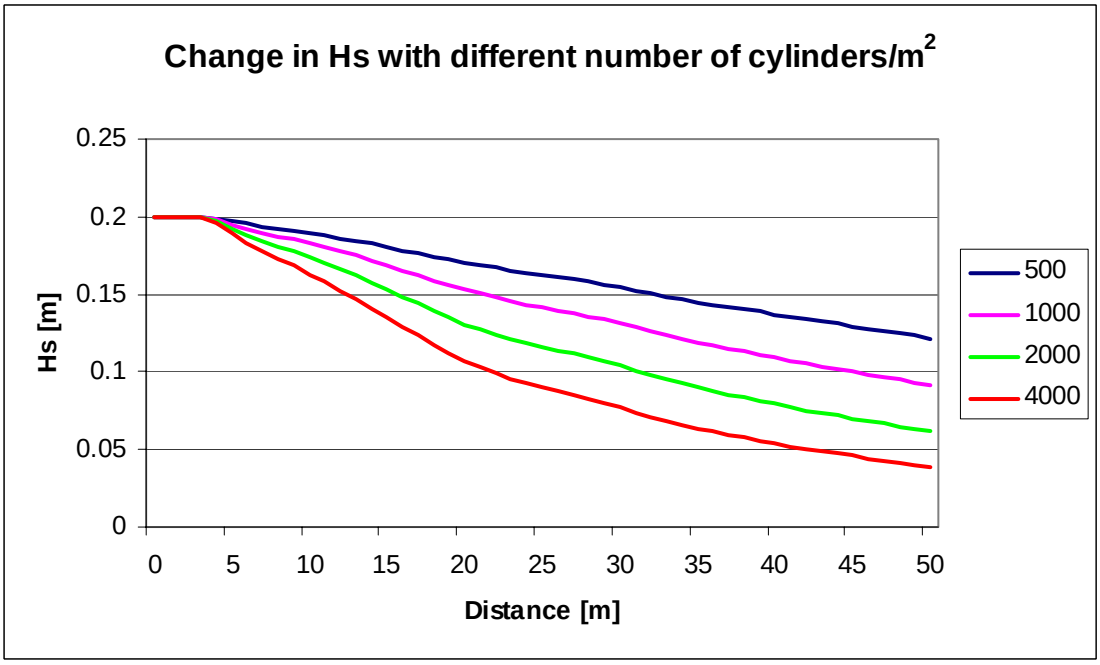


Figure 20: Wave attenuation with different densities

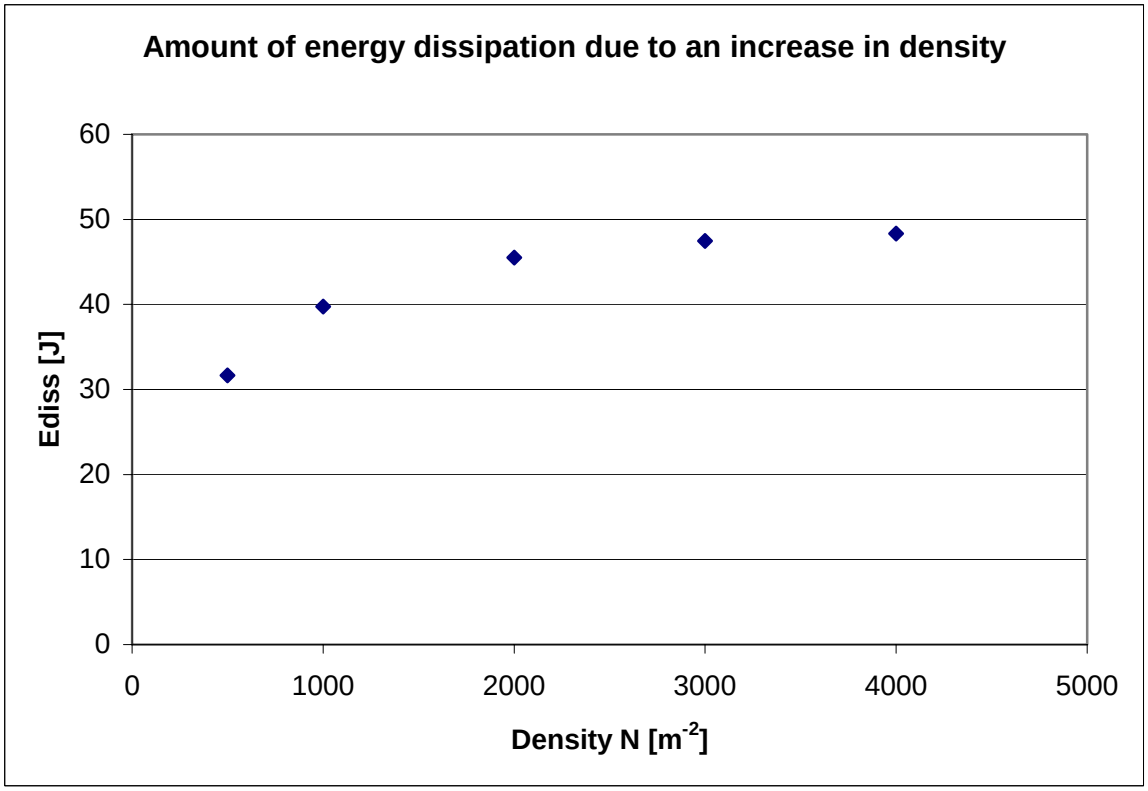


Figure 21: Relation between the amount of energy dissipation and stem density.

6.4 Influence of change in wave characteristics on wave attenuation

The wave height and period of the incoming waves influence the wave transmission and the amount of energy dissipation in the vegetation field.

6.4.1 Influence of wave height to the amount of wave attenuation

It is expected that the significant height of the incoming wave is of relatively large importance.
A wave with a large wave height contains more energy and is influenced more by the vegetation then a smaller wave. In the SWAN model the following input parameters were used and the significant wave height was varied, resulting in Figure 22.

Vegetation characteristics				Wave characteristics		Water level
bv	N	Cd (-)	hveg (m)	Hs (m)	Tp (s)	h (s)
0.004	1000	1	0.75	0.05-0.4	4.0	1

Table 4: Swan input parameters

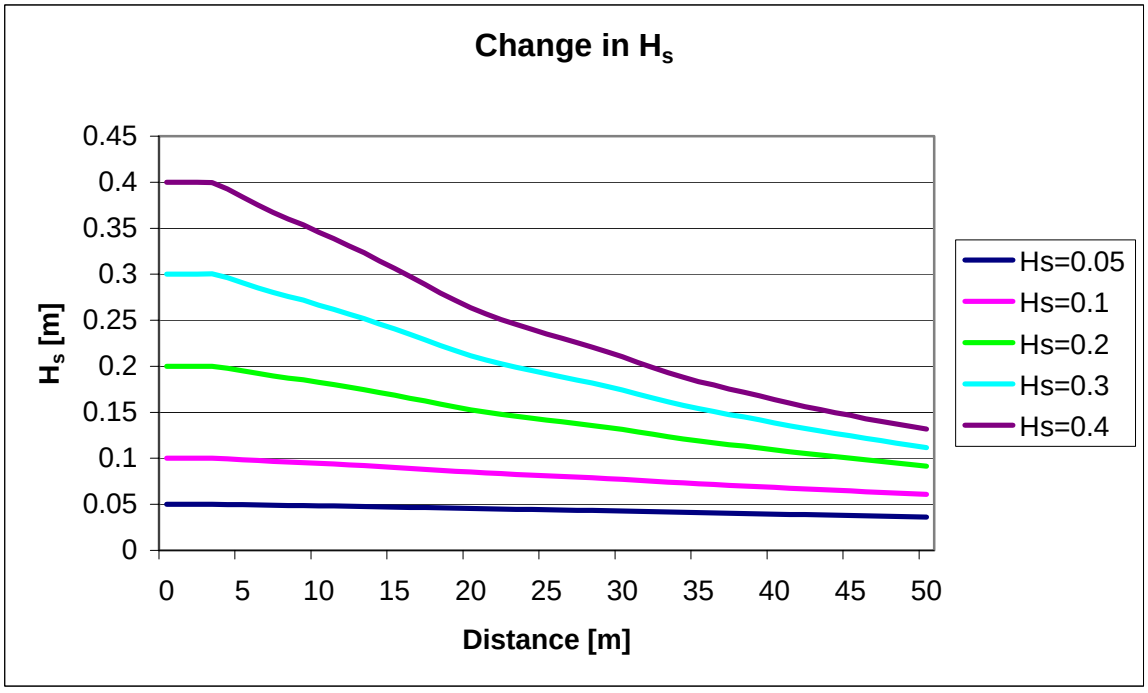


Figure 22: Decrease in significant wave height over vegetation

As was expected a higher incoming wave is affected more by the vegetation than a lower wave. The amount of dissipated energy in each case is shown in figure 23.

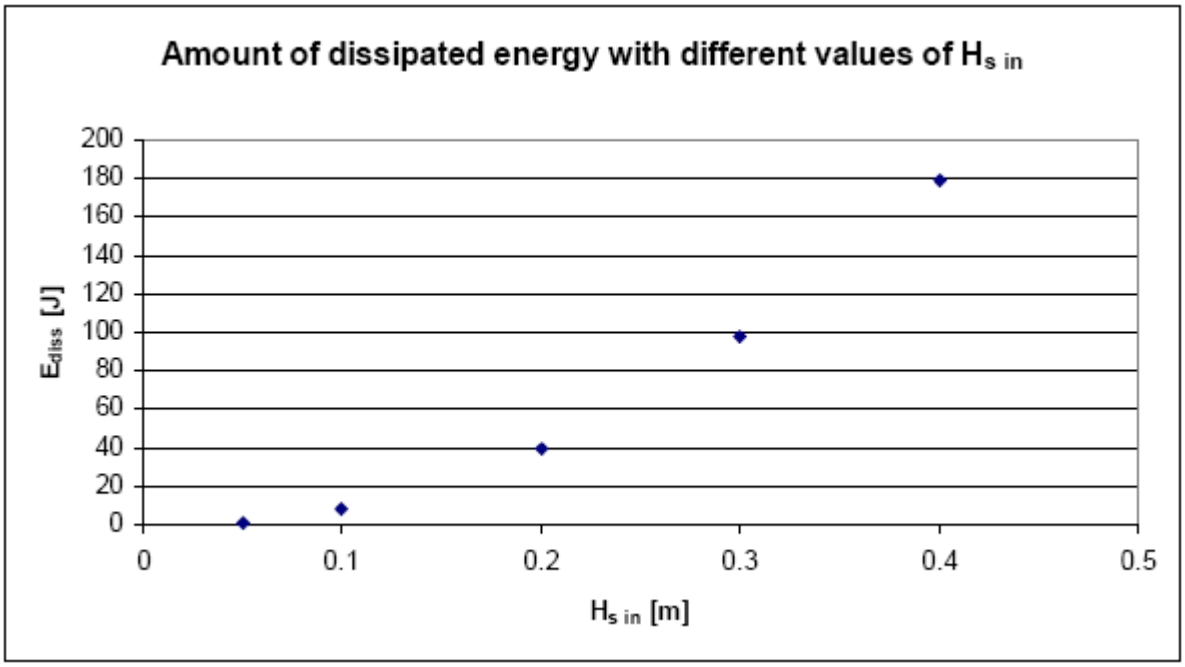


Figure 23: Energy dissipation at different incoming significant wave height.

The shape of figure 23 was expected, as the root mean square wave height is present to the third power in the Dalrymple et al. (1984) formulation.

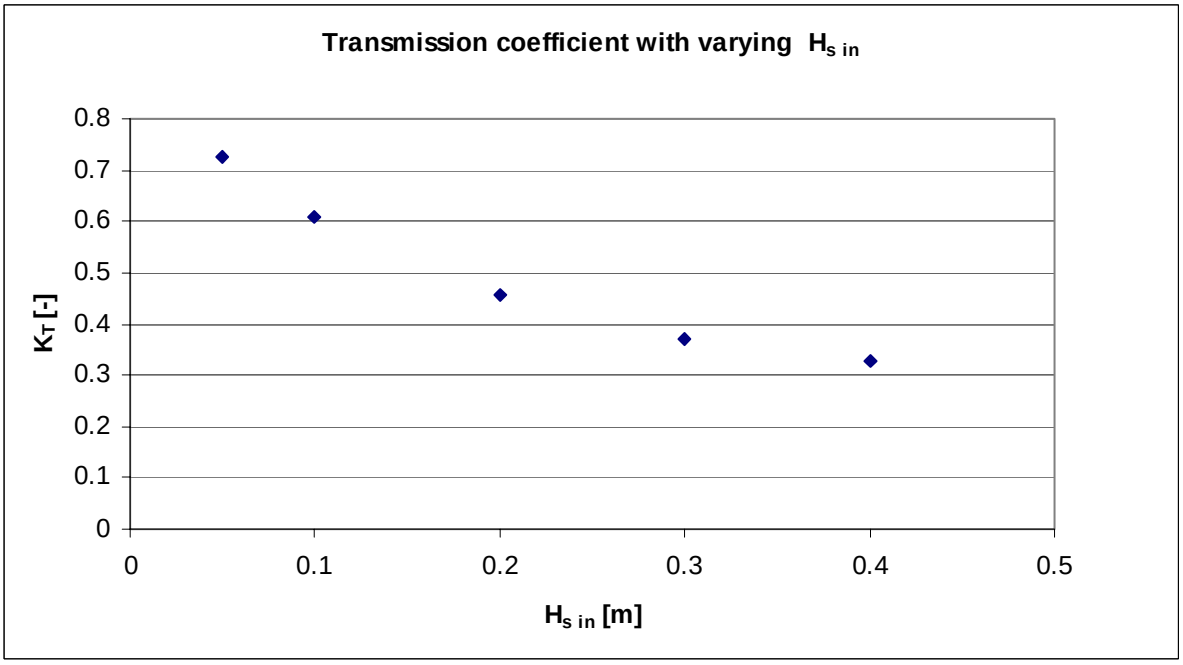


Figure 24: Relation between the transmission coefficient and the incoming significant wave height

6.4.2 Influence of change in wave frequency on wave attenuation

When a wave spectrum is considered, various waves of different frequencies are dissipated in different manners. From Appendix G and Figure 25 it can be seen that a spectrum with a large peak period and a low frequency range (lower peak frequency) dissipates more energy than a spectrum with a range of higher frequencies. In Figure 25 the amount of dissipated energy per frequency is shown for three cases:
Case A: Peak period of 6.25 s with spectral boundaries between 0.1 and 0.4 Hz
Case B: Peak period of 2.50 s with spectral boundaries between 0.3 and 0.6 Hz
Case C: Peak period of 2.85 s with spectral boundaries between 0.2 and 0.5 Hz

Vegetation characteristics				Wave characteristics		Water level
bv	N	Cd (-)	hveg (m)	Hs (m)	Tp (s)	h (s)
0.004	1000	1	0.75	0.05-0.2	Varying spectra	1

Table 5: SWAN model input

As the total amount of energy present in the spectrum is equal to the surface area under the spectral curve it appears that more energy is dissipated for a spectrum with larger peak periods.

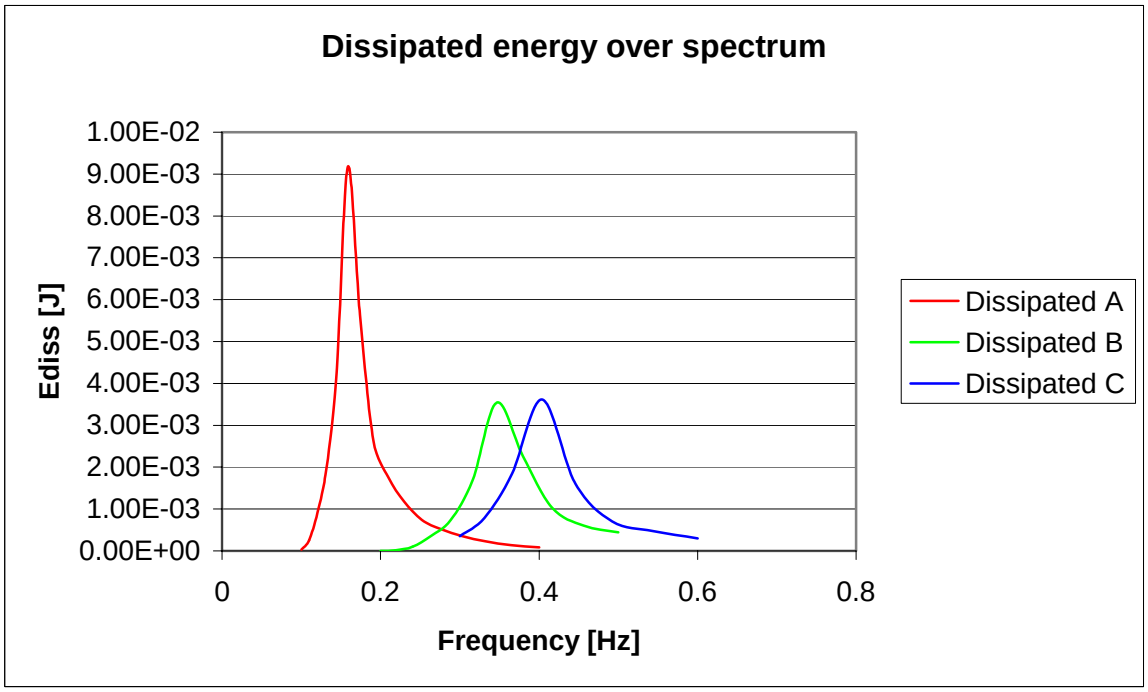


Figure 25: The difference between the incoming spectral energy and the spectral energy behind the vegetation, which are given in Appendix G.

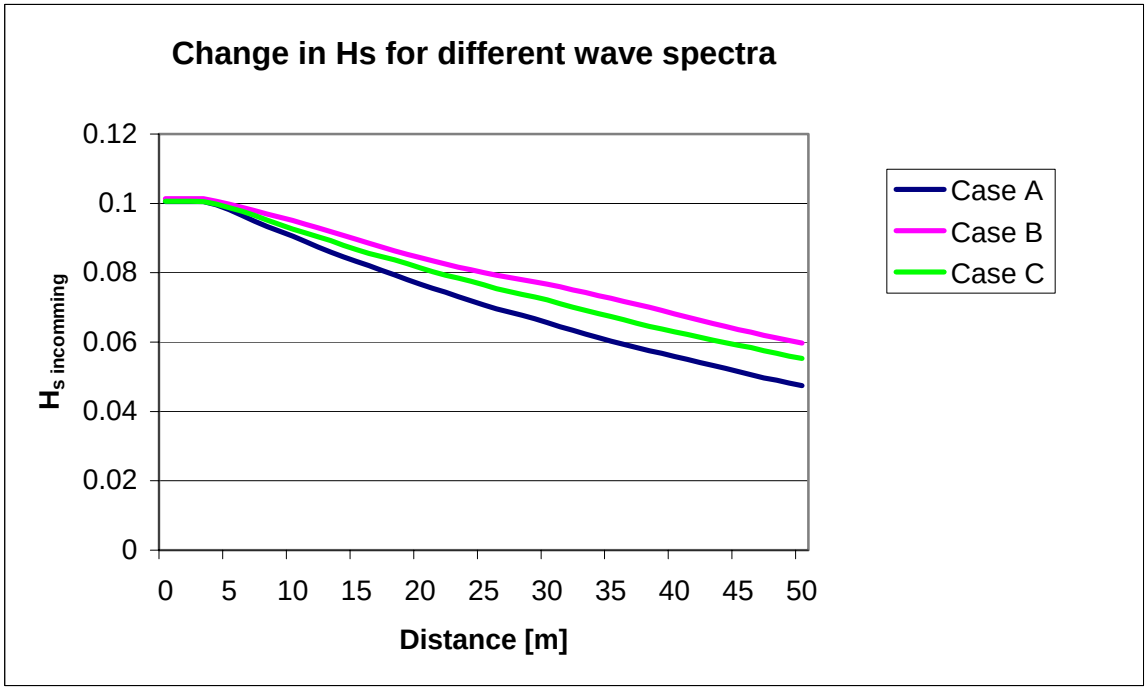


Figure 26: Change in Hs for different wave spectra

From Figure 25 can be concluded that wave spectrum A with low peak frequency and a low frequency range contains more energy. Because wave energy is proportional to H_s^2, in this frequency range the highest waves are present, which will be attenuated more by the vegetation
As was stated in section 3.3, on a scale of one single stem, a wave with a small wave period will cause more energy decrease then a long wave. This is among others dependent on the ratio between the obstacle size and the wavelength. On a larger scale, as considered in case of a vegetation field, waves with large peak periods contain more energy and have larger wave heights then other waves in the spectrum. Because wave energy is proportional to H_s^2, around the peak frequency the highest waves are present, which will be attenuated most by the vegetation, leading to the highest decrease in energy density.

7. Paulina Marsh case

7.1 Field measurements

The field research that was done at the Paulina Marsh in 2002, was executed by WL|Delft Hydraulics (2003), in association with the NIOO (Netherlands Institute for Ecology). The research consisted of wave measurements taken over a straight transect of the marsh and a vegetation measurement campaign. The measurements were carried out over a
26 meter long transect in the months of August and September. In this case the measurements done at August 10th are considered.

Eight wave gauges were placed in line over the marsh, indicated P0 to P7 in
Figure *27*, and the bathymetry that was measured is given in Figure 28.

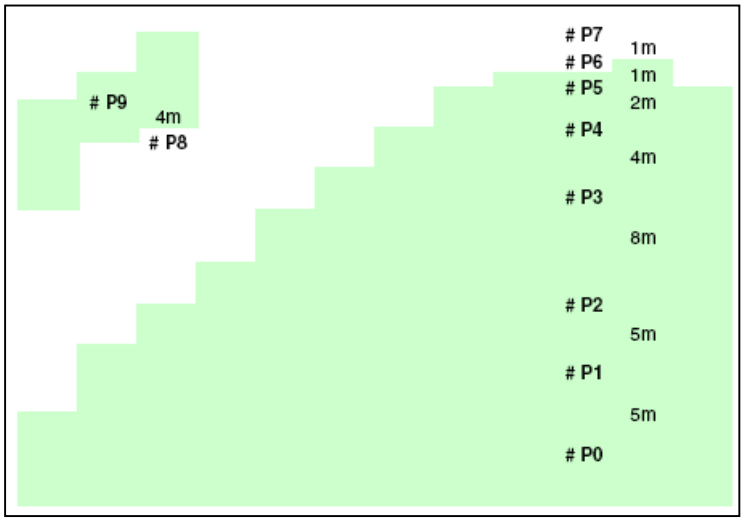


Figure 27 Location of the pressure sensors at the salt marsh. P0 is the landward side.

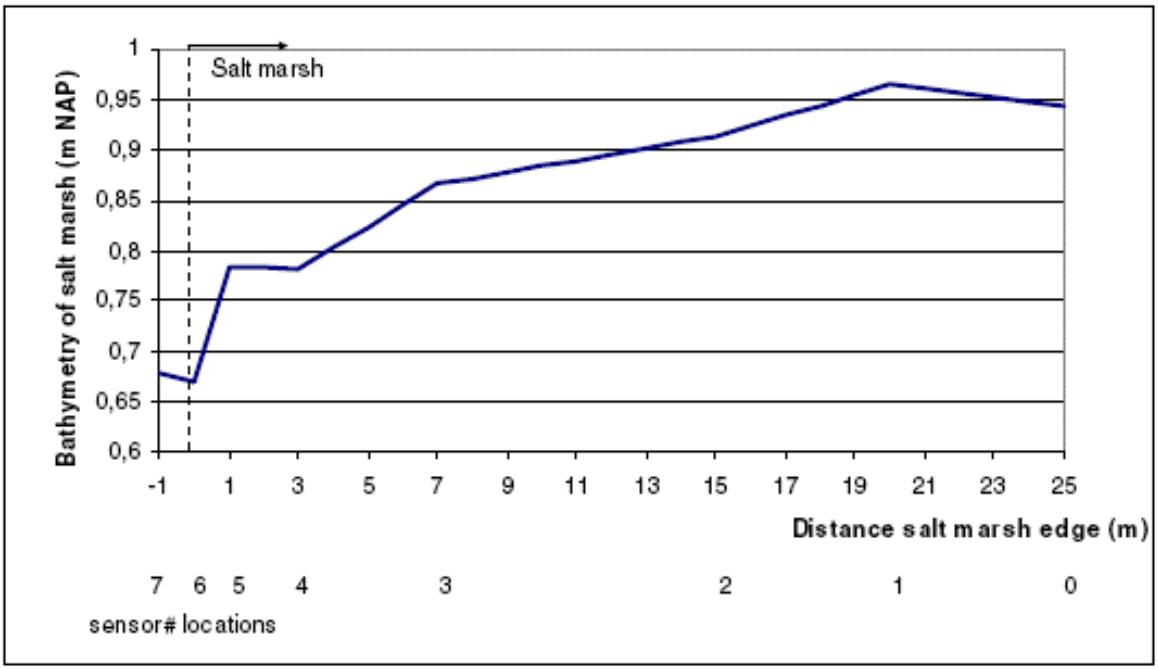


Figure 28: Bathymetry of the transect at the Paulina Marsh

Furthermore the vegetation on the Paulina Marsh was monitored. The dominant vegetation present on this marsh transect is *Spartina anglica*, a rather stiff species of halophytic vegetation. The results of the monitoring are given in Table 6.

Location	Plant height (cm)	Stem diameter (mm)	Stem density (m^{-2})
P0	41,75	4,3	872
P1	29,75	3,53	796
P2	38,28	3,9	620
P3	33,57	2,89	1476
P4	36,29	3,85	1308
P5	30,68	3,75	1704

Table 6: Plant characteristics of Spartina Anglica vegetation at Paulina schor.
From: WL|Delft Hydraulics (2003)

The wave conditions during the measurements were very moderate, with incoming wave heights most of the time below 10 centimetres.
The results of the wave measurements done at August 10th are given in Table 7.

Time:	Hs (cm)	Tp (s)	Water level (m)
16:30	6.79	6.4	2.57
17:15	6.53	3.56	2.19
18:00	5.88	2.13	1.81
18:30	7.85	2.29	1.47
18:45	8.56	2.29	1.28

Table 7: Wave measurements used in SWAN model

7.2 Model results

7.2.1 Homogeneous vegetation

Because the wave and bathymetry data are available over a linear transect of the Paulina Marsh, the model results will only be interpreted 1D over this transect line. A rectangular 2D grid was used to prevent interference of the model edges with the results (see Appendix B). The depth contours are taken constant over the grid width. The model setup that was used in the Paulina Marsh case is given in Figure 29, the grid cell spacing was set at 1m in x-direction and 2m in y-direction (50 by 50 cells).

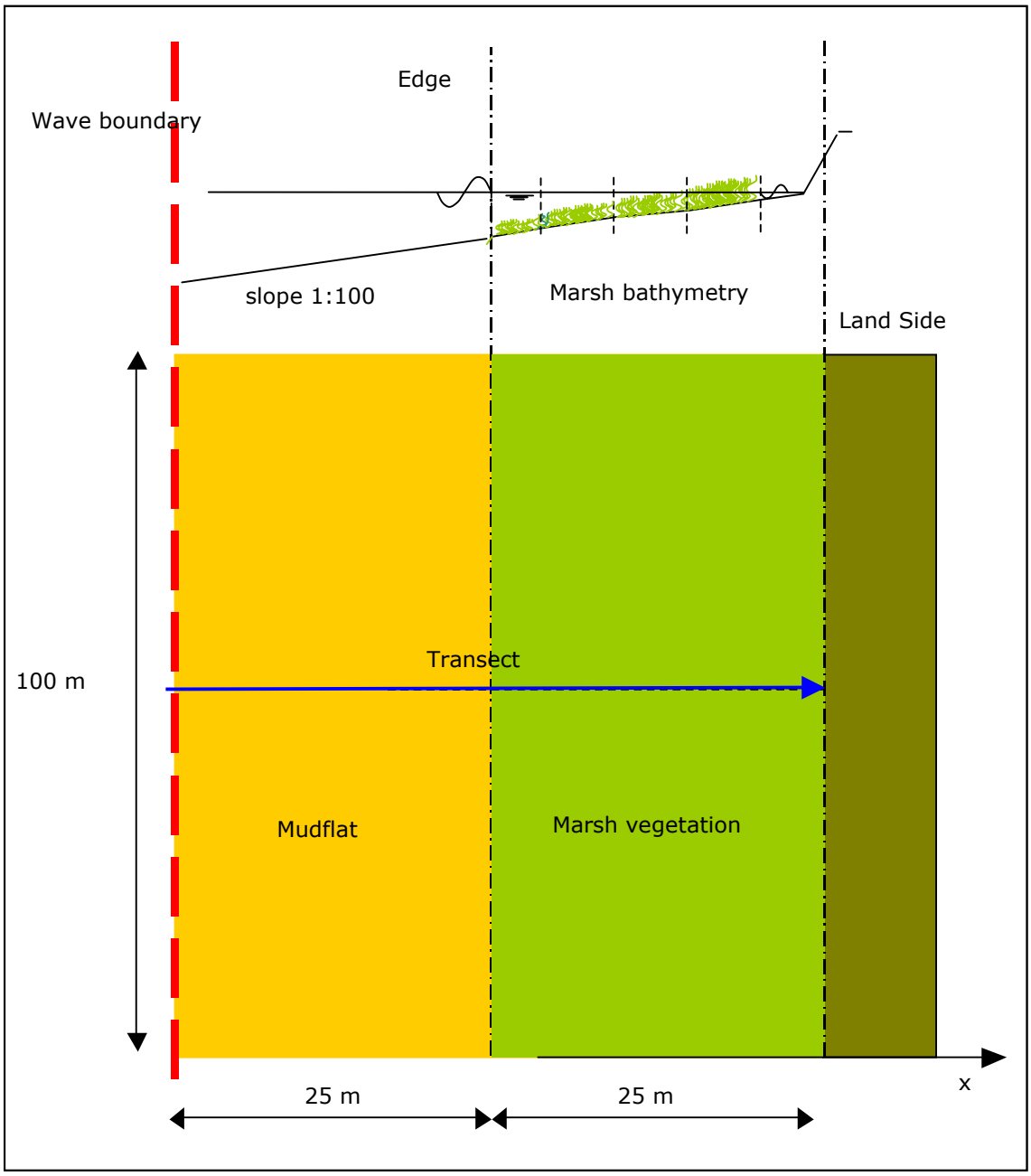


Figure 29: Model setup Paulina Marsh

The direction of the incoming waves was taken perpendicular to the marsh edge, as was the case when the measurements were done. The vegetation was considered homogeneous with the

Density: N = 1200 stems/m2
diameter: bv = 0.00375 m
mean vegetation height: αh of 0.4 m.

following characteristics, resulting in Figure 30.

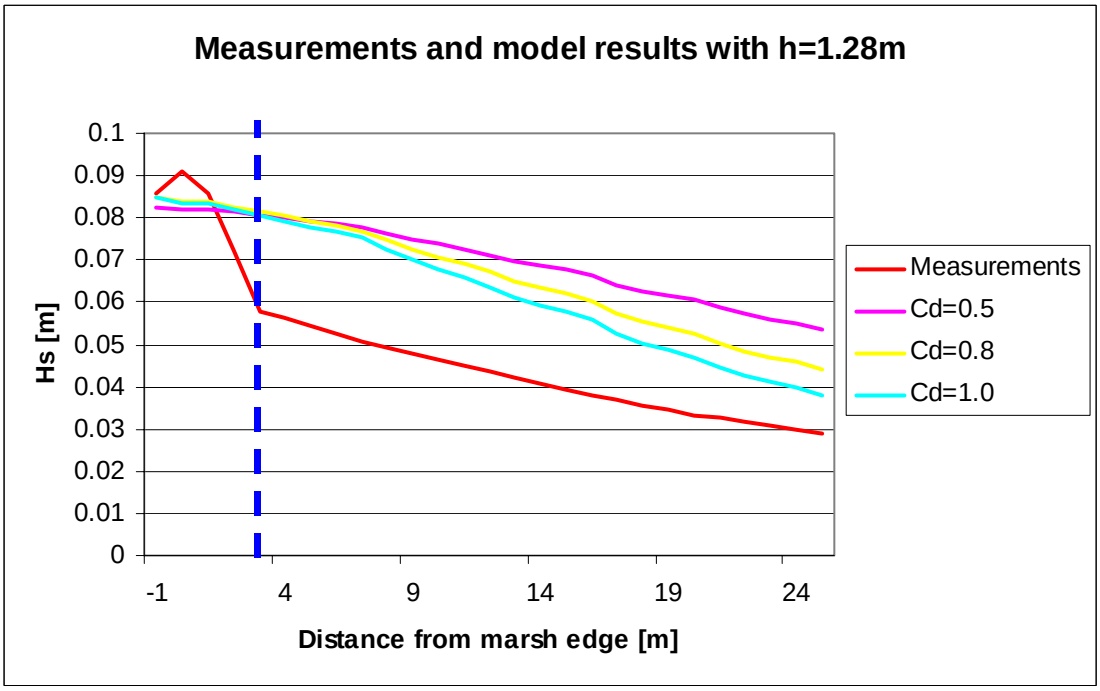


Figure 30: First results Paulina Marsh

The difference between the measurements and the model results is due to the influence of the marsh edge. Clearly the influence of the presence of a cliff at the marsh edge influences the wave propagation the first 4 meters. These edge influences are not taken into account in the model, resulting in an invalid representation of the real situation. A new wave boundary was set at x=3m to exclude these marsh edge effects. Now a good comparison can be made between the measured and the modelled wave transmission (figure 31 and 32). More model results can be found in Appendix H.

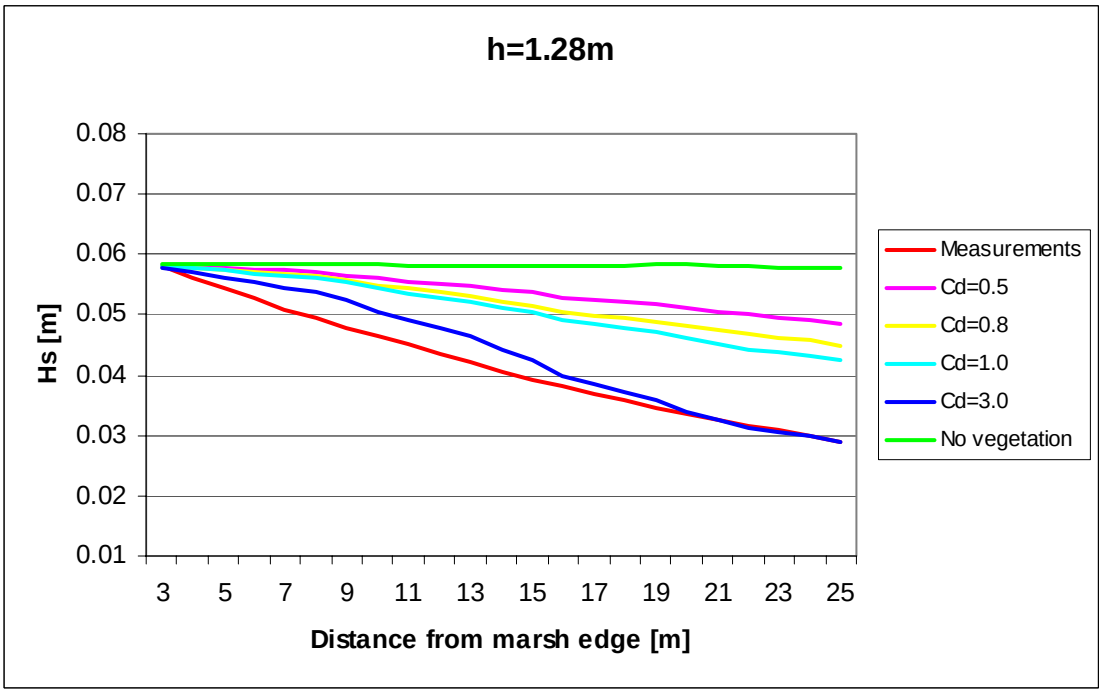


Figure 31: Wave damping over Paulina Marsh with h=1.28 m

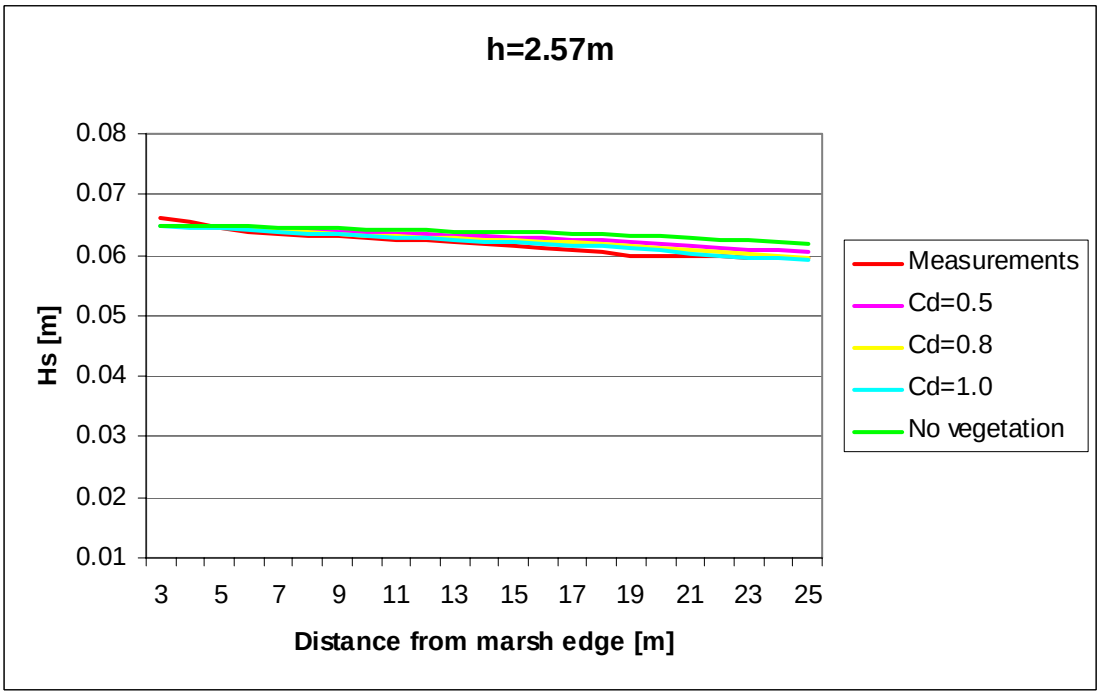


Figure 32: Wave damping over Paulina Marsh with h=2.57 m

It is clear that the influence of vegetation on waves diminishes as the relative vegetation height decreases. It can be seen that for the same wave conditions a lower water level results into more wave damping than in case of a higher water level and that at some point the waves are hardly influenced by the vegetation (see
Figure *32*).

In Figure 33 the drag coefficient, that was calibrated to fit the measurement results for each water level, are presented. This figure shows a decrease of the drag coefficient to zero for an ever-increasing water level.

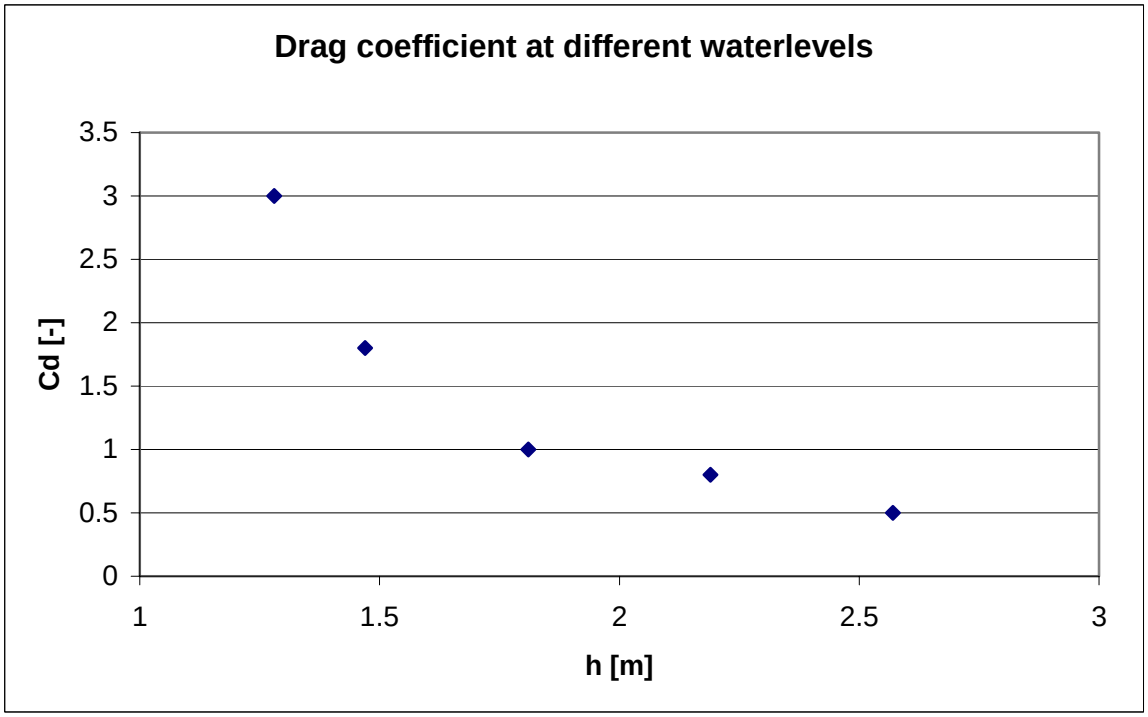


Figure 33: Calibrated drag coefficient at Paulina Marsh

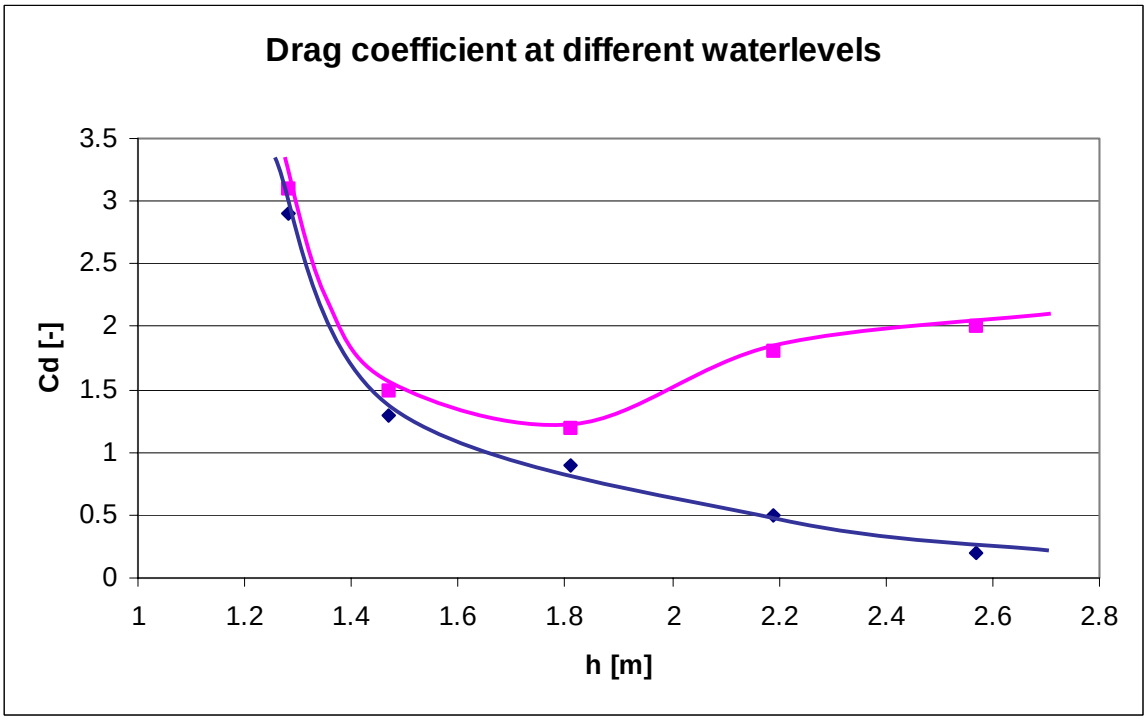


Figure 34: Drag coefficient boundaries

Figure 33 shows the best matching drag coefficient values. In figure 34 the upper and lower boundaries of the drag coefficient are given. In the area between the lines the drag coefficient values fulfil the amount of wave attenuation that was measured. It is seen that for a large relative

vegetation height (hence a low water level) the upper and lower boundaries approach each other and at some point might coincide. When the relative vegetation height decreases, the influence of the vegetation on waves diminishes and for various values of the drag coefficient the model matches the measured situation. This means that the vegetation hardly influences the waves.

What needs to be realized is that the calibrated drag coefficient is not the only uncertainty in the model. A mistake is being made by the averaging of the vegetation characteristics per zone. In reality, one square meter of marsh contains many different plants with different characteristics.

7.2.2 Horizontal variation of vegetation

As was mentioned in chapter 2 and Appendix A, a marsh is typically zoned. In each zone a different dominating plant species can thrive with different densities, diameters and heights. Therefore the amount of wave attenuation is different in each zone. At the Paulina Marsh the vegetation was intensively monitored and the marsh was roughly divided into 5 areas or zones, indicated A to E in Figure 35, with characteristics as presented in Table 8

location	transect length	Plant height (m)	Diameter (m)	Density (m-2)
A	4	0.36	0.0039	834
B	4	0.34	0.0037	708
C	8	0.36	0.0034	1048
D	5	0.35	0.0032	1392
E	5	0.33	0.0037	1506

Table 8: Modeled case

The situation with a water level of 1.28m was modelled for different values of the bulk drag coefficient. This results in the green line in Figure 36 for a drag coefficient of Cd = 3.0. Some differences are visible, in the zoned situation the wave height is damped more when the wave approaches the more dense zones.

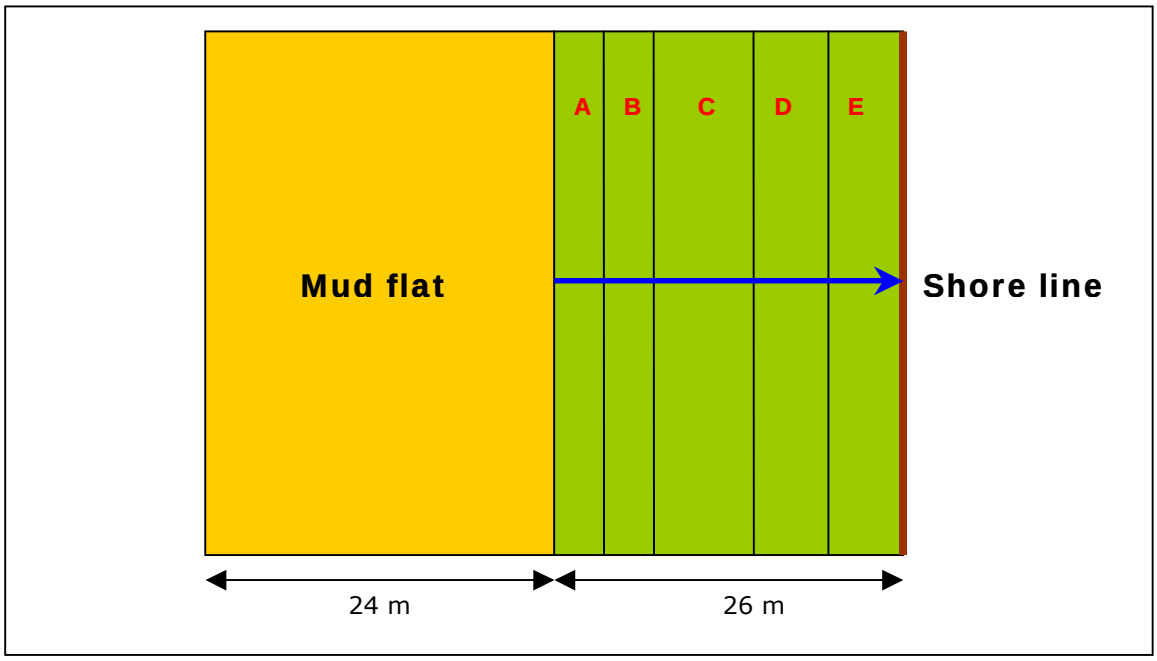


Figure 35: Modelled situation

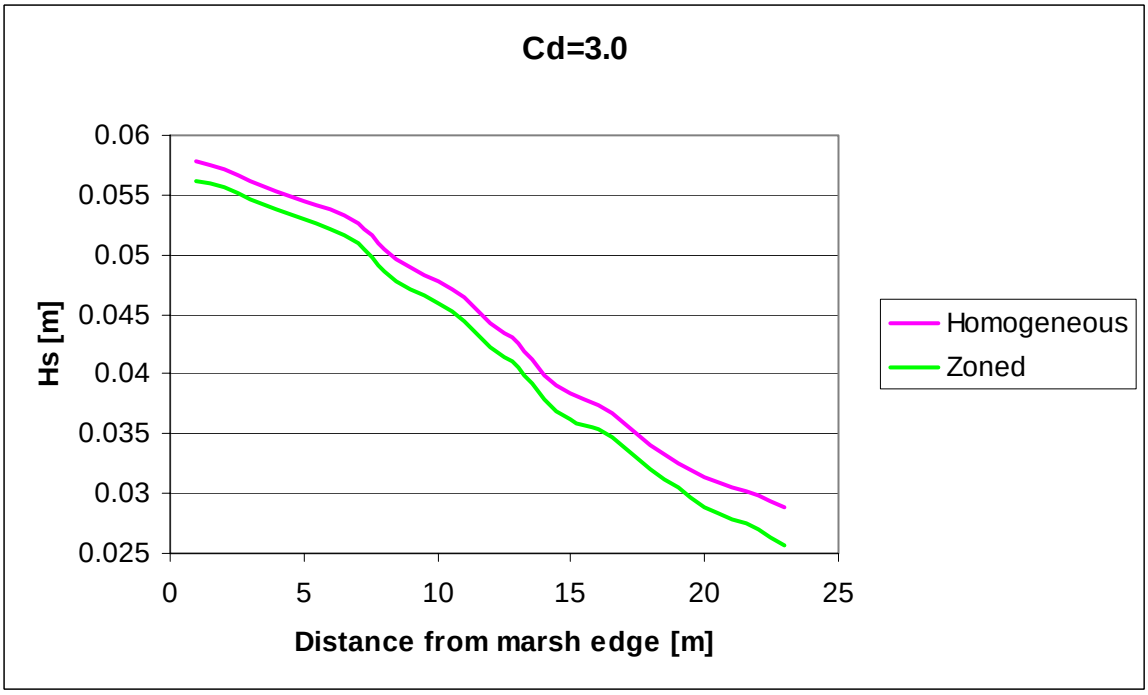


Figure 36: Wave attenuation over zoned and homogeneous vegetation at Paulina Marsh

The waves present at the Paulina Marsh during the measurement campaign were rather low, with wave heights most of the time below 10 cm. To give a better impression on the effect of horizontal zoning of vegetation in the model, a hypothetical marsh situation with the same bathymetry as the Paulina Marsh was modelled with a more pronounced zoning (Table 9), a significant wave height of 0.1 meter and a peak period of 4.0s. The wave transmission over the zoned vegetation was plotted against a situation with homogeneous vegetation with averaged vegetation characteristics of the zoned vegetation (table 10). The water level was set at 1.5 meter in both cases.

	Distance from marsh edge				
	0-5m	5-10m	10-25m	25-35m	35-50m
Density N [m^{-2}]	0	700	1000	1200	1500
Diameter bv [m]	0	0.003	0.005	0.005	0.008
vegetation height [m]	0	0.3	0.39	0.45	0.45
Drag coefficient Cd [-]	0	1	1	1	1

Table 9: Zoned situation

	Distance from marsh edge	
	0-5m	5-50m
Density N [m^{-2}]	0	1180
Diameter bv [m]	0	0.0058
vegetation height [m]	0	0.41
Drag coefficient Cd [-]	0	1

Table 10: Homogeneous vegetation (averaged values of table 9)

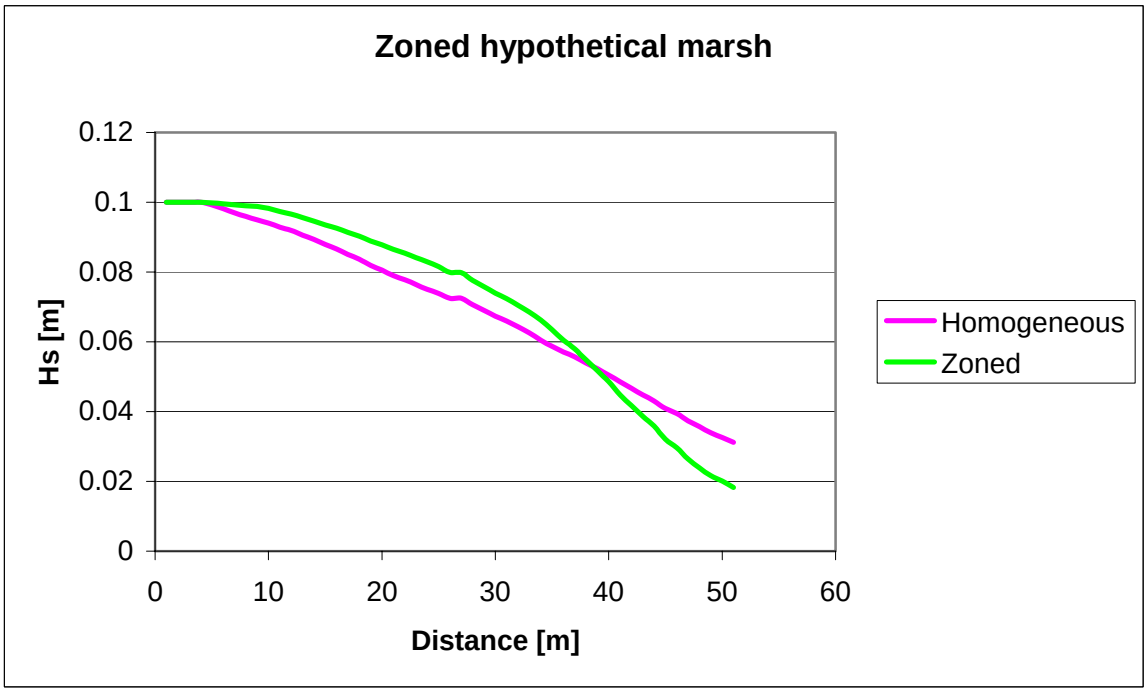


Figure 37: Wave attenuation over zoned and homogeneous vegetation at hypothetical marsh

In the zoned situation eventually more damping is observed. When waves arrive at the pioneer zone, the highest waves are first reduced in height. When the waves approach the coastline, the vegetation gets longer, thicker and denser, whereas the waves get shorter and lower. Therefore shorter waves can still be attenuated further down the marsh. It looks as if, with the zoning of the vegetation, nature has found the most effective vegetation configuration to attenuate waves.

8. Wave induced setup and secondary flows

Gradients in radiation stress that are a result of non-uniformities in the wave motion can induce both a rise in water level and currents in the water wherein the wave motion takes place. Without external forces (viscous damping, bottom shear stress), the sum of the radiation stress and the hydrostatic pressure force is constant as the waves go from deep to shallow water. When waves approach in shallow water, wave radiation stresses decrease due to energy dissipation induced by bottom friction and breaking. This decrease in radiation stress needs to be compensated by an increase in hydrostatic pressure force (conservation of momentum), resulting in a rise in water level towards the shoreline, shown in Figure 38.

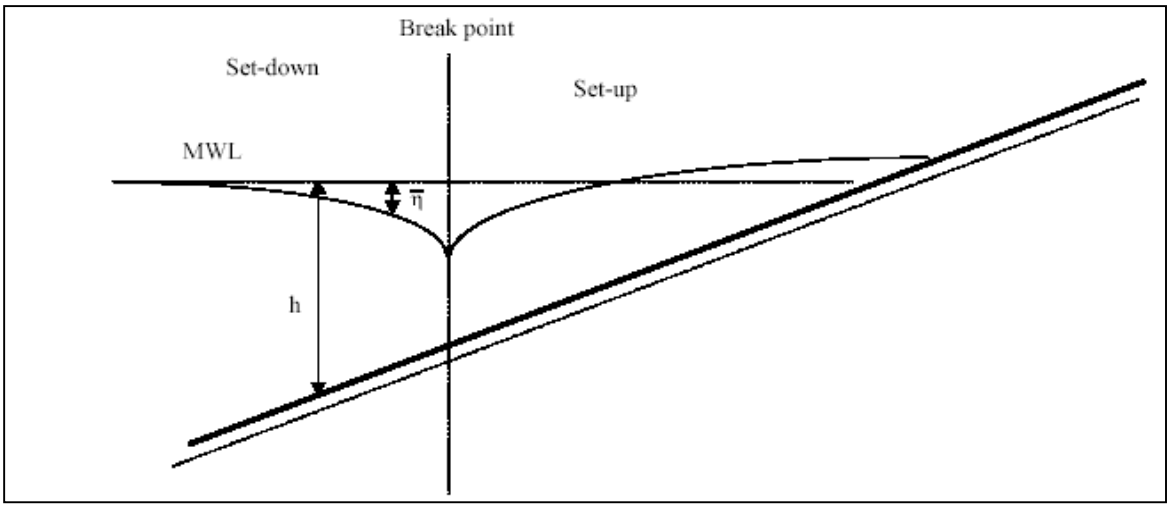


Figure 38: Schematization of wave set down and setup

In the area before the breaker zone wave energy dissipation can be neglected, therefore conservation of wave energy can be considered. When waves approach the breaker zone, on a sloping bottom, wave celerity decreases due to a decrease in water depth. Conservation of energy implies that a decrease in wave celerity causes an increase in wave radiation stress. Analogue to the situation described behind the breaker zone, an increase in radiation stress needs to be compensated by a decrease in pressure gradients (conservation of momentum), resulting in a decrease in water level (set down), see Figure 38.
When vegetation is present, extra energy dissipation due to wave- vegetation interaction causes larger gradients in radiation stress, resulting in wave setup. In patchy vegetation this can lead to a difference in setup between vegetated and non-vegetated areas. These setup differences can result in secondary flows.
To visualize this, two cases of patchy vegetation were modelled (see Figure 39). For both a grid of 125 by 500 meters was used, with a homogenous vegetation patch with characteristics as presented in Table 11.

Vegetation characteristics				Wave characteristics		Water level
b_v (m)	N (m^{-2})	Cd (-)	h_{veg} (m)	H_s (m)	T_p (s)	h (s)
0.004	1000	1	1.5	0.5	6.0	2

Table 11: SWAN model input

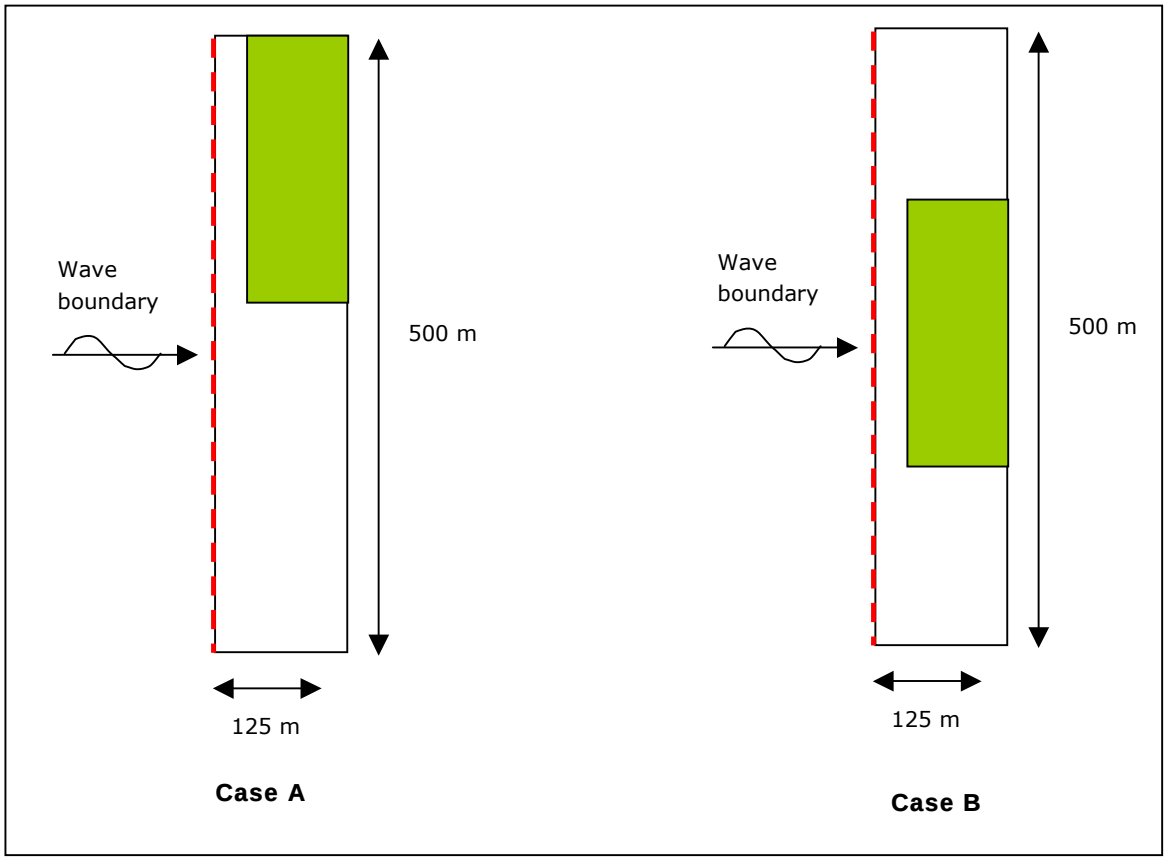


Figure 39: Model layout for wave setup cases

Case B will be studied in this section, for more results on case A see appendix H. As can be seen in

Figure 40 the wave attenuation in the vegetation causes wave setup in the vegetation and a small set down in front of the vegetation. Due to the setup differences, currents can originate as water will flow "downhill". In this case this results in a current out of the vegetation, as shown in figure 40. Although beyond the scope of this study, the impacts of these wave setup induced currents are thought to be of significant importance for the sediment transport in and out of the vegetation. Several dynamic processes as progression or degradation of a salt marsh and sediment accumulation in vegetation could be explained with this phenomenon.

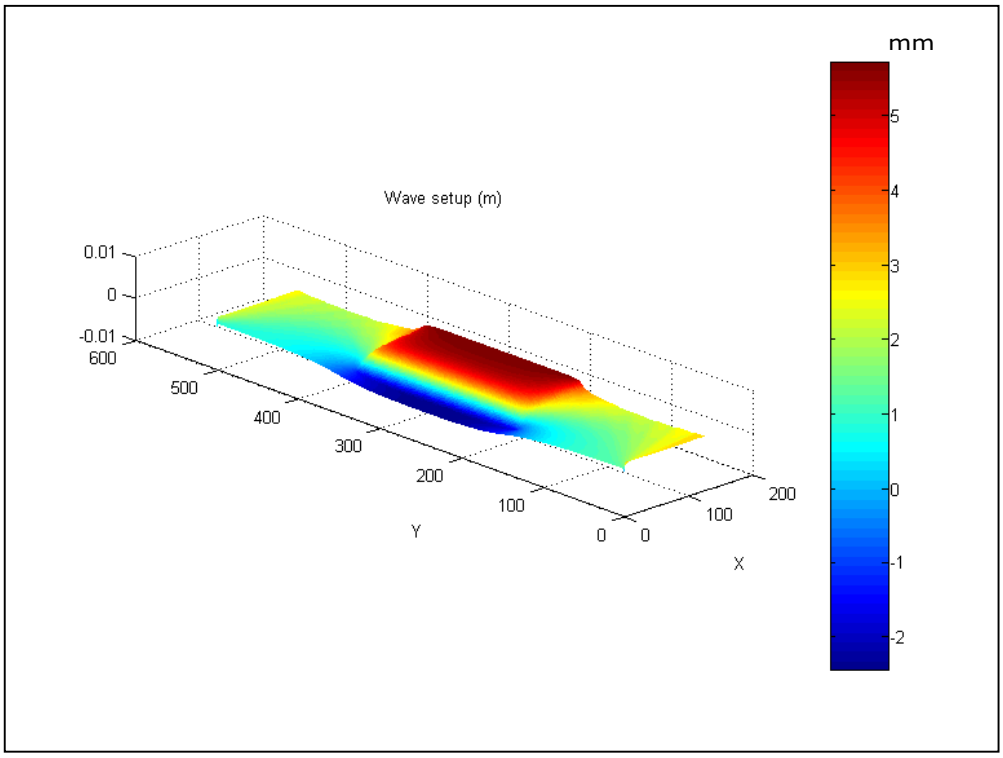


Figure 40: Wave setup in case B.

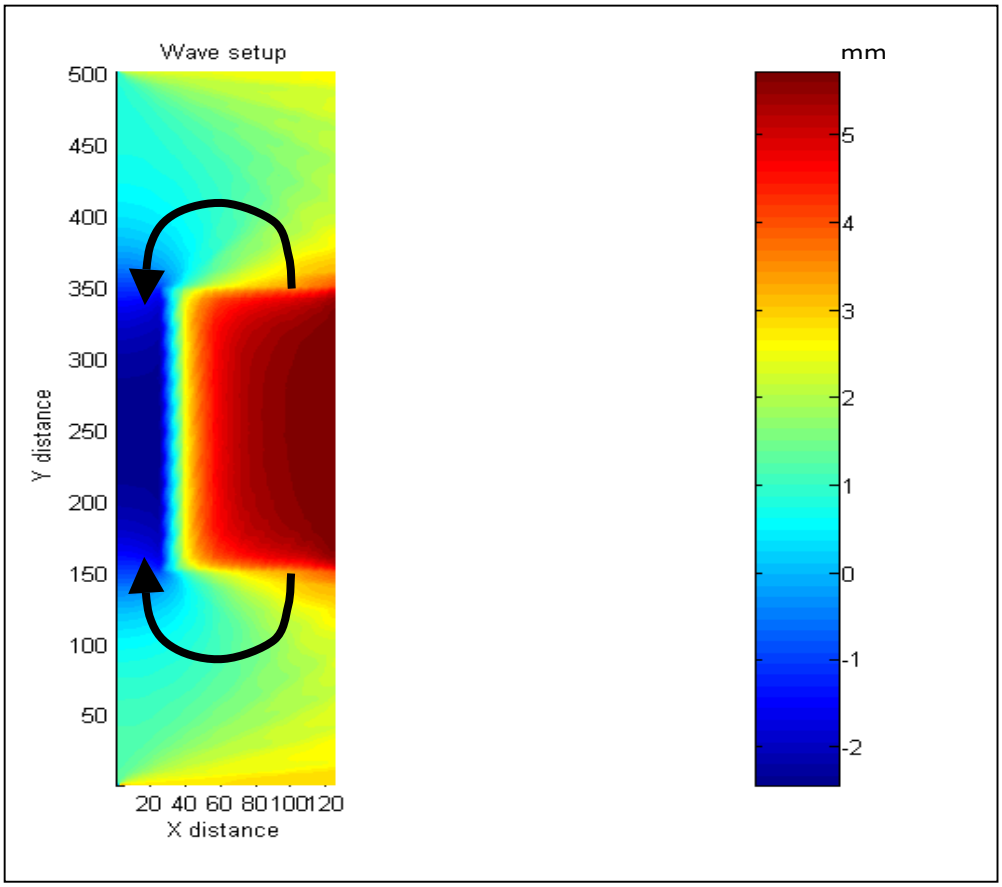


Figure 41: Top view wave setup and possible setup induced flow

9. Conclusions and recommendations

9.1 Conclusions

In this section the conclusions that were drawn throughout the research are stated in chronologic order, followed by the general conclusion on the fulfilment of the objective that was stated in section 1.2.2.

- The best analytical approximation of wave attenuation in vegetation, and the most suitable to implement in SWAN, was found to be the Dalrymple formulation.
- This formulation is based on modelling vegetation as vertical cylinders. By varying the drag coefficient, vegetation density, height and diameter different types of stiff and flexible vegetation fields can be modelled.
- It was found valid to vertically subdivide the vegetation into segments, and to add up the energy dissipation per segment to form the total amount of energy dissipation over the plant height. This was implemented in the SWAN model; the result was an adapted SWAN model in which vegetation can be horizontally and vertically varied.
- The drag coefficient C_d is the only parameter in the formulation that cannot be determined directly by measurements; hence it needs to be calibrated on physical model tests or field measurements.
- The drag coefficient in oscillating flow turned out not have a constant value, but to be dependent on the Reynolds number and hence the flow regime. The flow regime for waves through a vegetation field is determined by both wave and vegetation characteristics.
- The dependency of the drag coefficient on wave characteristics was determined by the horizontal orbital velocity and the peak period, and could best be described by the relation between the drag coefficient and the Keulegan-Carpenter number.
- The stem configuration, stem diameter, relative vegetation height, and relative spacing determine the dependency of the drag coefficient on vegetation characteristics. In sparse vegetation, the drag coefficient approaches the value for flow around one cylinder, with increasing density the drag coefficient decreases due to wake interference and sheltering.
- A number of processes that are not accounted for in the Dalrymple formulation are discounted in the drag coefficient. Therefore it is not physically correct to refer to the C_d that is used in the model, as the drag coefficient.
- A mistake is being made by the averaging of the vegetation characteristics per zone. In reality, one square meter of marsh contains many different plants with different characteristics. This deviance is also accounted for in the drag coefficient.
- The adapted SWAN model was validated on flume test results (Mendez and Losada *2004*). The model results and the physical model tests matched; therefore the implementation was found successful.
- A sensitivity analysis showed the validity of the expected characteristic relations between the amount of wave damping and the varying vegetation and wave parameters. However the dependency of the drag coefficient on these parameters was not taken into account.
- The model was applied on measurements done at the Paulina Marsh, a range of the drag coefficient between 0.5 and 3.0 was found.
- Horizontal zonation of vegetation resulted into more wave damping.
- With the adjusted SWAN model, differences in wave setup between areas with and without vegetation were detected.

The objective that was formulated at the start of this research was:

> The objective of this thesis is to make SWAN suitable to model situations with vegetated foreshores. The model has to be applicable on all types of halophytic vegetation.

General conclusion:

> The implementation of vegetation in SWAN was found successful for all types of vegetation by varying the value of the drag coefficient. However, due to the dependency of the drag coefficient on wave and vegetation characteristics, the model can only be applied on specific situations where wave and vegetation measurements have been taken.

9.2 Recommendations

From previously stated conclusions, the following recommendations are done:

- More field measurements are required at foreshores with different types of vegetation (f.i. mangroves, reed) in order to determine if the model is really suitable to model wave attenuation over any type of vegetation.
- More research needs to be done on the dependency of the drag coefficient on wave and vegetation characteristics. When more is known about these relations, a first prediction can be made on the value of the drag coefficient in a specific situation. The following relations should be examined:

  - The relation between the Keulegan-Carpenter number and the drag coefficient in oscillating flow should be determined for different situations. These relations can be used to obtain a good first estimate on the value of the drag coefficient in the field. An elaboration on this recommendation of a physical model test to obtain this relation is given in section 9.3.

  - More needs to be known about the processes that take place inside the vegetation field in order to describe the processes that determine the value of the drag coefficient.

  - An inventory should be made on the processes that are not accounted for in the Dalrymple formulation. The attribution of these processes to the wave attenuation should be known in order to filter any non-drag related phenomena out of the drag coefficient. In the Dalrymple formulation this means replacing the coefficient $\tilde{C}_d$ by (C_d +λ) in which C_d is the real drag coefficient and λ contains all non-drag related influences that were included in $\tilde{C}_d$.

- The adjusted SWAN model with vegetation implementation should be combined with Delft3dFLOW in order to determine the influence of flow on waves and vice versa in vegetated areas.
- Secondary flows due to setup differences in vegetation fields can then be visualized in Delft3dFLOW and morphological computations could be done in order to determine if sediment is imported or exported in a patchy vegetation field.

9.3 Recommended flume experiments

In a wave flume physical model tests should be performed with homogeneous (artificial) vegetation.
Tests should be performed with constant conditions (water level, vegetation characteristics), only varying the wave conditions. The amount of wave damping can be measured and the drag coefficient can be computed.
When repeated for different water levels, a relation between the drag coefficient and the Keulegan-Carpenter number (wave conditions) can be obtained.

These experiments can be repeated for different combinations of vegetation density, diameter and relative spacing between the stems.
With these results it could be examined if an empirical relation can be found between the drag coefficient and the vegetation characteristics for given wave conditions.

List of references

- Armstrong, W., Wright, E.J., Lythhe, S., Gaynard, J.T. (1985). Plant zonation and the effects of the spring-neap tidal cycle on soil aeration in a Humber salt marsh. Journal of Ecology 73, pp. 323-329.
- Asano, T.; Deguchi, H.; Kobayashi, N., (1993). Interaction between water waves and vegetation. In Edge, B.L. (Ed.), Proceedings of the Twenty-Third Coastal Engineering Conference. Am. Soc. of Civil Engineering., New York, pp. 2710-2723
- Baptist,M.J. (2005), Modelling floodplain biogeomorphology. Phd. thesis Delft University of Technology.
- Battjes, J.A. (2001): Short Waves. Lecture notes for the course CT4320, Faculty of Civil Engineering, Delft University of Technology.
- Booij, N., R.C. Ris and L.H. Holthuijsen, (1999), A third-generation wave model for coastal regions, Part I, Model description and validation, J.Geoph.Research, 104, C4, 7649-7666
- Booij, N., Haagsma, IJ.G., Kieftenburg, A.T.M.M., Ris, R.C., van der Westhuizen, A.J., Zijlema, M. (2004), SWAN user manual, Cycle III version 40.41.
- Booij, R. (1992), Turbulentie in de waterloopkunde, college ct 5312 (in dutch). Delft University of Technology.
- Boorman, L.A. (1999), Salt marshes-present function and future change. Mangroves and Salt Marshes 3, pp. 227-241.
- Burger, B. (2005), Wave attenuation in Mangrove vegetation. M.Sc. thesis Delft University of Technology.
- Chapman, V.J. (1976). Coastal vegetation. University of Auckland. Oxford Pergamon 1976
- Cooper, A. (1982). The effects of salinity and waterlogging on the growth and cation uptake of salt marsh plants. The new Phytologist 90, pp. 263-275.
- Dalrymple, R.A.; Kirby, J.T., Hwang, P.A. (1984). Wave diffraction due to areas of energy dissipation *Journal of Waterway, Port, Coastal and Engineering*, 10, (1), 67-69
- Dijkema, K.S. (1987), Geography of salt marshes in Europe. Zeitschrift für Geomorphologie, 31/4, pp. 489-499
- Dijkema, K.S., Bossinade, J.H., Bouwsema, P., De Glopper, R.J. (1990), Salt marshes in the Netherlands Wadden Sea: rising high tide levels and accretion enhancements. In: J.J. Beukema, W.J. Wolff, J.J.W.M. Brouns, eds. Expected effects of climatic change on marine coastal ecosystems. Dordrecht, Kluwer, pp. 173-188
- Elwany, M.H.S.; O'Reily, W.C.; Guza, R.T.; Flick, R.E..the Joint North Sea Wave Project (JONSWAP), Dtsch. Hydrogr. Z. Suppl., 12, A8
- Elwany, M.H.S.; O'Reily, W.C.; Guza, R.T.; Flick, R.E. (1995). Effects of Southern California kelp beds on waves. Journal of waterway, port, coastal and ocean engineering, 121/2, 143-150
- Erchinger, H.F. (1985), Dünen, Watt und Salzwiesen. Der Niedersachsische Minister für Ernährung, Landwirtschaft und Forsten, pp. 1-59.
- Hasselmann, K., T.P. Barnett, E. Bouws, H. Carlson, D.E. Cartwright, K. Enke, J.A. Ewing, H. Gienapp, D.E. Hasselmann, P. Kruseman, A. Meerburg, P. Müller, D.J. Olbers, K. Richter, W. Sell and H. Walden, 1973: Measurements of wind-wave growth and swell decay during the Joint North Sea Wave Project (JONSWAP), *Dtsch. Hydrogr. Z*. Suppl., 12, A8
- H. Houwing, E.J. et al (1995), Salt marshes and sea level rise: plant dynamics in relation to accretion enhancement techniques. IMAU-report R95-27.
- Heideman, J.C. and Sarpkaya, T.(1985): Hydrodynamic forces on Dense Arrays of Cylinders. 17th annual Offshore technology conference Houston, Texas.

- Huiskens, A.H.L. (1990), Possible effects of sea-level changes on salt marsh vegetation. In: J.J. Beukema, W.J. Wolff, J.J.W.M. Brouns, eds. Expected effects of climatic change on marine coastal ecosystems. Dordrecht, Kluwer, pp. 167-172.
- Janssen-Stelder, B.M. (2000). A synthesis of salt marsh development along the main land coast of the Dutch Wadden Sea. PhD thesis, University of Utrecht.
- Komen, G.J., Cavaleri, L., Donelan, M., Hasselmann, K., Hasselmann, S. and P.A.E.M. Janssen, 1994: Dynamics and Modelling of Ocean Waves, Cambridge University Press, pp. 532
- Massel S.R., Furukawa, K., Brinkman, R.M., (1999), Surface wave propagation in mangrove forests , Fluid Dynamics Research, no. 24, p. 219-249
- Mazda Y., Magi, M., Kogo, M., Hong, P.N ,(1997), Mangroves as a coastal protection from waves in the Tong King delta, Vietnam
- Mazda, Y., Wolanski, E., King, B., Sase, A., Ohtsuka, D., Magi, M.,(1997) Drag forces due to vegetation in mangrove swamps. Mangroves and salt marshes 1, pp. 199-199, 1997.
- Mendez, F.J.; Losada, I.J. (2004). An empirical model to estimate the propagation of random breaking and nonbreaking waves over vegetation fields. Coastal Engineering, 51, 103-118
- Mitsch, W.J. and Gosselink, J.G. (2000), Wetlands, John Wiley & Sons, New York,.
- Mőller, I.; Spencer, T.; French, J.R., (1996). Wind wave attenuation over saltmarsh surfaces: Preliminary results from Norfolk, England. Journal of Coastal Research, 12/4, 1009-1016
- Mőller, I.; Spencer, T; French, J.R.; Dixon, M. (1999). Wave transformation over salt marshes: A field and numerical study from North Norfolk, England. Estuarine, coastal and shelf science (1999) 49, 411-426
- Mőller, I.; Spencer, T. (2002). Wave dissipation over macro-tidal saltmarshes: Effects of marsh edge typology and vegetation change. Journal of Coastal Research, SI 36, 506-521
- Nepf, H.M. (1999): Drag, turbulence and diffusion in flow through emergent vegetation. Water recources research, VOL. 35, No.2, pp. 479-489, February 1999.
- Nixon, S.W. (1980), Between coastal salt marshes and coastal waters- a review of speculation and research on the role of salt marshes in estuarine productivity and water chemistry. In: P. Hamilton and K.B. Mc Donnald, eds., Marine Science II: Estuarine and wetland processes, pp. 437-525
- Orsen, R., Panageotou, W., Leatherman, S.P. (1985): Response of tidal salt marshes to the U.S. Atlantic and Gulf coast to rising sea level. Journal of Coastal Research 1., pp 29-37
- RIKZ (2004) Bodemdalingstudie Waddenzee 2004. Vragen en onzekerheden opnieuw beschouwd. Rapport RIKZ/2004.025
- Schiereck, G.J. (2001). Introduction to Bed, bank and shore protection. Engineering the interface of soil and water. Delft university press.
- Seymour, R.J. (1996) Discussion of "Effects of Southern California kelp beds on waves", Journal of waterway, port, coastal and ocean engineering. 122 (4), 207-208.
- Van de Koppel, J., van der Wal, D., Bakker, J.P., Herman, P.M.J. (2005): Self-Organization and Vegetation Collapse in Salt Marsh Ecosystems. The American Naturalist Vol. 165, No1
- WAMDI group, 1988: The WAM model - a third generation ocean wave prediction model, J. Phys. Oceanogr., 18, 1775-1810
- White, B.L., Nepf, H.M. (2003): Scalar transport in random cylinders at moderate Reynolds number. Journal of Fluid Mechanics vol. 487 2003, pp. 43-79.
- Whitham, G.B., 1974: Linear and nonlinear waves, Wiley, New York, 636 p.
- WL | Delft Hydraulics (1995) Golfdemping door riet. Author:Verheij, H.J.
- WL | Delft Hydraulics (2003) Wave attenuation by vegetation. Author: A. Mol. Project reference Z2837

- WL | Delft Hydraulics (2004, March). Vegetation friction factor algorithm. Authors: De Vries, M.B.; Roelvink, D.

A

p

Appendices

Appendix A: Salt marshes

A.1 Introduction

The salt marshes along the Dutch Wadden Sea are considered important nature reserve areas where plant and animal communities develop in close interaction with the hydraulic and geomorphologic processes.
In the Netherlands salt marshes can be found around the Wadden Sea coast in the north, and along the south west coast, in the province of Zeeland. The locations are indicated red in Figure 42. Before more can be said about the wave attenuating properties of salt marshes more needs to be known about the marsh shape. Because salt marshes are in a state of dynamic equilibrium with the surrounding environment, it is important to get insight into the most important processes that attribute to the altering shape of the marsh. This way, future marsh developments and the altering wave attenuating skills of the marsh vegetation can be predicted.

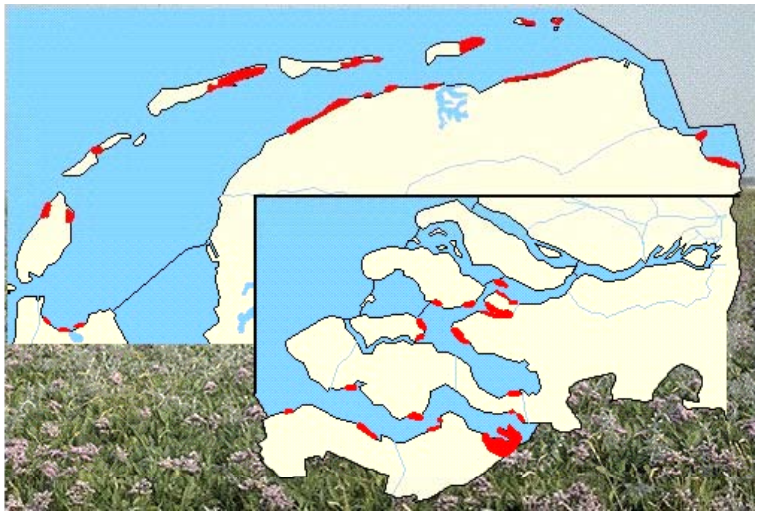


Figure 42 Overview of salt marsh locations along the Dutch coast (from:www.kweldervisie.nl)

Salt marshes are part of the inter-tidal flats and are situated at the upper part of these flats. They are bordered by mudflats at the sea side and are backed mostly by dykes or dunes. A top view of a natural salt marsh (see figure 42) reveals a typical branched pattern of channels, which are important because of their drainage function. At the seaside edge a cliff can appear, indicating the edge of the marsh.
Salt marches are coastal ecosystems that are being influenced by waves and tide. They develop favourably on gently sloping shores with little wave energy and sufficient sediment supply (e.g. Janssen-Stelder, *2000* after: Dijkema, *1987*). Therefore salt marshes can usually be found in the sheltered areas behind offshore barrier islands, behind spits, in estuaries and in protected bays with shallow water (Chapman, *1976*). Additional important factors are sufficient surface elevation, tidal amplitude and drainage to allow periods of soil aeration necessary for plant growth (Janssen-Stelder, *2000* after: Armstrong et al., *1985*). These are the perfect circumstances for pioneer vegetation to develop. The development of pioneer vegetation stimulates further sedimentation.



Figure 43: "De schorren" Marsh at Texel (from:www.waddenzee.nl)

A.2 Salt marsh vegetation

Marshes are vegetated by halophytes, vegetation that can thrive in a salt-water environment. The vegetation plays an important role in preventing erosion by armouring the soil with its roots and by absorbing wave energy.
Indirectly marshes permit the reduction of design criteria for flood defence embankments at their landward margin.

The tidal range determines the (equilibrium) height of the marshes. The vegetation on salt marshes is typically zoned, meaning different species thrive at different parts of the marsh. Physical factors affecting zonation include salt stress, availability of nutrients, and submersion stress associated with elevation. The vegetation is spread and patchy at the edges of the marsh (pioneer zone) and gets denser and more uniform when approaching land. The highest zone is home to the least salt resistant species. Typically, density and length of the plants increase with the soil elevation. Pioneer and salt marsh vegetation have an important influence on erosion and sedimentation of the Dutch salt marshes (Janssen-Stelder, *2000* after Dijkema et al., *1990*).

The zonation is modified by the process of erosion and sedimentation induced by waves and tidal movements. The seaward extent of the marsh vegetation is determined by the ability to withstand stress induced by waves and tidal inundation, the water and soil salinity and soil aeration (Janssen-Stelder, *2000* after: Cooper, *1982*). The landward extend of the vegetation is mainly affected by intra-and inter-specific competition (Janssen-Stelder, *2000* after: Huiskens, *1990*).
The salt marsh vegetation in the Wadden Sea can be divided into four zones, each with its own specific dominant vegetation, according to Erchinger (Janssen-Stelder, *2000* after: Erchinger, *1985*) (see Figure 44).

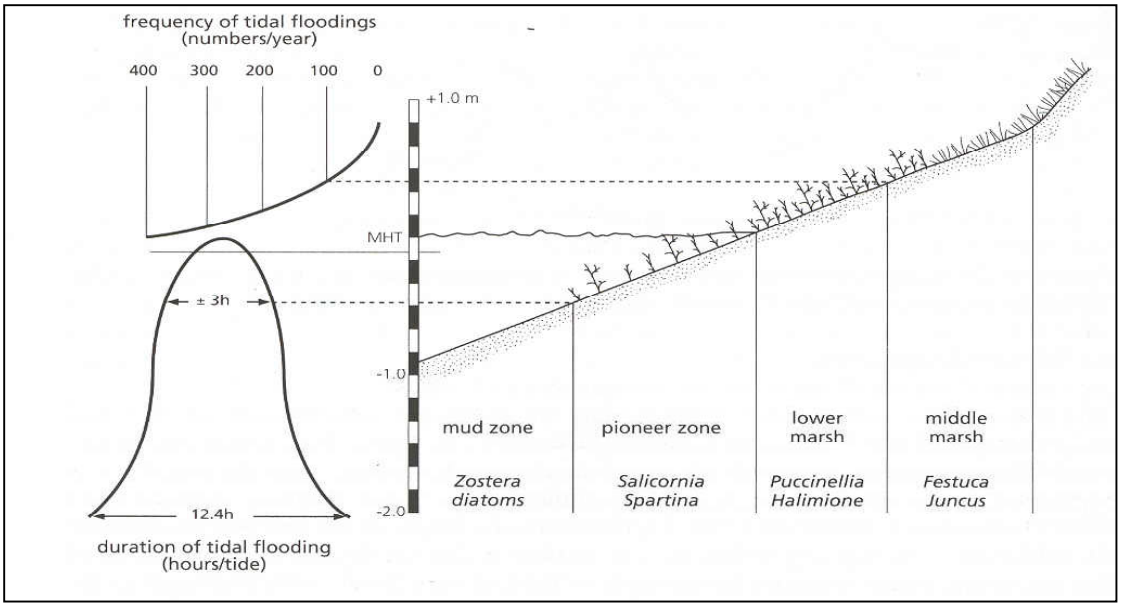


Figure 44: typical zonation of a Wadden Sea marsh after: Erchinger, (1985)

The first zone is the bare mudflat, located near the lower inter-tidal flat. The accumulation on this part depends on the local turbulence during tidal flooding.
Dominant vegetation are macrophytes such as eelgrass (*Zostera marina*). (see Appendix A.2 for pictures)
The second zone is the pioneer zone. This zone contains the pioneer vegetation and accumulation is higher than on the bare mudflat, because of a lower flow velocity due to the presence of vegetation. This zone is frequently flooded (twice a day).
In the pioneer zone, the plant growth starts approximately 40 cm below the MHWL line (Wadden sea quality status report), only the species Glasswort (*Salicornia dolichostachya*) and cordgrass (*Spartina anglica*) are able to settle and survive the prevailing extreme conditions of this zone. As soon as the conditions allow it, Sea Poa (*Puccinellia maritima*) will settle.
The third zone, the lower marsh zone, is flooded only during spring and storm tides (100-400 times per year). A dense vegetation cover is present, resulting in a high accumulation rate. This area is characterized by Sea Poa, in combination with Sea Lavender (*Limonium vulgare*). On clayish or brackish, ungrazed marshes, Sea Aster (*Aster tripolium*) can be found. On well drained higher parts of the low marsh Sea purslane (*Halimione portulacoides*) is the dominant species.
The fourth zone, the middle marsh, is only flooded during storm tides and therefore receives a rather small amount of sediment. The sediment that is supplied to this zone is completely caught by the dense vegetation. The characteristic plant species that thrive here are Creeping Fescue (*Festuca ruba*) and Mid Rush (*Juncus gerardi*), sometimes in combination with Sea wormwood (*Artemisia maritima*).

A.3 Dynamics of salt marshes

The shape and dimensions of salt marshes are continuously altering. On the one hand salt marshes can extend seaward or retreat toward the coastline, on the other hand sand settles on, or erodes from the marsh surface changing the height of the marsh. The change in shape of a salt marsh is a continuous ensemble between accretion, erosion and land subsidence and rise due to the presence of vegetation. These effects are caused by a number of processes, which will be described in the following paragraphs.
It is stated that only a short description of the dynamics of the salt marsh is given to get a better insight in the behaviour of the marsh in time. With this information, the expected future developments can be modelled, taking into account the response to sea level rise, the effect of storm surges, gas mining etc.

A.3.1 General sediment transport

The soil of a salt marsh is typically very fine-grain clay mixed with humus, carried to the estuary and coastline from freshwater rivers and land.
Tidal currents are responsible for the sediment transport between the marsh and the bordering mudflat (Janssen-Stelder, *2000* after: Houwing et al., *1995*). Waves may contribute during storm events, when sediment is being stirred up by the wave orbital movement and wave generated turbulence. The sediment is then being transported by wave induced and tidal currents. Storm events contribute to the sedimentation on the salt marsh as long as the supplied sediment is sufficient; otherwise erosion may occur (Janssen-Stelder, *2000).*

Storm events lead to large sediment transports between marshes and bordering mud flats, sometimes leading to net erosion, sometimes to net accretion of the salt marsh. During a storm, high waves can erode the transition area between mud flat and salt marsh, leading to a retreat of the salt marsh. The sediment that is being eroded can settle at the lower mud flat, flattening and lengthening the inter-tidal profile. In the mean time, erosion of the marsh allows the mudflat profile to extend further landward and again provide a flatter, wider profile and increasing wave attenuation. The retreat of the salt marsh progressively reduces the salt marsh extent. This can continue until the entire marsh has vanished and the mudflat extends to the coastline. This process of salt marsh deterioration during storms occurs in areas where salt marsh development is limited to a narrow area such as along the Wadden Sea (Janssen-Stelder, *2000*). In these areas sometimes man made constructions like brushwood groins are deployed to prevent this from happening.

In general there are three major sources supplying sediment to the marshes: sand, silt and clay particles carried landward by wave action, deposition of organic material from outside the system and in-situ deposition of organic material from salt marsh vegetation (Orson et al., *1985*).

A.3.2 Effects of vegetation

Sediment that is transported into the marsh can be trapped by the vegetation. Dense vegetation will cause a decrease in near-bed turbulence and hence stimulate accretion (Boorman, *1999*). The height of the vegetation influences the effectiveness with which the sediment is being trapped. The roots of the plants also play an important role in erosion prevention. The roots armour the soil, reducing the amount of bed erosion. The marsh vegetation can also cause land subsidence. Bed consolidation is caused by the subtraction of water from the soil by the vegetation present on the marsh (Janssen-Stelder, *2000*).

The pioneer zone is of particular significance to the development of a salt marsh.
When a positive accretion balance is maintained in this transition zone between mudflat and marsh area, there is no problem in concerning salt marsh development during sea level rise (Dijkema et al, *1990*). The transition between the bare mudflat and the vegetated marsh is characterized by an increase in shear strength. This often results into cliff formation at the transition area between the bare mudflat and the marsh. The location of the cliff depends on the amount of erosion and accretion in the pioneer zone, especially during storm surges. On the one hand erosion of the marsh edge leads to retreat of the edge. On the other hand, in front of the retreating marsh edge, new sediment will settle and hence accretion of the marsh takes place. These processes are shown in figure 45. During salt marsh development (A), the sediment layer thickens. Degeneration (B) is characterized by eroding cliffs, but re-growth occurs at the same time. Further down, pioneer marsh plants form a new sediment-catching kernel. (Van de Koppel, Herman, *2005*)

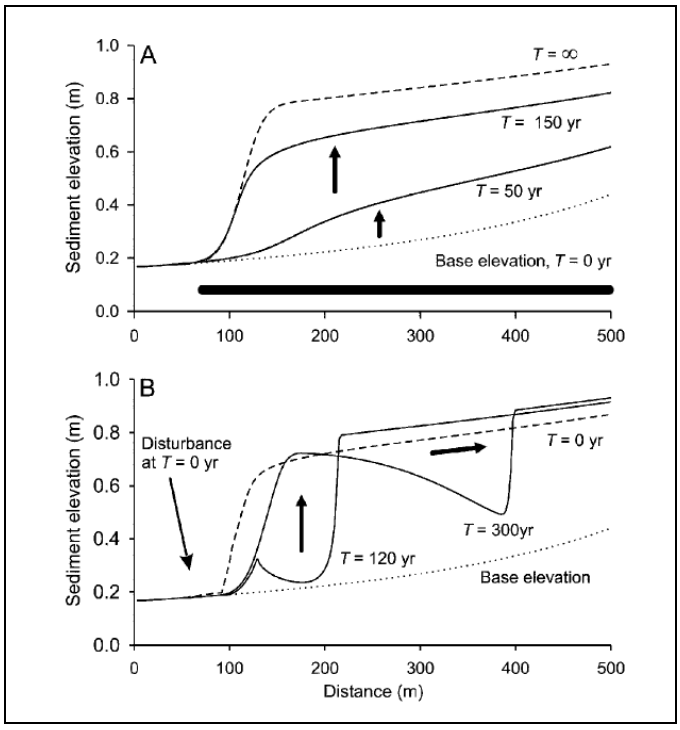


Figure 45: Salt marsh generation (A), and degeneration and re-growth (B)

A.3.3 Seasonal influences on salt marshes

In summer a thick mud layer builds up on the bare parts of the salt marsh. This sediment can be stirred up by storms and be transported further up the salt marsh. In winter, most of the vegetation will die and be washed away, and marshes lose most of their wave attenuating skills. Most severe storms occur in winter when there is minimal obstruction for waves to reach the shoreline. Therefore the situation on salt marshes in winter, during a storm at high water spring tide will be normative when determining the safety of a dike behind a salt marsh area. The remains of the vegetation will then have little influence on waves. This decrease in wave attenuation for shorter vegetation will be validated in the model.
In Figure 46 a marsh in winter and in summer are shown.

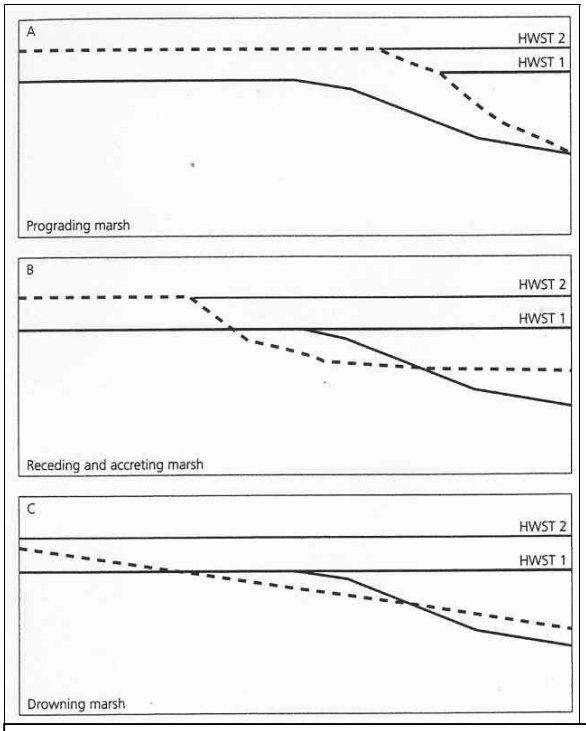


Figure 46 marsh in winter (left) and in summer (right).

A.3.4 Effects of sea level rise

An important issue these days is sea level rise as a result of a rise in mean temperature on earth. This may have consequences for the marsh ecosystem. During rapid sea level rise, sedimentation cannot keep up and salt marshes drown. A slowly rising sea level causes an increase in flooding frequency and duration of flooding, leading to an increase in sedimentation.

Orson et al. (1985) propose three general models of salt marsh response to sea level rise:



(HWST: High Water Spring Tide)

A. Propagating or advancing marsh model:
marsh can expand both laterally and vertically when accretion rates are higher than rates of coastal submergence. This situation may occur when large rivers are present supplying great amounts of sediment allowing further propagation of the marsh.

B. Receding and accreting marsh model:
The marsh may remain stable if the sediment input equals the rate of coastal submergence so that the surface elevations are maintained. The seaward edge of the marsh (pioneer zone) will erode but deposition upon the remaining marsh can keep pace with sea level rise.

C. Drowning marsh model:
The marsh system could drown if rates of coastal submergence exceed the marsh ability to accrete vertically. The salt marsh vegetation is unable to deal with the increased stress caused by the increased inundation and dies. The subsequent loss of ability to trap sediment may result in sediment loss and lowering of the marsh surface.

Figure 47: Possible responses of salt marshes to sea- level rise (Janssen-Stelder after Orson et al. 1985)

Presently, model B applies for the mainland salt marsh areas of the Dutch Wadden Sea. In general, a positive accretion balance occurs in the marsh zone itself because a dense vegetation cover stimulates sedimentation and prevents erosion. In the pioneer zone however, the vegetation cover is not so dense and is unable to decrease the wave energy sufficiently. A negative accretion balance may develop in the pioneer zone. A height deficit can develop between the marsh and the pioneer zone because of the accretion deficit of the pioneer zone. This can lead to cliff formation and receding of the salt marsh (Dijkema et al., *1995*).

A.3.5 Gas mining

The variation of the bottom level on the Wadden marsh and in the pioneer zone is on the one hand due to erosion and sedimentation, on the other hand due to gas mining (RIKZ *2004*). Rijkswaterstaat and Alterra are intensively monitoring the whole Wadden area to map bottom descent and to predict vegetation change in the future due to land subsidence. Sedimentation and erosion are also intensively monitored and the results of the bottom descent are continuously compared to the amount of erosion and sedimentation on the marsh. Since 1987 the marshes of Ameland have been monitored, both on bottom level changes and on changes in vegetation. It was found that despite the large bottom descent due to gas mining (26 cm in 2003) (RIKZ *2004*) no changes in vegetation occurred that could be related to this bottom descent. This is partly due to siltation. This rate increases when the area inundates more frequently, but also without bottom descent siltation takes place constantly. On many locations near the edge of the marsh and close to creeks, the siltation has been sufficient to completely compensate the bottom descent.
Other factors involved in sedimentation, besides vegetation and wave and tide action, include the physico-chemical deposition due to the flocculating action of sodium on suspended soil colloids and the physical effect of fresh water overlying salt water (Chapman, *1976*). These effects won't be further elaborated on in this thesis.

A.3.6 Salt marsh vegetation



Eelgrass (*Zostera marina*)



Glasswort
(*Salicornia dolichostachya*)



Cord grass (*Spartina Anglica*)



Sea pow (*Puccinellia Maritima*)



Sea Lavender
(*Limonium Vulgare*)



Sea Aster (*Aster tripolium)*



Sea purslane
(*Halimione portulacoides*)



Creeping Fescue
(*Festuca ruba*)



Mid Rush (*Juncus gerardi*)



Sea wormwood
(*Artemisia maritima*)

Appendix B. Edge influences in SWAN

A problem with 1D schematizations is that wave energy flows out via the long sides of the model. This is because SWAN does not 'feel' borders along the sides of the model. So a wave will propagate in the wave direction, but at the same time, the wave energy will spread over the side borders of the model, causing a strong decrease in wave height. Figure 48 illustrates this problem. The figure shows a wave at the boundary (left side of schematization) with wave height H_0 and wave width W_0. After some time, the wave width has increased to W_1 because of the spreading of the wave under an angle θ. The result is a decrease in wave height to H_1. The solution to this problem is to choose a large schematization width, so that $W>L$, in which L is the schematization length. In this case, the wave will still spread out over the side borders, but the middle line of the section (the measurement transect) will not have been affected by this phenomenon yet when the wave has travelled a distance L.

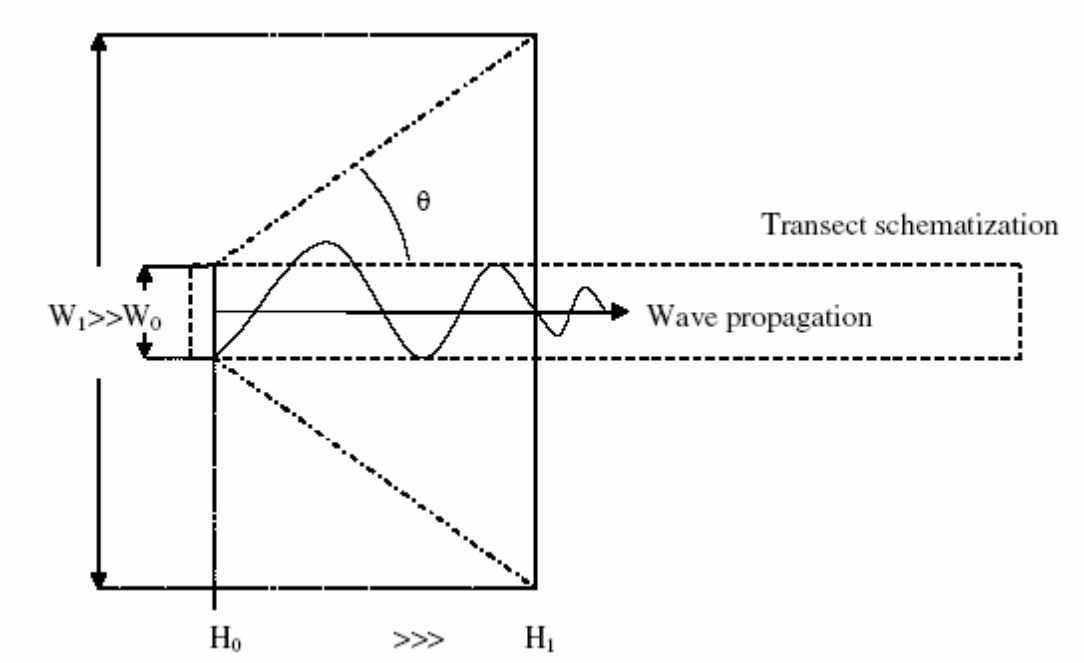
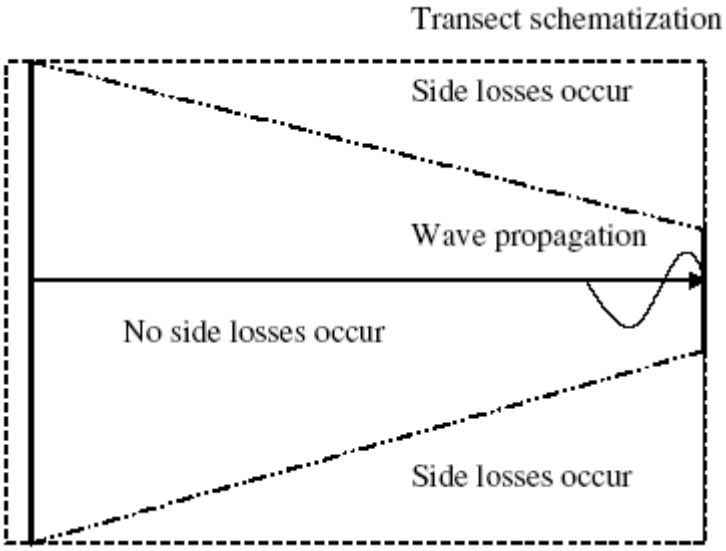


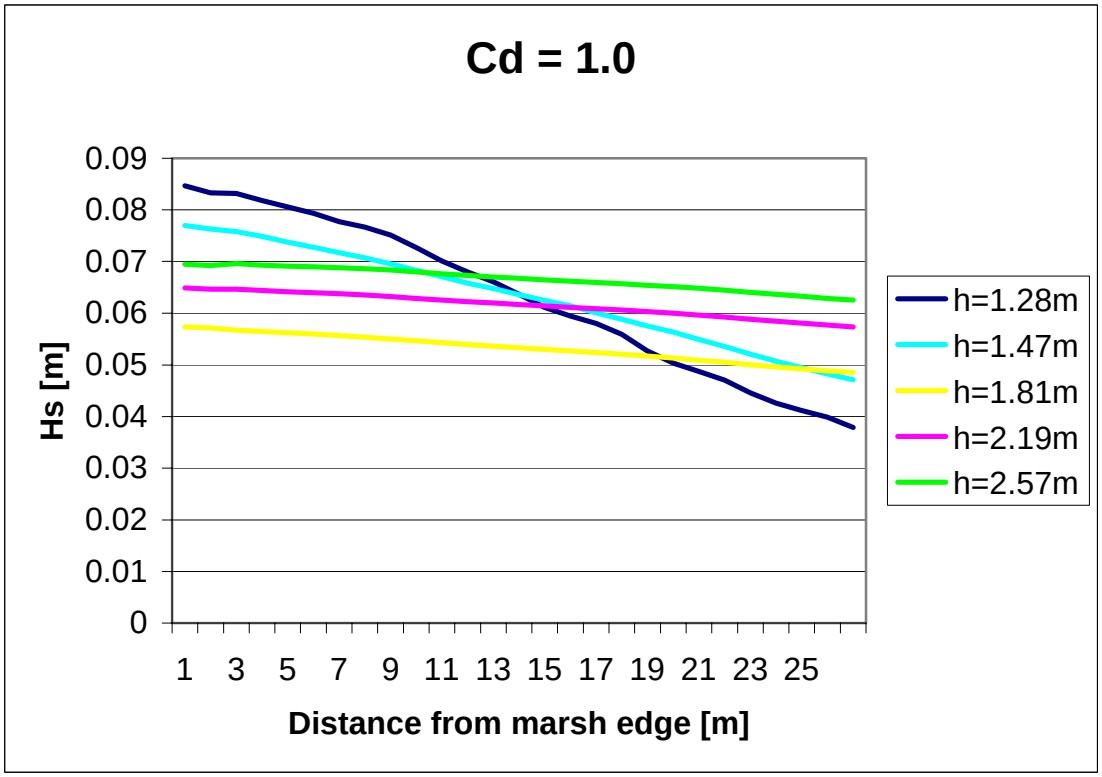
Figure 48: wave energy losses over the model edges

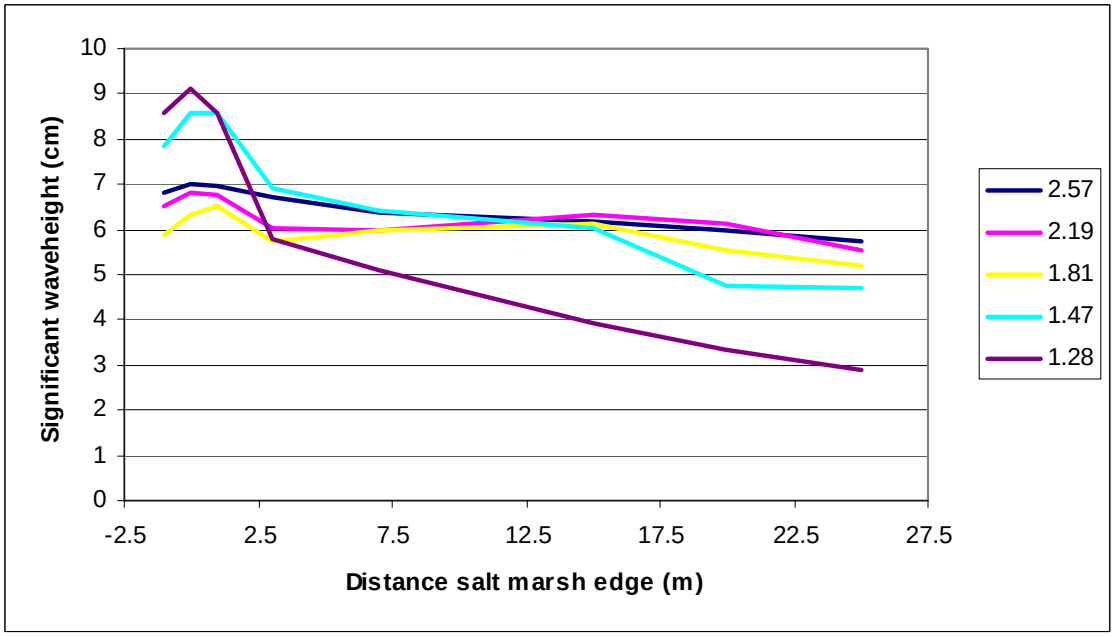
In order to make a correct model, the width of the model will have to be chosen much larger than the length. The figure shows the area where waves are affected by energy losses through the along sides and the area that is not yet affected by this energy loss.
The angle at which the side losses occur is θ = 30º. In the cases considered in this thesis the width was chosen at least twice the size of the transect length, so the results over the transect are unaffected by energy losses. Another important edge influence in SWAN is the influence of the JONSWAP spectrum on the upper wave boundary. In the model results a small discontinuity is seen that is caused by the shape of this wave spectrum.



From: WL Delft Hydraulics (2003) Author: A. Mol.

Appendix C Results of first indication Dalrymple formulation





Appendix D SWAN Source Code

D.1 General description SWAN source code

SWAN has been released under public domain (http://fluidmechanics.tudelft.nl/SWAN) and is integrated in WL | Delft Hydraulics DELFT3D modelling package (DELFT3D-WAVE module). SWAN is an open source code program; anyone may make adaptations for own use. SWAN source code is written in fixed form Fortran 90. The source code comprises different so-called subroutines. In the main program (*swanmain*) these subroutines are called upon. The most important subroutine used in this implementation is *swancom2*. This subroutine contains some dissipation formula's e.g. bottom friction, wave breaking and white capping.

D.2 Working with SWAN

All routines are compiled with a Fortran 90 compiler and linked to form the executable *swan.exe*. This executable reads an input file that contains the user-defined information. In the input file physical processes as e.g. bottom friction, white capping and breaking can be activated or deactivated, wave and wind spectra parameters as well as the desired output parameters (e.g. H_s, T_p etc.) can be defined. In the input file a reference is made to several other files. The information about the bathymetry is read from a bottom file (**.bot*), whereas for the output a file contains the output locations (**.loc file*). The output is stored in a table, spectra or block format. A computational grid can be defined in the input file or the grid can be read from an external grid (**.grd*) file.

D.3 Input of vegetation parameters

The vegetation input parameters in the model are the drag coefficient, density, diameter and vegetation height.
Three types of spatial configuration of the vegetation are possible.
Horizontally and vertically homogeneous
Horizontally variable and vertically homogeneous
Horizontally and vertically variable

This input is handled by the subroutine INPVEG

D.4 Scource code Subroutine INPVEG

```
SUBROUTINE INPVEG (ILMAX, LAYH, VEGDRGL, VEGDIL, VEGDEL, IX)

    INTEGER ILMAX
    REAL LAYH(ILMAX), VEGDRGL(ILMAX), VEGDIL(ILMAX), VEGDEL(ILMAX)


     IF (IX.LT.5) THEN

        LAYH    = (/0.2,0.2,0.1/)
          VEGDRGL = (/0.,0.,0./)
          VEGDIL  = (/0.,0.,0./)
          VEGDEL  = (/0.,0.,0./)

        ELSE

        IF (IX.GE.5 .AND. IX.LT.10) THEN

        LAYH    = (/0.1,0.1,0.1/)
          VEGDRGL = (/22.62,22.62,22.62/)
          VEGDIL  = (/0.003,0.003,0.003/)
          VEGDEL  = (/700,700,700/)

        ELSE
        IF (IX.GE.10 .AND. IX.LT.25) THEN

        LAYH    = (/0.13,0.13,0.13/)
        VEGDRGL = (/22.62,22.62,22.62/)
        VEGDIL  = (/0.005,0.005,0.005/)
          VEGDEL  = (/1000,1000,1000/)
        ELSE
        IF (IX.GE.25 .AND. IX.LT.35) THEN

        LAYH    = (/0.15,0.15,0.15/)
        VEGDRGL = (/22.62,22.62,22.62/)
        VEGDIL  = (/0.005,0.005,0.005/)
          VEGDEL  = (/1200,1200,1200/)

        ELSE
        LAYH    = (/0.15,0.15,0.15/)
          VEGDRGL = (/22.62,22.62,22.62/)
          VEGDIL  = (/0.008,0.008,0.008/)
          VEGDEL  = (/1500,1500,1500/)
     ENDIF
    ENDIF
    ENDIF
    ENDIF
    RETURN
    END
```

D.5 Vertical averaging of parameters

To obtain the contribution of each vegetation layer the input parameters are multiplied in the subroutine PARVE.

```
! d      = water depth
! Nlayer = number of layers in grid point
!
! Per layer is known:
!
! LAYH      (thickness of the layer),
! VEGDRAG   (drag coeff.),
! VEGDIA    (vegetation diameter),
! VEGDEN    (density)
!
! ********************************
!
!
!          ---------- n
!
!          ---------- 2
!           _ d
!          --|-------- 1
!            |
!          --|-------- 0
!
!
! ********************************
!
! LAY, Cd, BV, DEN are vectors with the size of the numbers of layers inputted.
! The vegetation parameters of the different layers are averaged throughout the water
colom.
! With these averaged parameters the dissipation due to vertical varying vegetation can
be ! calculated. This Subroutine checks in which layer the water level is present.
Subsequently
! the vegetation parameters up to the layer where the water level is in, are used to
calculate a ! weighed average.
! With this average the dissipation due to the vegetation can be calculated.
!
!
!IL = layer counter
!ILMAX = Number of layers
!
        SUBROUTINE PARVE (ILMAX, LAYH, VEGDRGL, VEGDIL, VEGDEL, VEGDRAG  ,
     &          VEGDIA, VEGH, VEGDEN, DEP2, LAYPART)
```

```
      USE SWCOMM3
!
          INTEGER ILMAX
          REAL LAYH(ILMAX), VEGDRGL(ILMAX), VEGDIL(ILMAX), VEGDEL(ILMAX)
          REAL VEGDRAG(MCGRD),VEGDIA(MCGRD), VEGH(MCGRD), VEGDEN(MCGRD),
     &     DEP2(MCGRD)

          INTEGER IL, IK, IM
          REAL  SUMLAYH, SUMLAYH1, SUMLAYH2, VEGDRAGAV, VEGDIAAV, VEGDENAV,
     &  LAYPART

          SUMLAYH    = 0.
          SUMLAYH1   = 0.
          SUMLAYH2   = 0.
          VEGDRAGAV  = 0.
          VEGDIAAV   = 0.
          VEGDENAV   = 0.
          LAYPART    = 0.

      DO IL = 1, ILMAX
        SUMLAYH = SUMLAYH + LAYH(IL)
      ENDDO
!
      IF (DEP2(KCGRD(1)).GT.SUMLAYH) THEN
       DO IL = 1, ILMAX
         VEGDRAGAV = VEGDRAGAV + (VEGDRGL(IL) * LAYH(IL))
           VEGDIAAV  = VEGDIAAV  + (VEGDIL(IL)  * LAYH(IL))
         VEGDENAV  = VEGDENAV  + (VEGDEL(IL)  * LAYH(IL))
           ENDDO
       VEGDRAG(KCGRD(1))  = VEGDRAGAV  / SUMLAYH
       VEGDIA(KCGRD(1))   = VEGDIAAV   / SUMLAYH
       VEGDEN(KCGRD(1))   = VEGDENAV   / SUMLAYH
         VEGH(KCGRD(1))     = SUMLAYH

      ELSE IF (DEP2(KCGRD(1)).LT.LAYH(1)) THEN
        VEGDRAG(KCGRD(1)) = VEGDRGL(1)
        VEGDIA(KCGRD(1))  = VEGDIL(1)
        VEGDEN(KCGRD(1))  = VEGDEL(1)
        VEGH(KCGRD(1))    = DEP2(KCGRD(1))

      ELSE
             DO IL = 1, ILMAX
           SUMLAYH1 = SUMLAYH1 + LAYH(IL)
           IF (DEP2(KCGRD(1)).LE.SUMLAYH1) THEN
            DO IM = 1, IL-1
```

```
          SUMLAYH2 = SUMLAYH2 + LAYH(IM)
          ENDDO
          LAYPART = DEP2(KCGRD(1)) - SUMLAYH2
          DO IK = 1, IL-1
          VEGDRAGAV = VEGDRAGAV + (VEGDRGL(IK) * LAYH(IK))
          VEGDIAAV  = VEGDIAAV  + (VEGDIL(IK)  * LAYH(IK))
          VEGDENAV  = VEGDENAV  + (VEGDEL(IK)  * LAYH(IK))
          ENDDO
           VEGDRAG(KCGRD(1)) = (LAYPART * VEGDRGL(IL) + VEGDRAGAV)
     &                 / DEP2(KCGRD(1))
            VEGDIA(KCGRD(1))  = (LAYPART * VEGDIL(IL)  + VEGDIAAV)
     &                 / DEP2(KCGRD(1))
            VEGDEN(KCGRD(1))  = (LAYPART * VEGDEL(IL)  + VEGDENAV)
     &                 / DEP2(KCGRD(1))
            VEGH(KCGRD(1)) = DEP2(KCGRD(1))
             EXIT
              END IF
               ENDDO
        ENDIF
        RETURN
        END
```

D.6 Subroutine SVEG

The actual energy dissipation of the vegetation is calculated by the subroutine SVEG.

```
!**********************************************************************
!
     SUBROUTINE SVEG (DEP2    ,AC2     ,
    &            IMATDA  ,KWAVE   ,SPCSIG  ,
    &            IDCMIN  ,IDCMAX  ,
    &            ISSTOP  ,DISSC1  ,VEGDRAG ,VEGDIA  ,
    &            VEGH    ,VEGDEN )
!
!**********************************************************************
!
     USE SWCOMM3
     USE SWCOMM4
     USE OCPCOMM4
!
!  0. Authors
!
!    40.55: Bastiaan Burger, Martijn Meijer
!
!  1. Updates
!
!    40.55, May. 05: implementation of vegetation friction formula
!
```

```
!  2. Purpose
!
!     Computation of the source terms due to vegetation friction
!
!  3. Method
!
!     The energy dissipation due to vegetation is described by a
!     Morrison type equation, modeling the plants as vertical,
!     noncompliant cylinders, neclecting swaying motions induced by
!     waves. Vegetation characteristics that are used as input are:
!     drag coefficient, vegetation height, plant density and diameter.
!
!
!     SVEGEO = (1/(2*SQRT(PI)) * RHO * VEGDRAG * VEGDEN * VEGDIA
*((KWAVE*GRAV)/2*SPCSIG)**3 * ((A + B)/C) * HRMS**3
!
!     with
!
!     HRMS = HSIG*SQRT(2)
!     A = (SINH(K*VEGH))**3

!     B    = 3*SINH(K*VEGH)
!     C = 3*K*((COSH(KD)**3)
!
!
!  4. Argument variables
!
!     SPCSIG: Relative frequencies in computational domain in sigma-space 30.72
!
      REAL    SPCSIG(MSC)                                    30.72
!
!     INTEGERS :
!     --------
!
!     IX          Counter of gridpoints in x-direction
!     IY          Counter of gridpoints in y-direction
!     IS          Counter of relative frequency band
!     ID          Counter of the spectral direction
!
!     ITER        Number of iteration i.e. number of full sweeps
!
!
!     MXC         Maximum counter of gridppoints in x-direction
!     MYC         Maximum counter of gridppoints in y-direction
!     MSC         Maximum counter of relative frequency
!     MDC         Maximum counter of directional distribution
!     ISSTOP      Maximum counter of wave component in frequency
!                 space that is propagated
!
!     REALS:
```

```
!    ---------
!
!    DD          Spectral direction band width
!    DS          Width of the frequency band
!    GRAV        Gravitational acceleration
!    KD          Wavenumber * Depth
!    SVEGEO      Sourceterm for the vetatationfriction to be stored in the array IMATDA
!
!    one and more dimensional arrays:
!    --------------------------------
!
!    DEP2      2D    Depth
!    ESIN      1D    Sin per spectral direction (id)
!    ECOS      1D    Cos per spectral direction (id)
!    IMATDA    2D    Coefficients of diagonal of matrix
!    KWAVE     2D    Wavenumber function of frequency and IC
!    DISSC1    2D    Dissipation coefficient, function of sigma and theta
!    VEGDRAG   2D    Spatially variable drag coefficient
!    VEGDEN    2D    Spatially variable vegetation density
!    VEGDIA    2D    Spatially variable vegetation diameter
!    VEGH      2D    Spatially variable vegetation height
!
!  7. Common blocks used
!
!
!  8. Subroutines used
!
!    ---
!
!  9. Subroutines calling
!
!    SOURCE
!
! 10. Error Messages
!
!    ---
!
! 11. Remarks
!
!    ---
!
! 12. Structure
!
!    -----------------------------------------------------------
!
!    -----------------------------------------------------------
!
! 13. Source text
!
```

```
      REAL    :: VEGDRAG(MCGRD), VEGDIA(MCGRD), VEGH(MCGRD),
     &           VEGDEN(MCGRD)
!
      INTEGER  ID     ,IS     ,ISSTOP
      REAL     KD     ,KVEGH  ,SVEGEO,   ADUM,   BDUM,   CDUM
!
      REAL     DEP2(MCGRD)             ,
     &         AC2(MCGRD,MDC,MSC)       ,
     &         IMATDA(MDC,MSC)          ,
     &         DISSC1(MDC,MSC)          ,
     &         KWAVE(MSC,ICMAX)
!
      INTEGER  IDCMIN(MSC)             ,
     &         IDCMAX(MSC)
      SAVE IENT
      DATA IENT/0/
      IF (LTRACE) CALL STRACE (IENT,'SVEG')
          DO  IS = 1, ISSTOP
        KD    = KWAVE(IS,1) * DEP2(KCGRD(1))
        KVEGH = KWAVE(IS,1) * VEGH(KCGRD(1))
        ADUM  = (SINH(KVEGH))**3
        BDUM  = 3*SINH(KVEGH)
        CDUM  = 3*KWAVE(IS,1)*(COSH(KD))**3

        SVEGEO1 = (1/(2*SQRT(PI))) * VEGDRAG(KCGRD(1)) *
     &          (VEGDEN(KCGRD(1))) * VEGDIA(KCGRD(1)) *
     &          ((KWAVE(IS,1)*GRAV)/(2*SPCSIG(IS)))**3*
     &          ((ADUM + BDUM)/CDUM)

        DO IDDUM = IDCMIN(IS) , IDCMAX(IS)
          ID = MOD ( IDDUM - 1 + MDC , MDC ) + 1

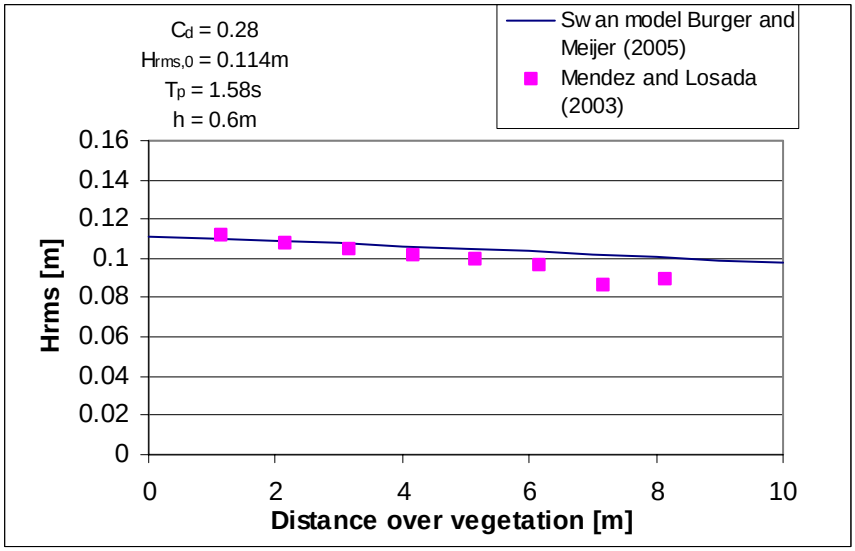
           SVEGEO = SVEGEO1 *
     &       SQRT(SPCSIG(IS)*AC2(KCGRD(1),ID,IS))

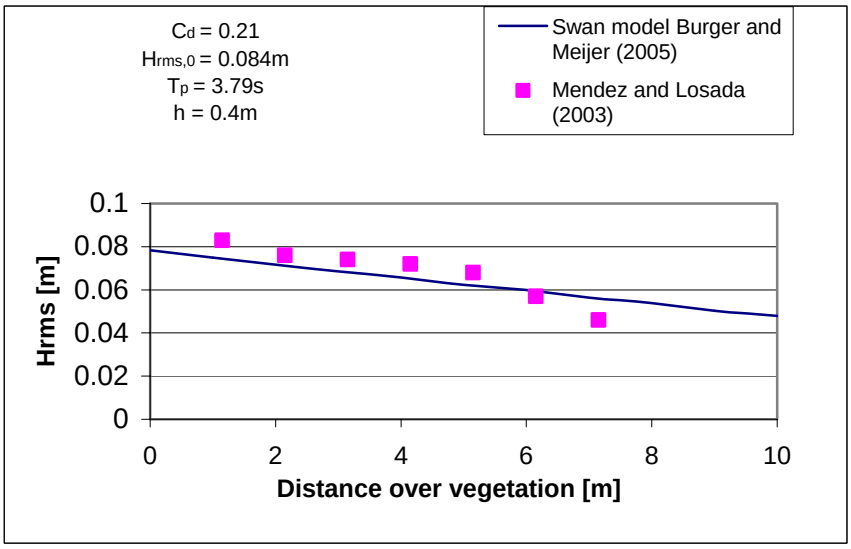
!        *** store the results in the array IMATDA ***
!
          IMATDA(ID,IS) = IMATDA(ID,IS) + SVEGEO
          DISSC1(ID,IS) = DISSC1(ID,IS) + SVEGEO

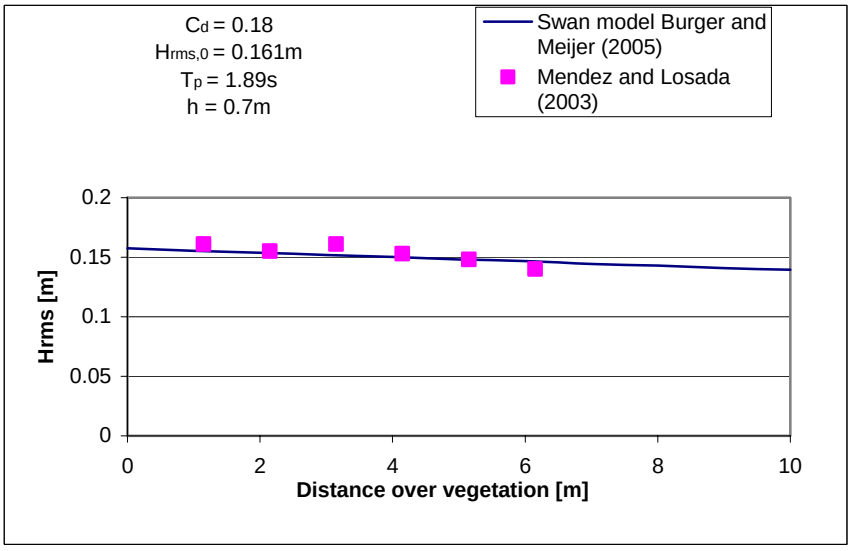
        END DO
         CONTINUE
      END DO

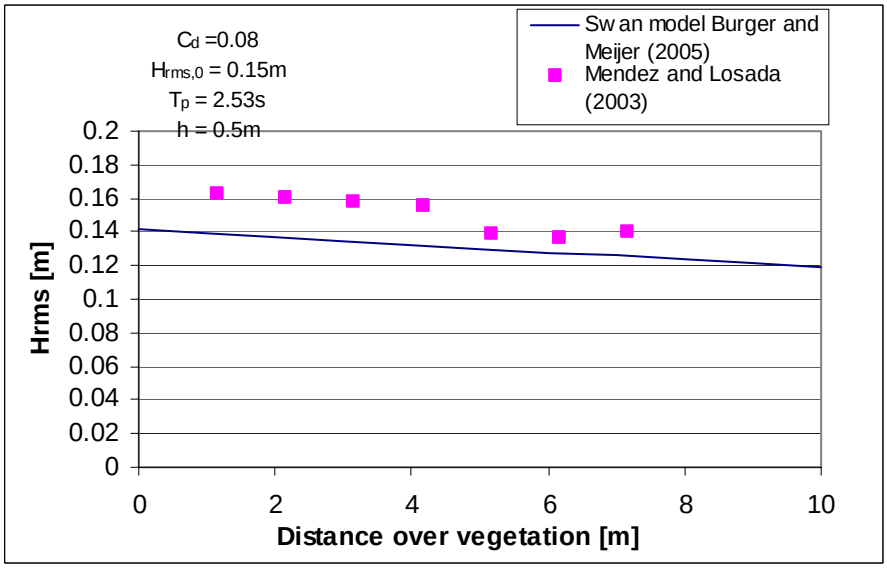
!     End of subroutine SVEG
      RETURN
      END
```

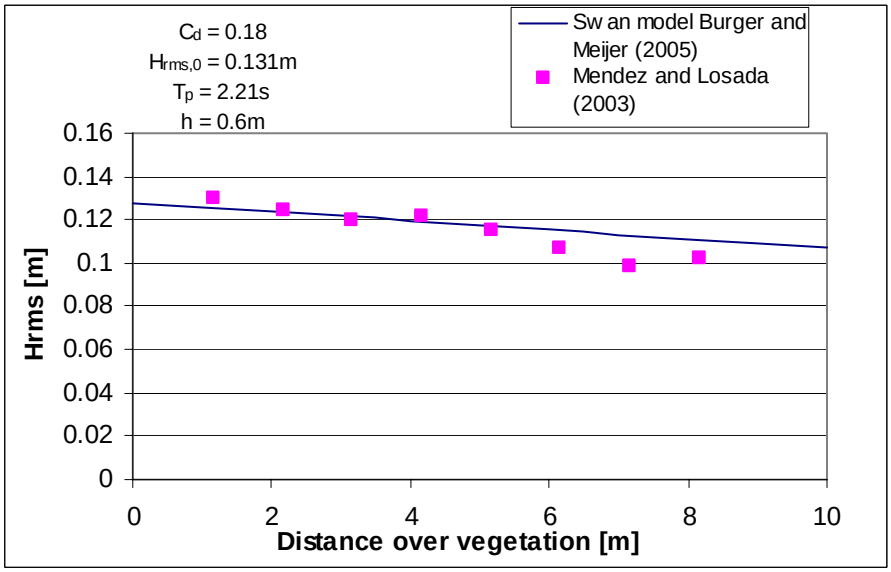
Appendix E Validation on physical model results

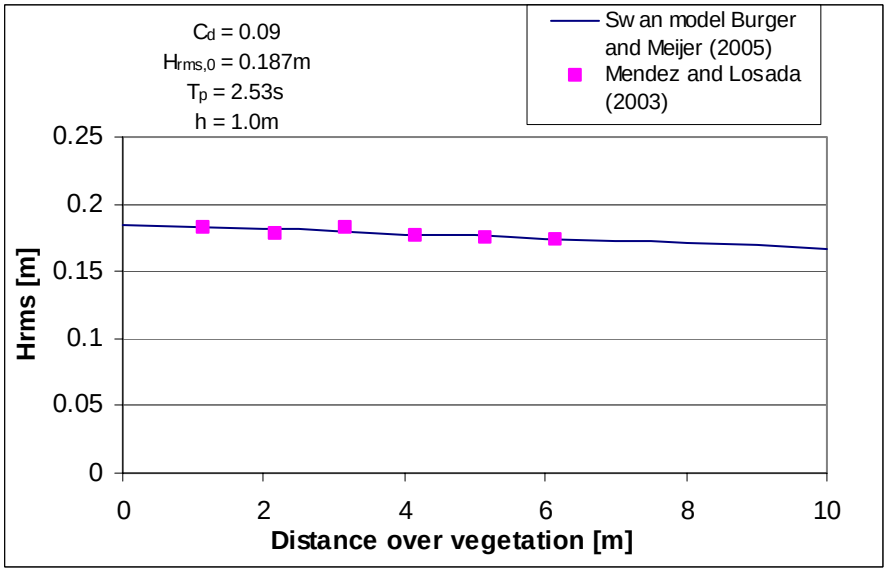








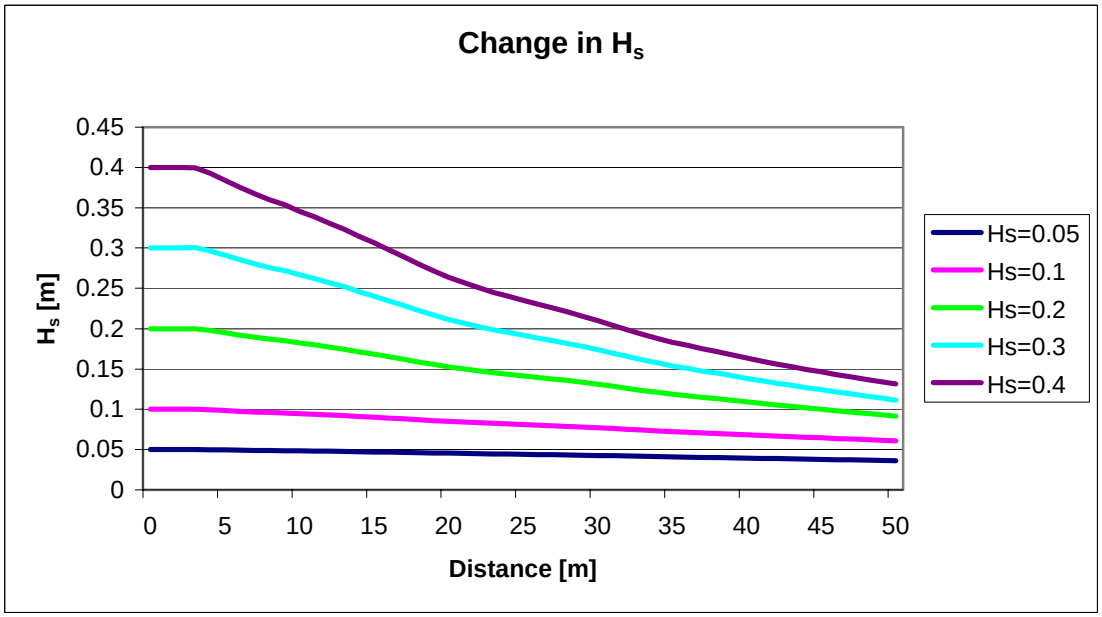


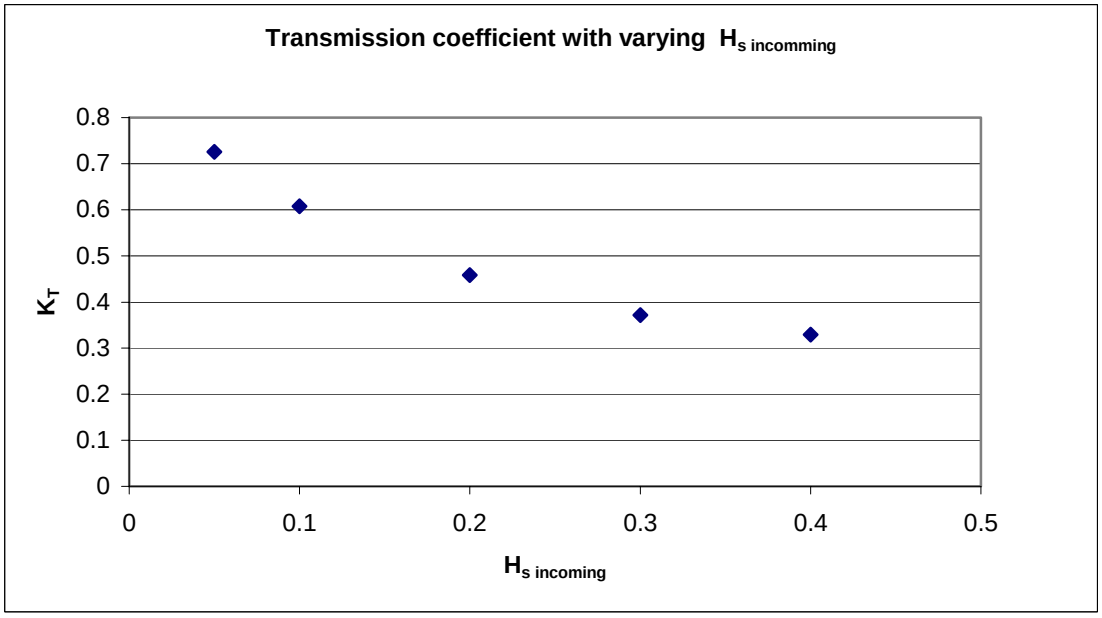


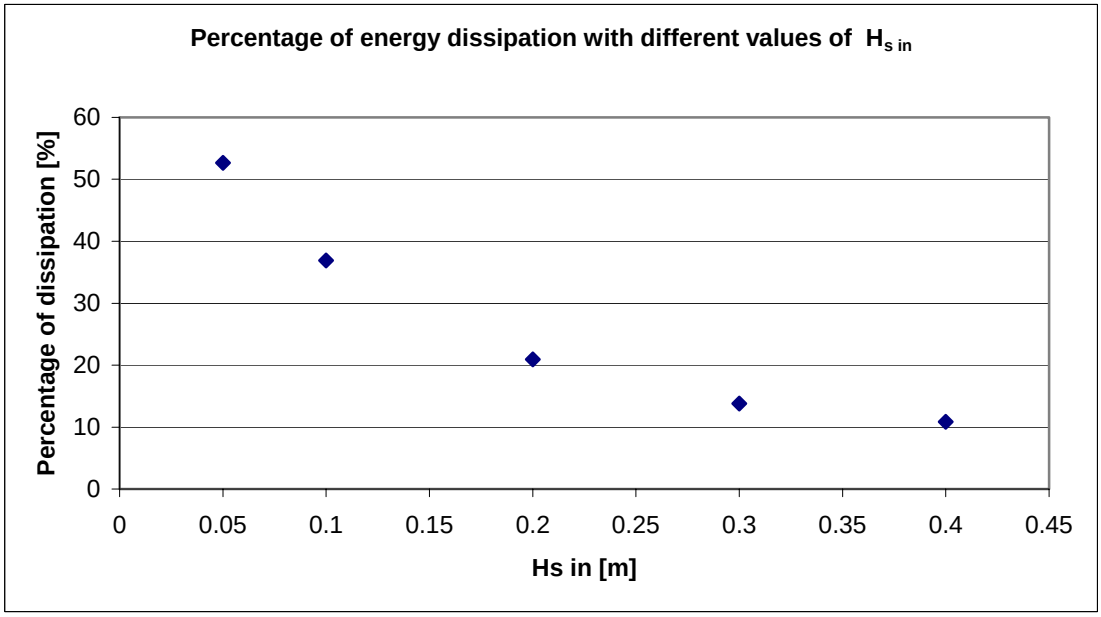
Physical model results Burger and Meijer vs. Mendez and Losada

Appendix F Sensitivity analyses

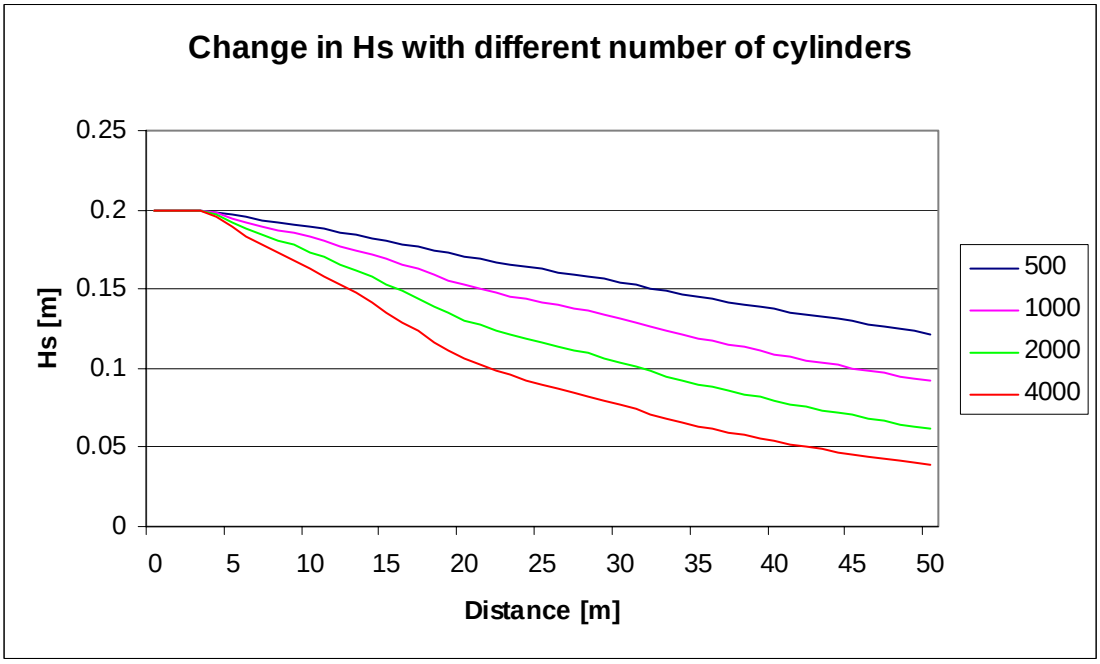
F.1 Change in H_s

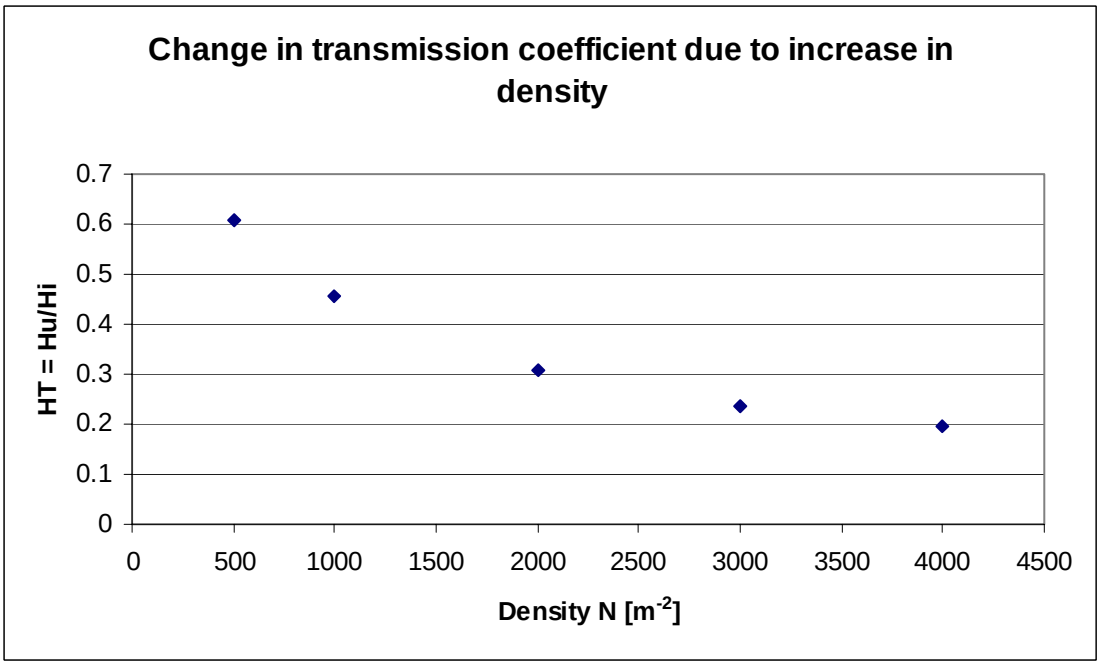


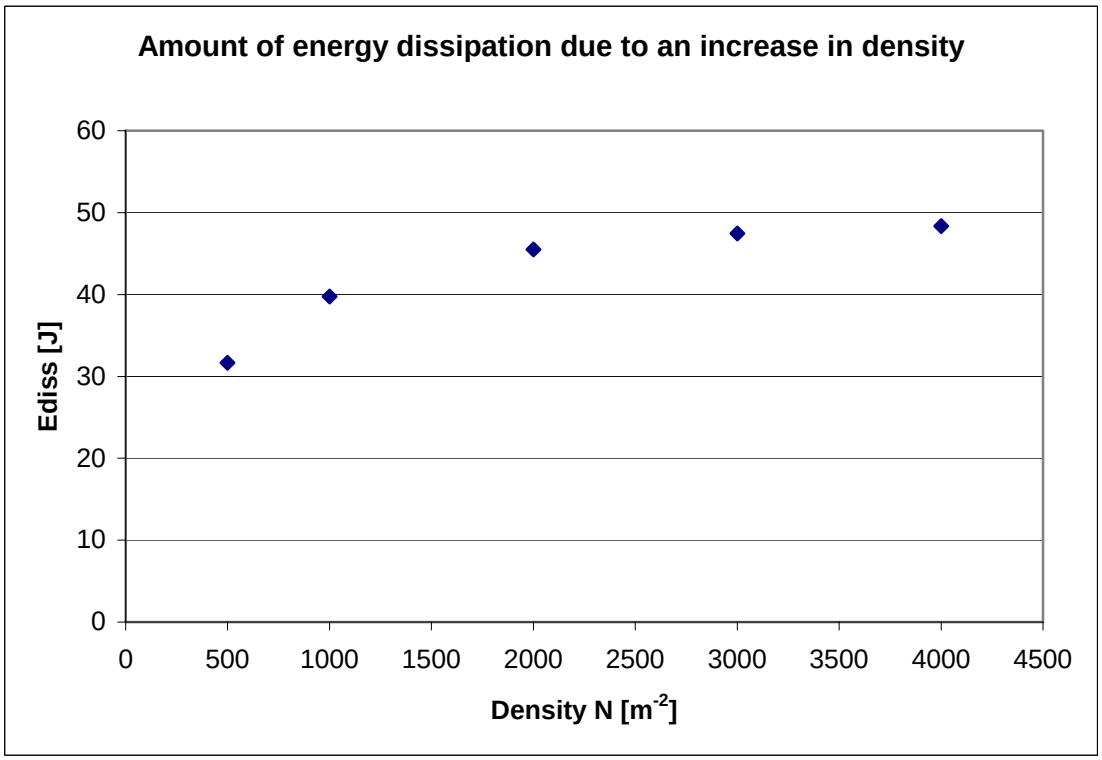


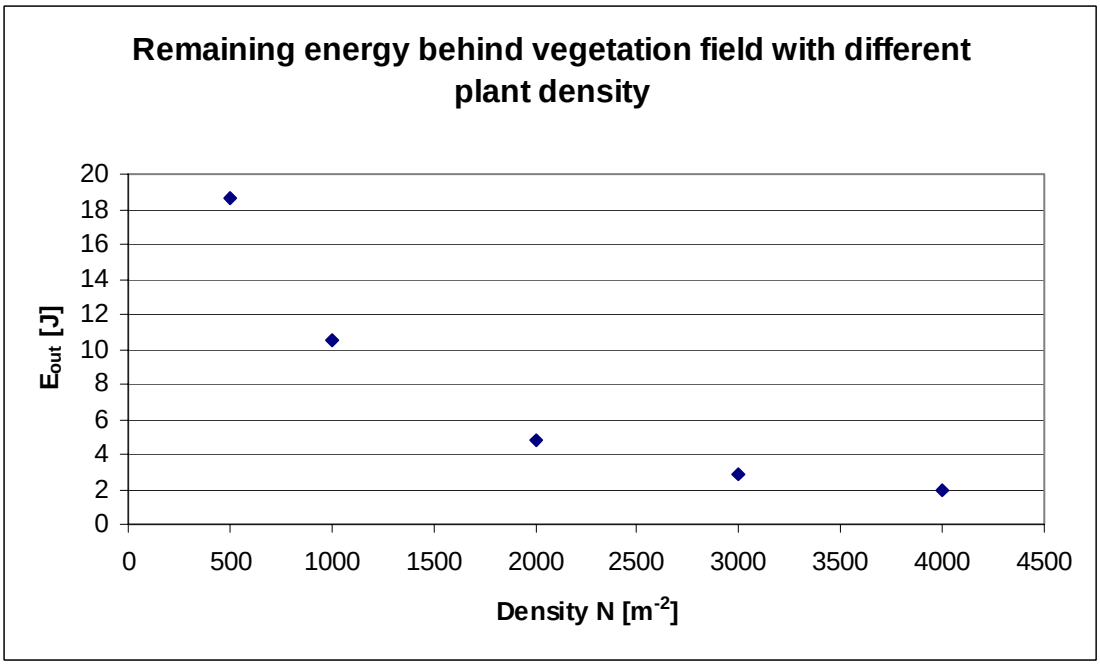


F.2 Change in N

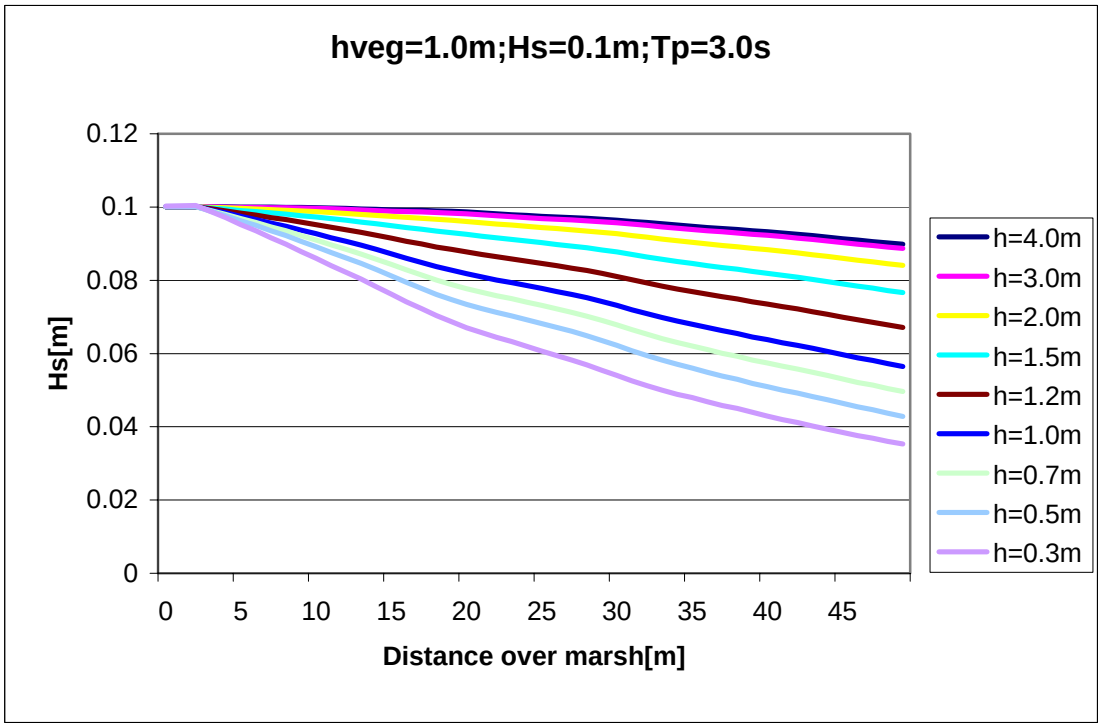


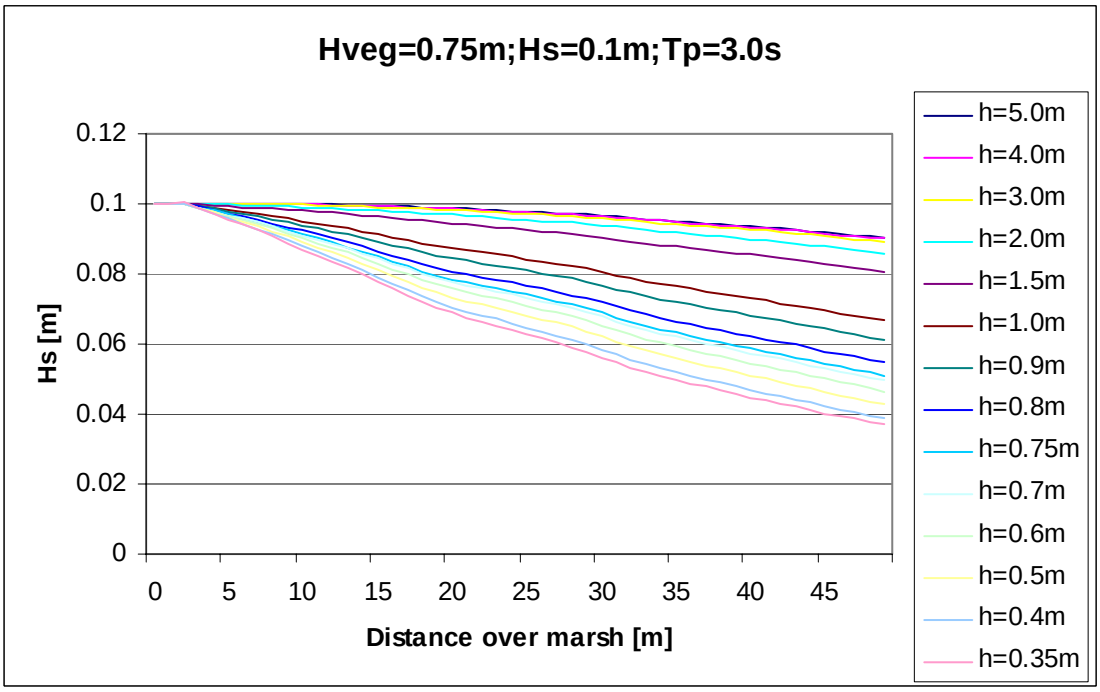

Change in transmission coefficient due to increase in density
HT = Hu/Hi
0.7
0.6
0.5
0.4
0.3
0.2
0.1
0
0
500
1000
1500
2000
2500
3000
3500
4000
4500
Density N [m-2]


Amount of energy dissipation due to an increase in density
Ediss [J]
60
50
40
30
20
10
0
0
500
1000
1500
2000
2500
3000
3500
4000
4500
Density N [m-2]

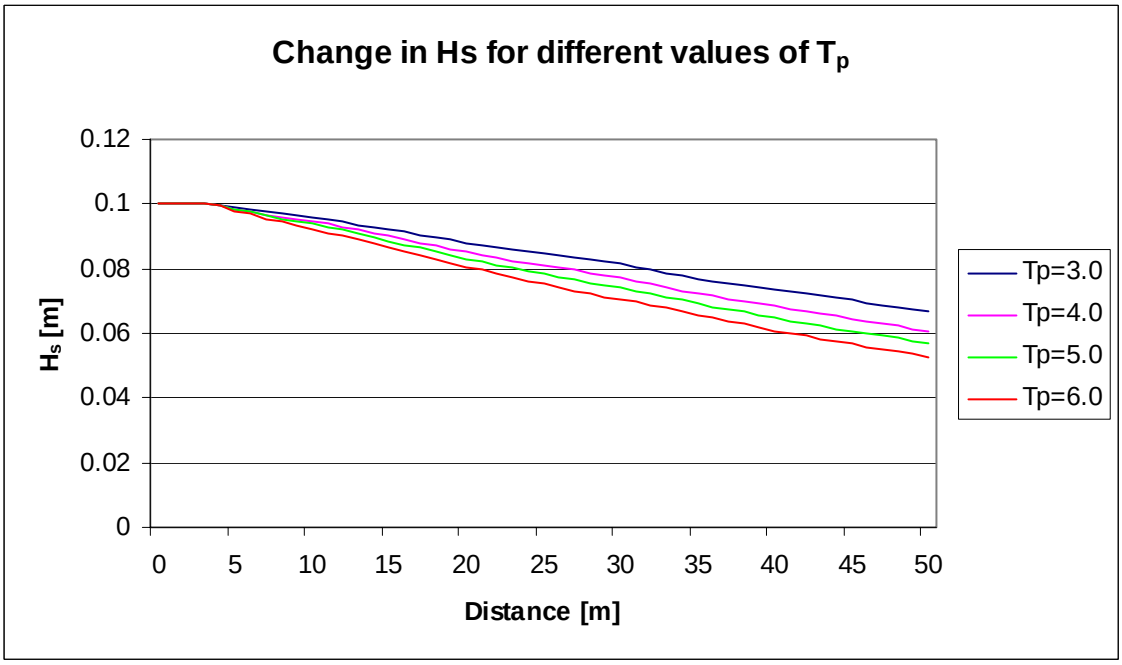


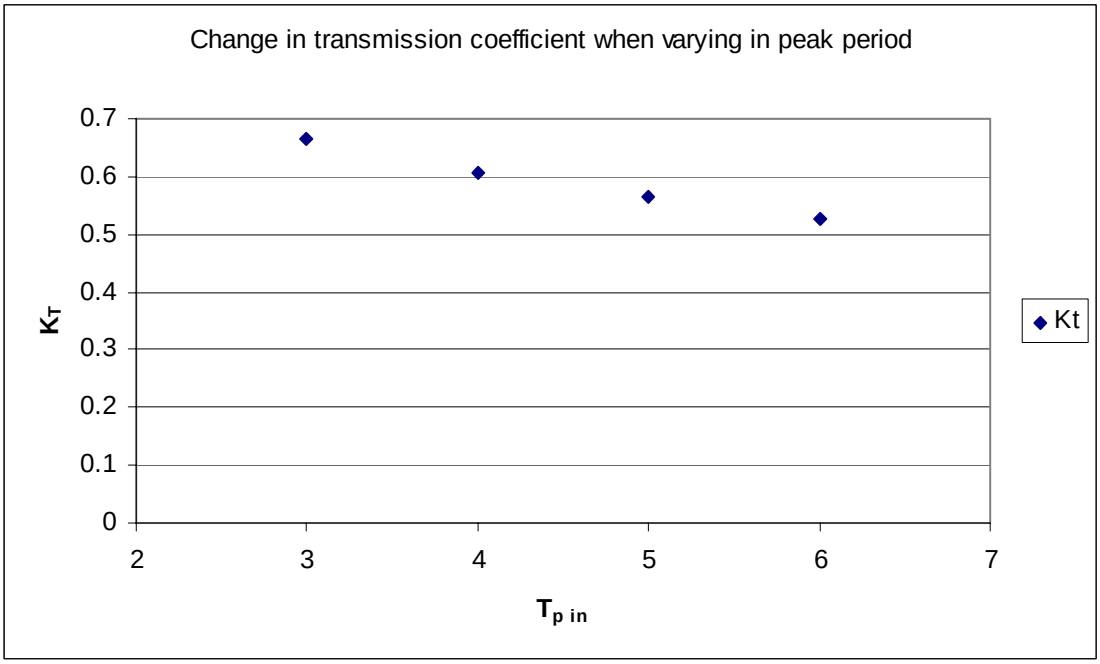
F.3 Change in relative vegetation height

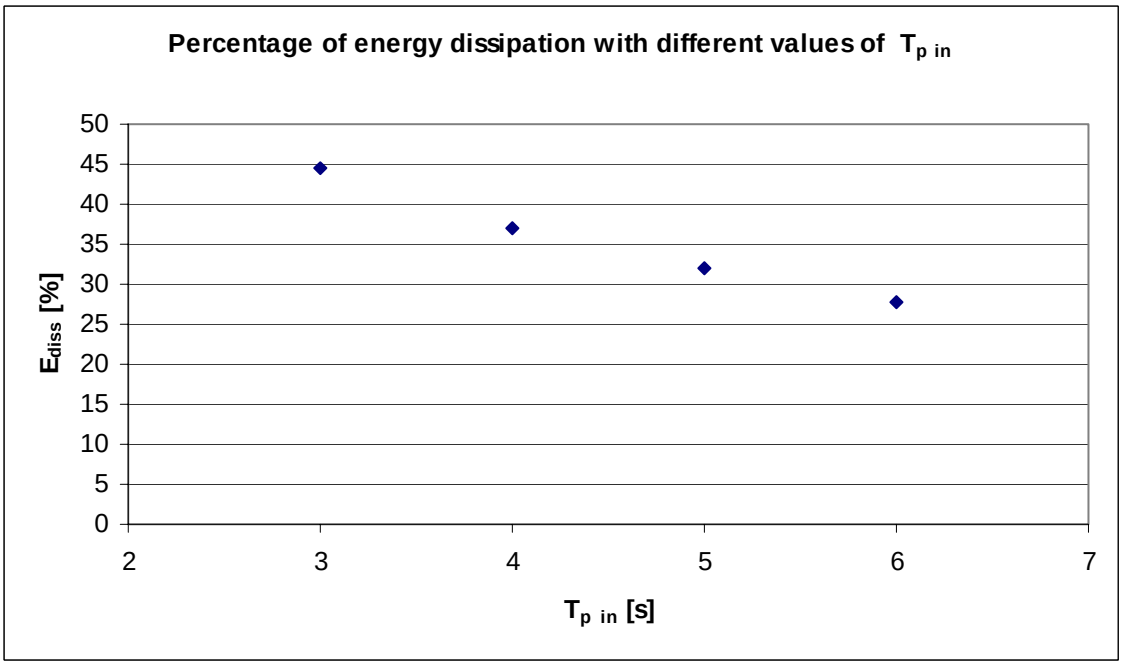


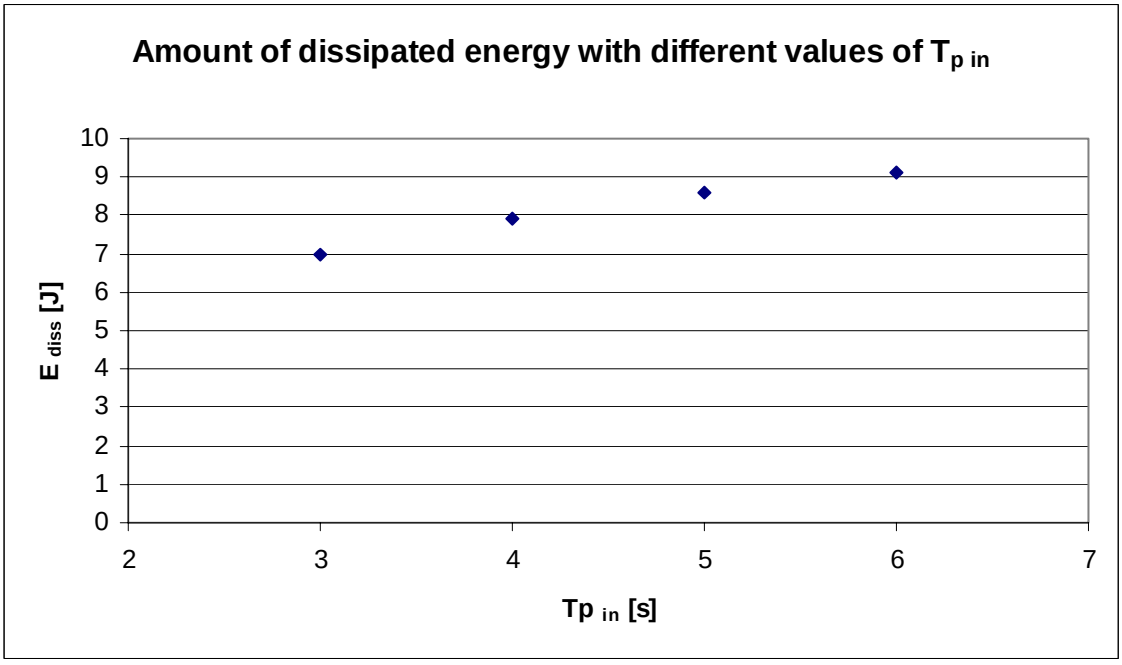

Hveg=0.75m;Hs=0.1m;Tp=3.0s
Hs [m]
0.12
0.1
0.08
0.06
0.04
0.02
0
0
5
10
15
20
25
30
35
40
45
Distance over marsh [m]
h=5.0m
h=4.0m
h=3.0m
h=2.0m
h=1.5m
h=1.0m
h=0.9m
h=0.8m
h=0.75m
h=0.7m
h=0.6m
h=0.5m
h=0.4m
h=0.35m

F.4 Change in Tp

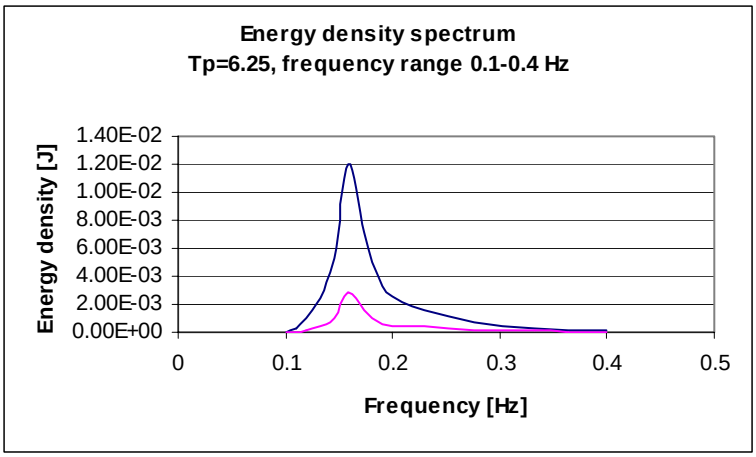


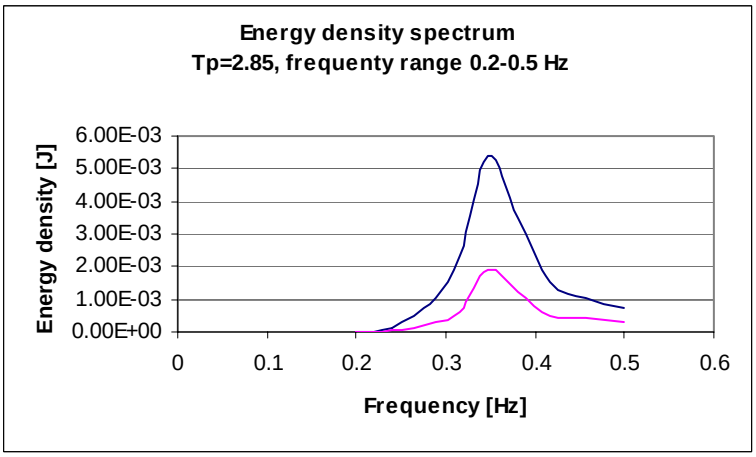


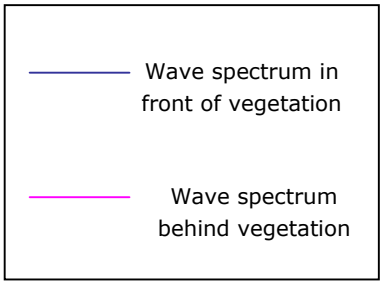

Percentage of energy dissipation with different values of $T_{p\ in}$
E_{diss} [%]
50
45
40
35
30
25
20
15
10
5
0
2
3
4
5
6
7
$T_{p\ in}$ [s]

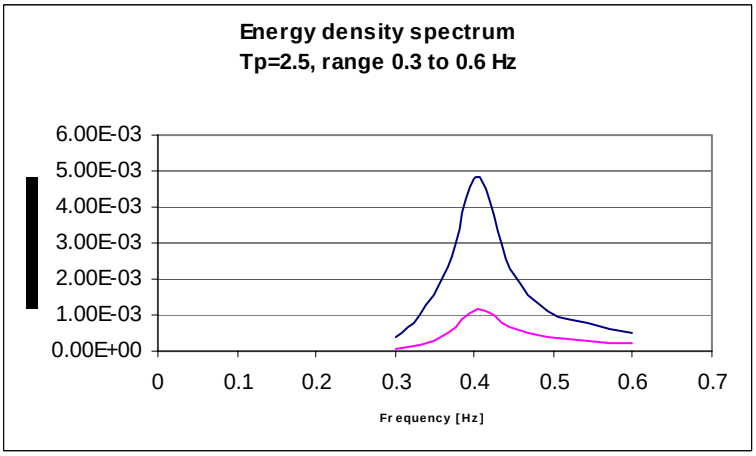

Amount of dissipated energy with different values of $T_{p\ in}$
E_{diss} [J]
10
9
8
7
6
5
4
3
2
1
0
2
3
4
5
6
7
Tp_{in} [s]

Appendix G: Energy density spectra



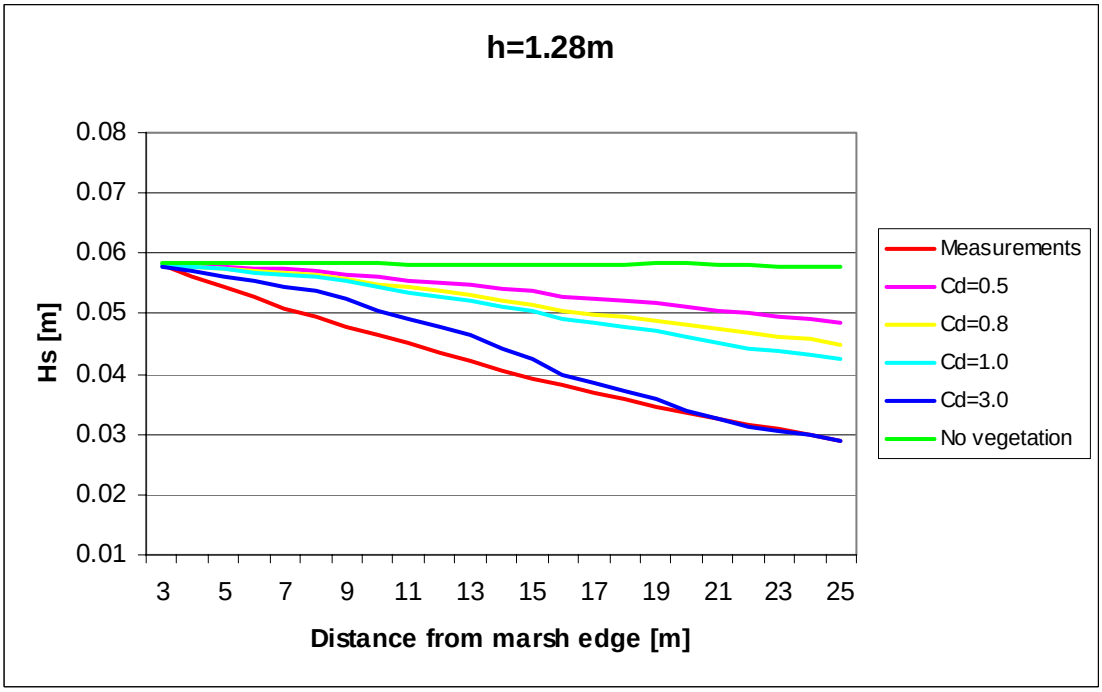


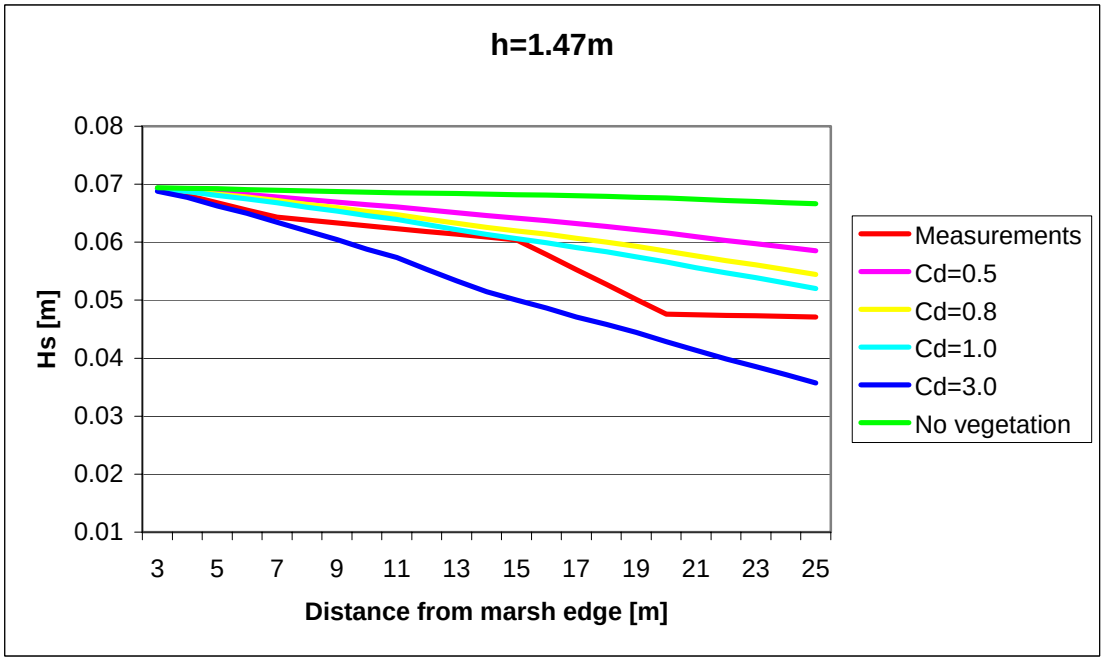


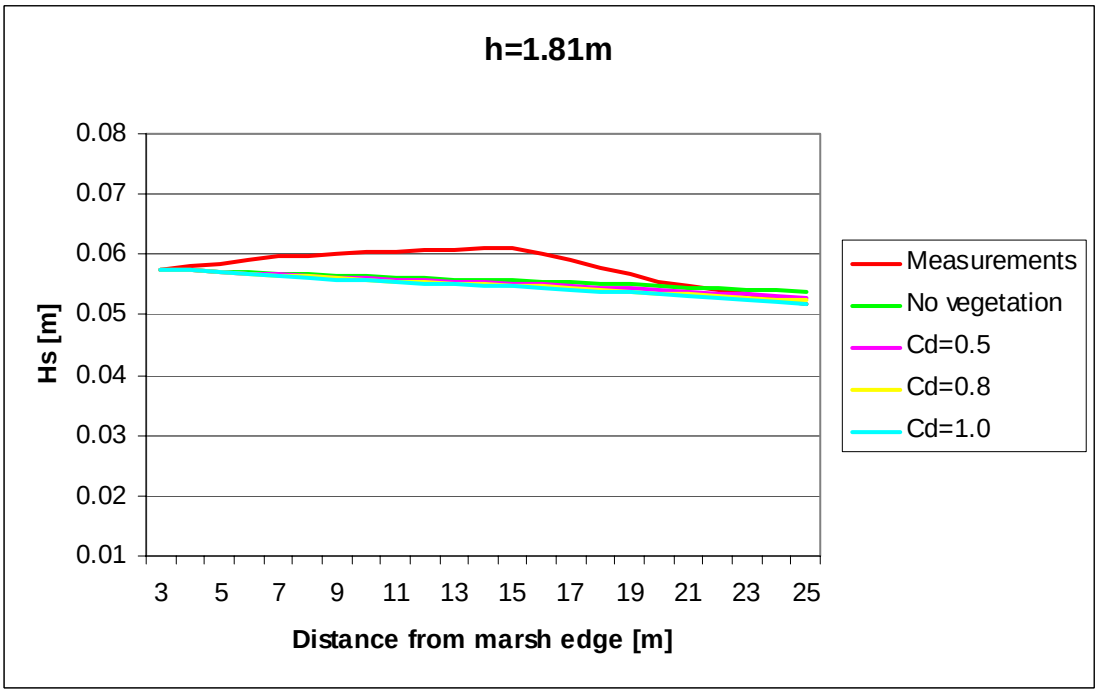


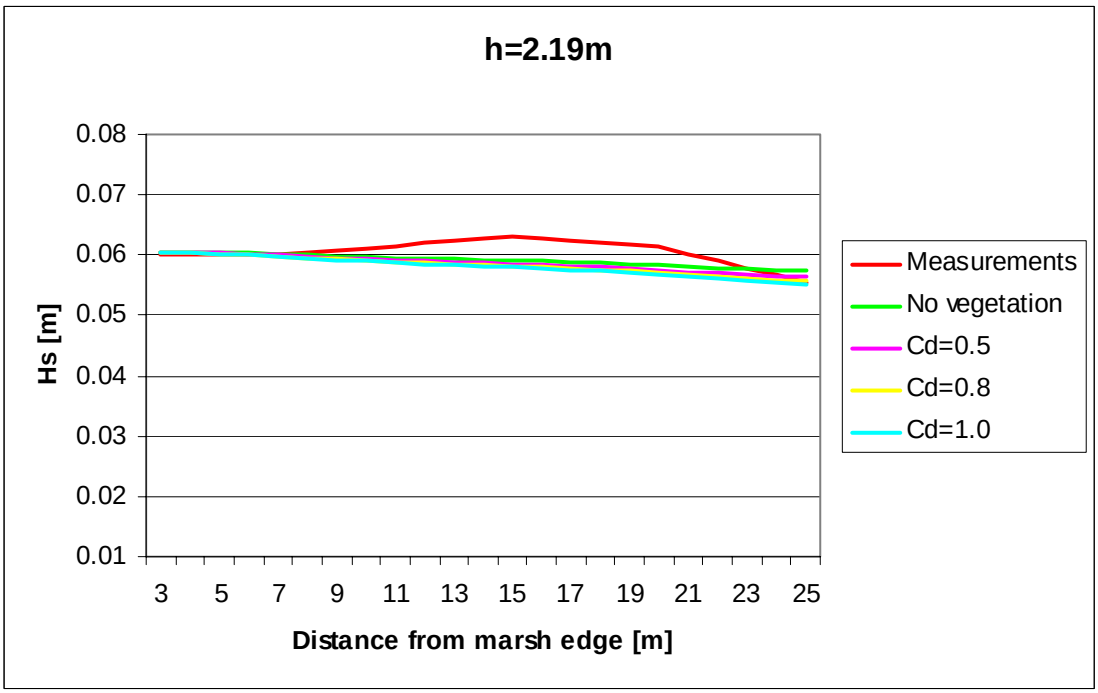
Appendix H Model results Paulina Marsh

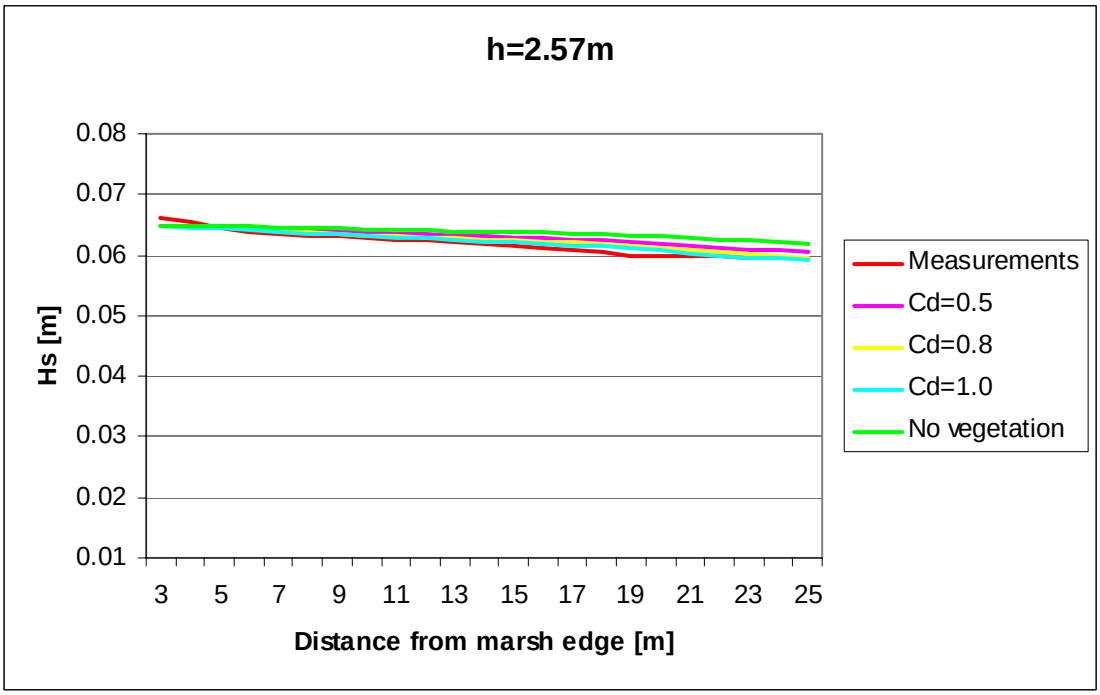
H.1 Results for various values of C_d



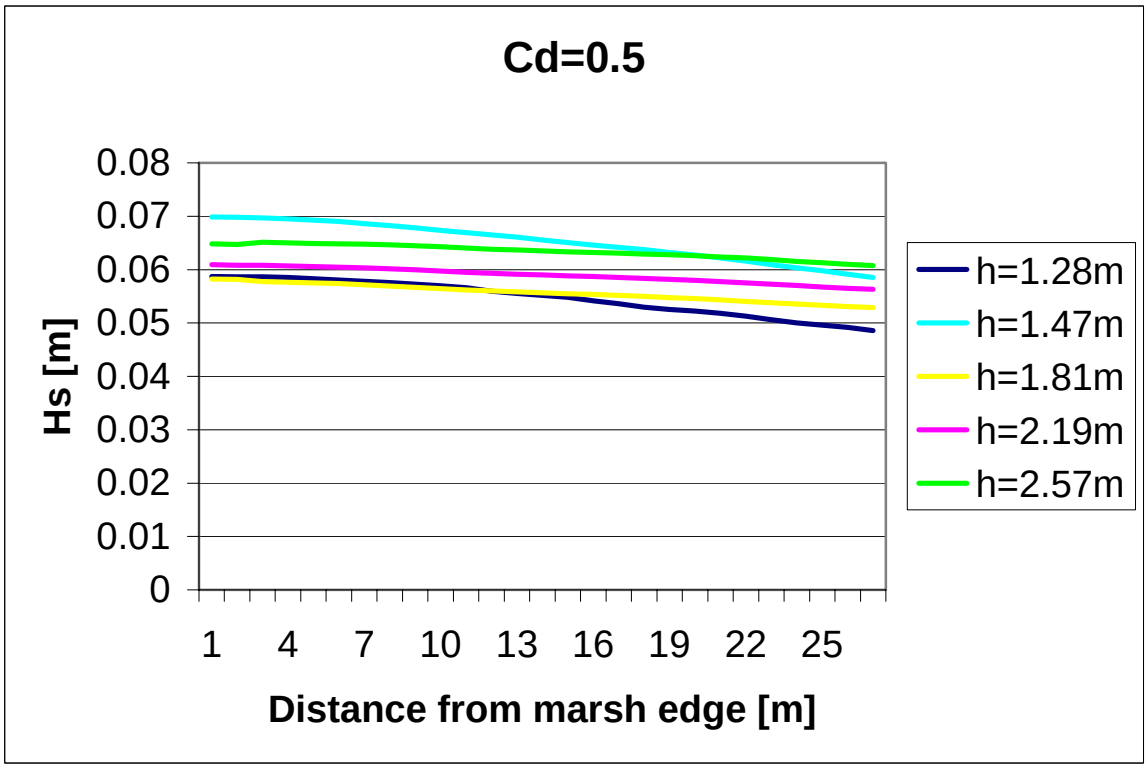


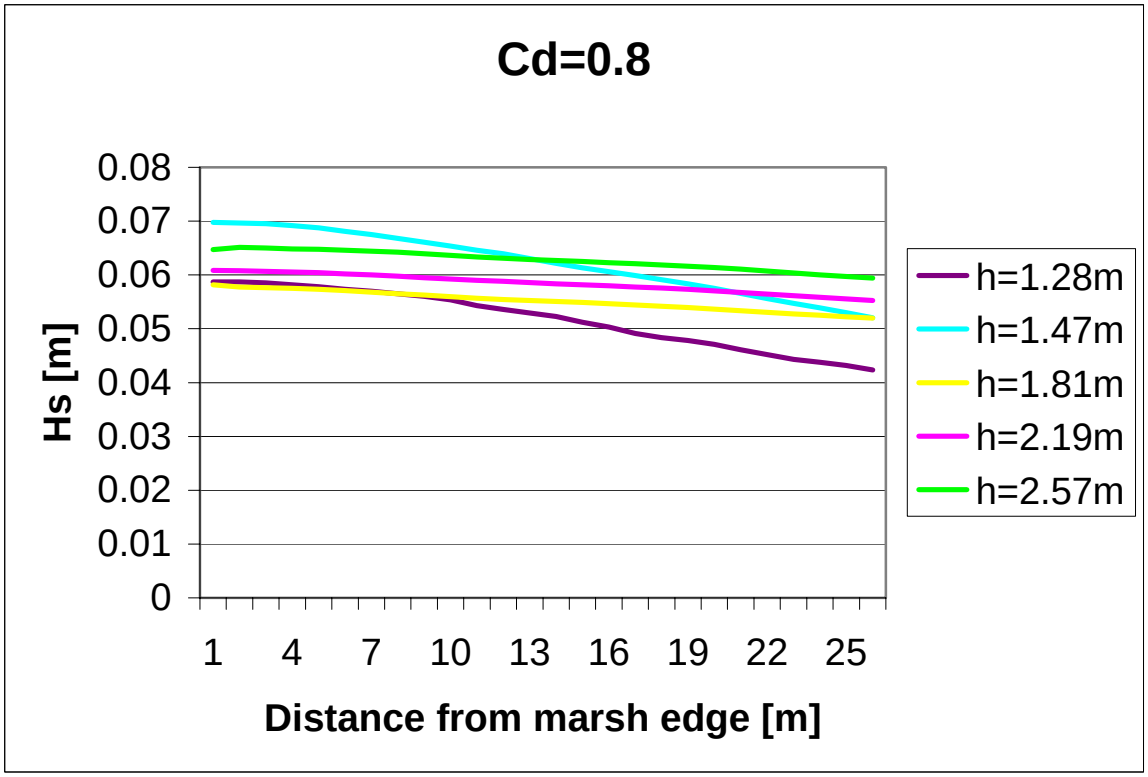

h=1.81m
0.08
0.07
0.06
0.05
0.04
0.03
0.02
0.01
Hs [m]
3 5 7 9 11 13 15 17 19 21 23 25
Distance from marsh edge [m]
Measurements
No vegetation
Cd=0.5
Cd=0.8
Cd=1.0

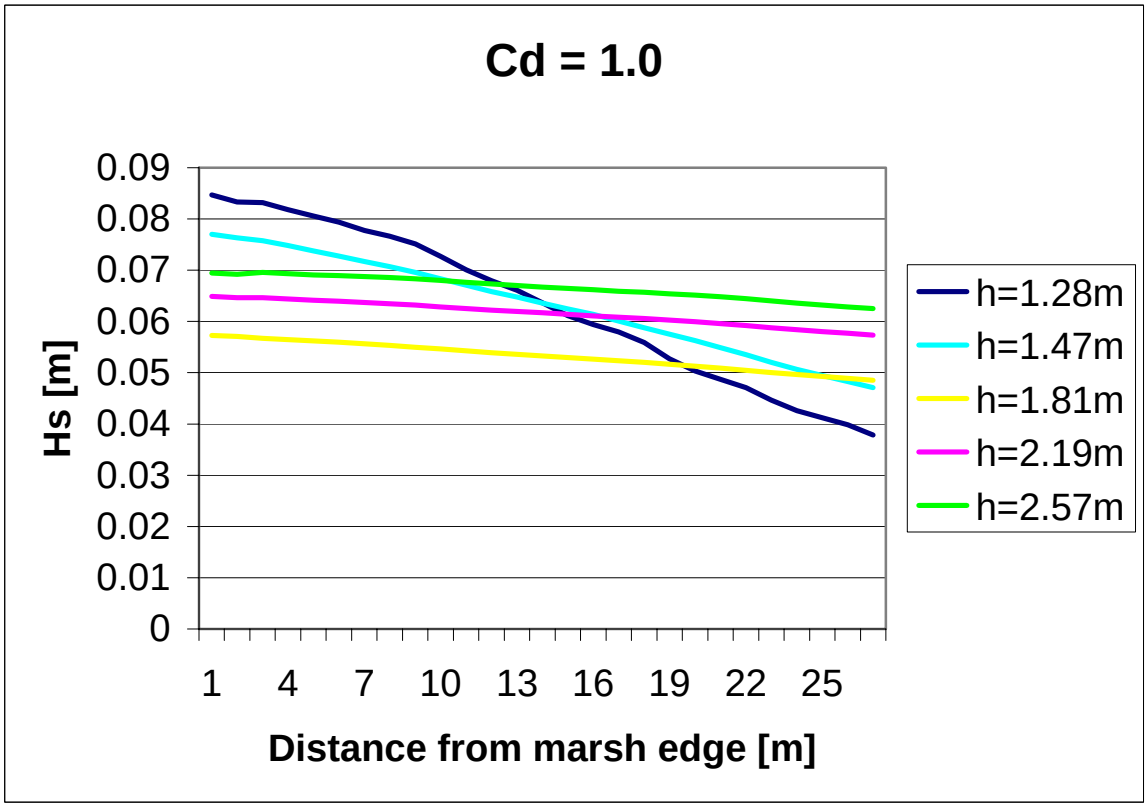

h=2.19m
0.08
0.07
0.06
0.05
0.04
0.03
0.02
0.01
Hs [m]
3 5 7 9 11 13 15 17 19 21 23 25
Distance from marsh edge [m]
Measurements
No vegetation
Cd=0.5
Cd=0.8
Cd=1.0



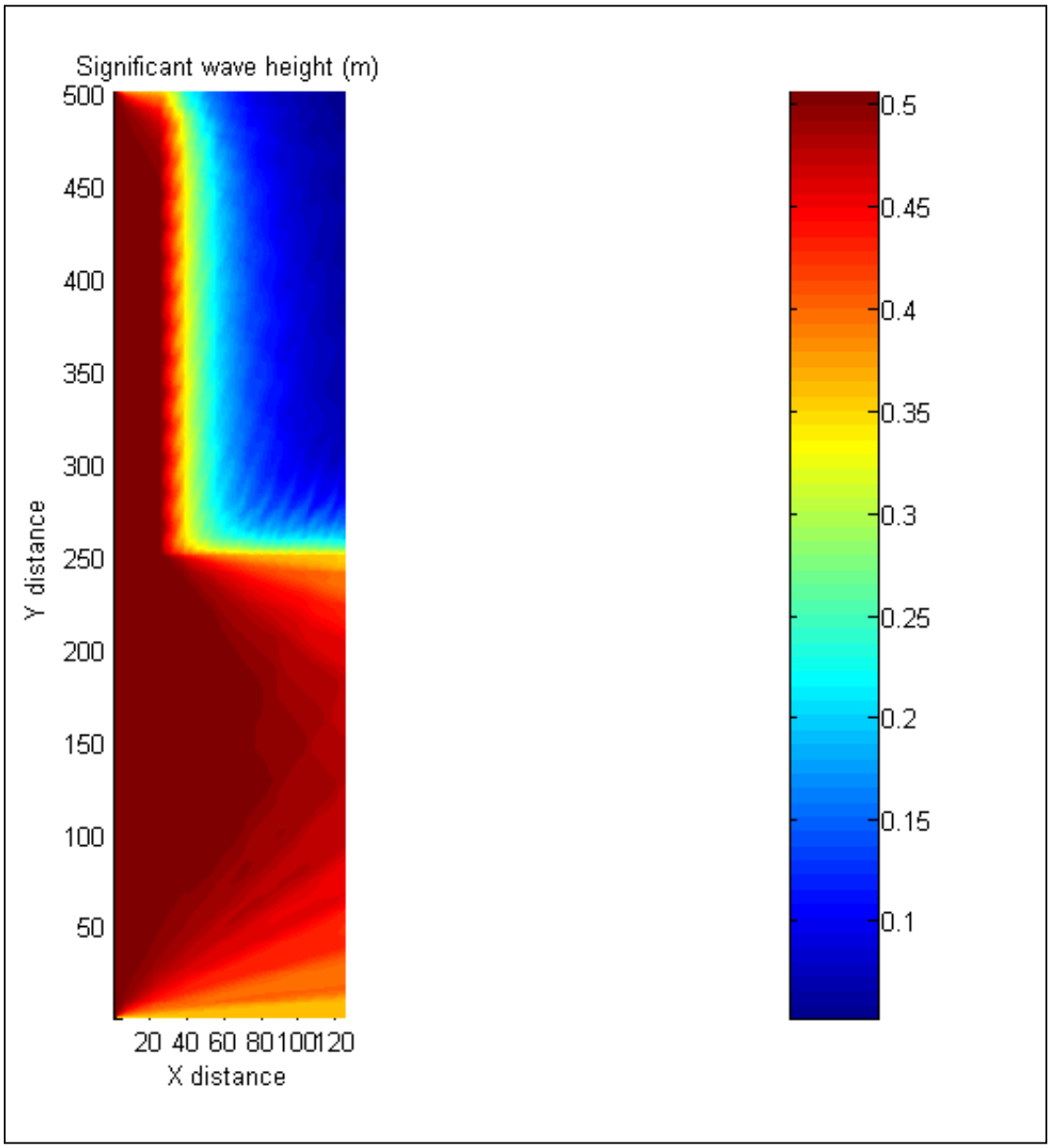
H.2 Constant drag coefficient assumed



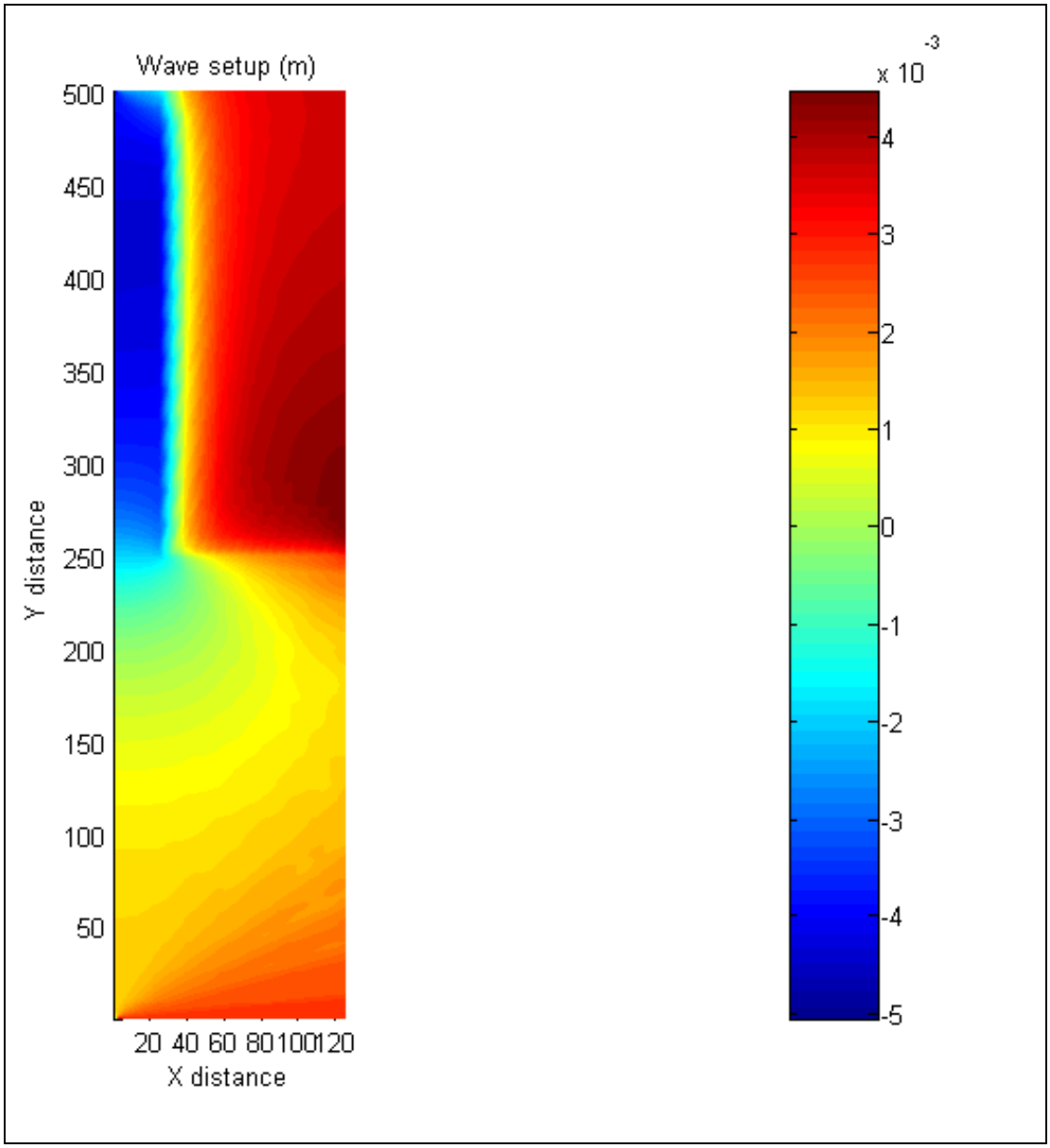

Cd=0.8
0.08
0.07
0.06
0.05
0.04
0.03
0.02
0.01
0
Hs [m]
1
4
7
10
13
16
19
22
25
Distance from marsh edge [m]
h=1.28m
h=1.47m
h=1.81m
h=2.19m
h=2.57m


Cd = 1.0
0.09
0.08
0.07
0.06
0.05
0.04
0.03
0.02
0.01
0
Hs [m]
1
4
7
10
13
16
19
22
25
Distance from marsh edge [m]
h=1.28m
h=1.47m
h=1.81m
h=2.19m
h=2.57m

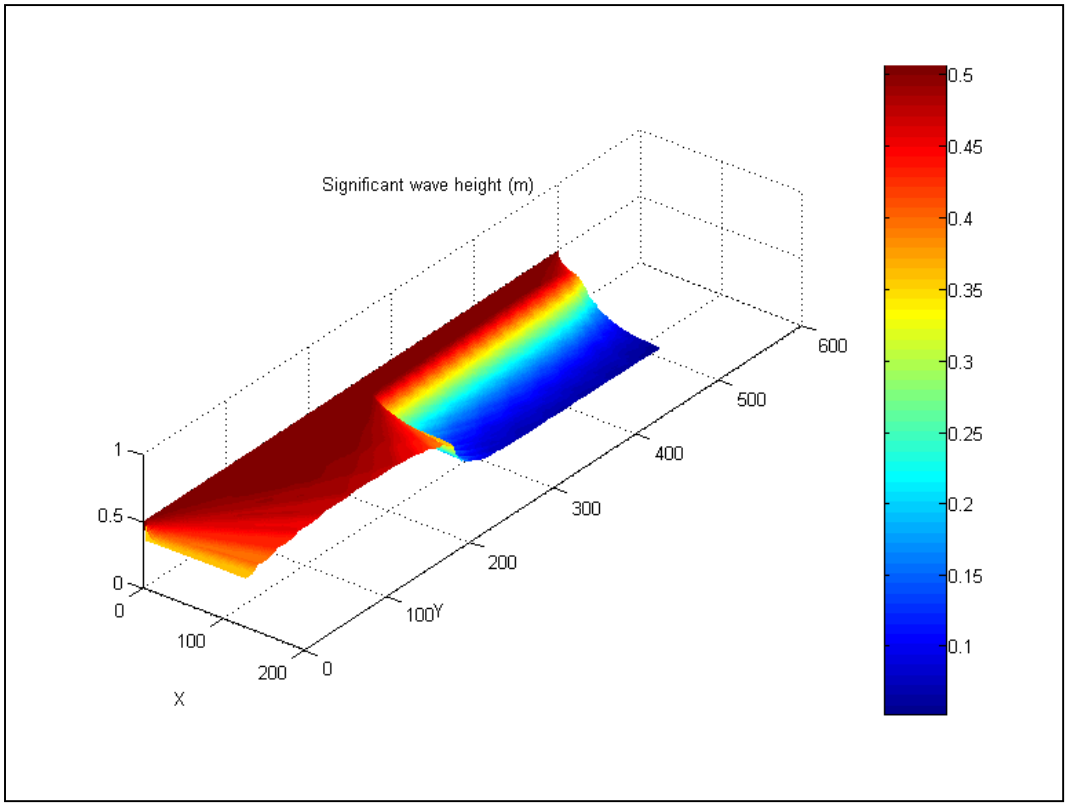
Appendix I Wave setup



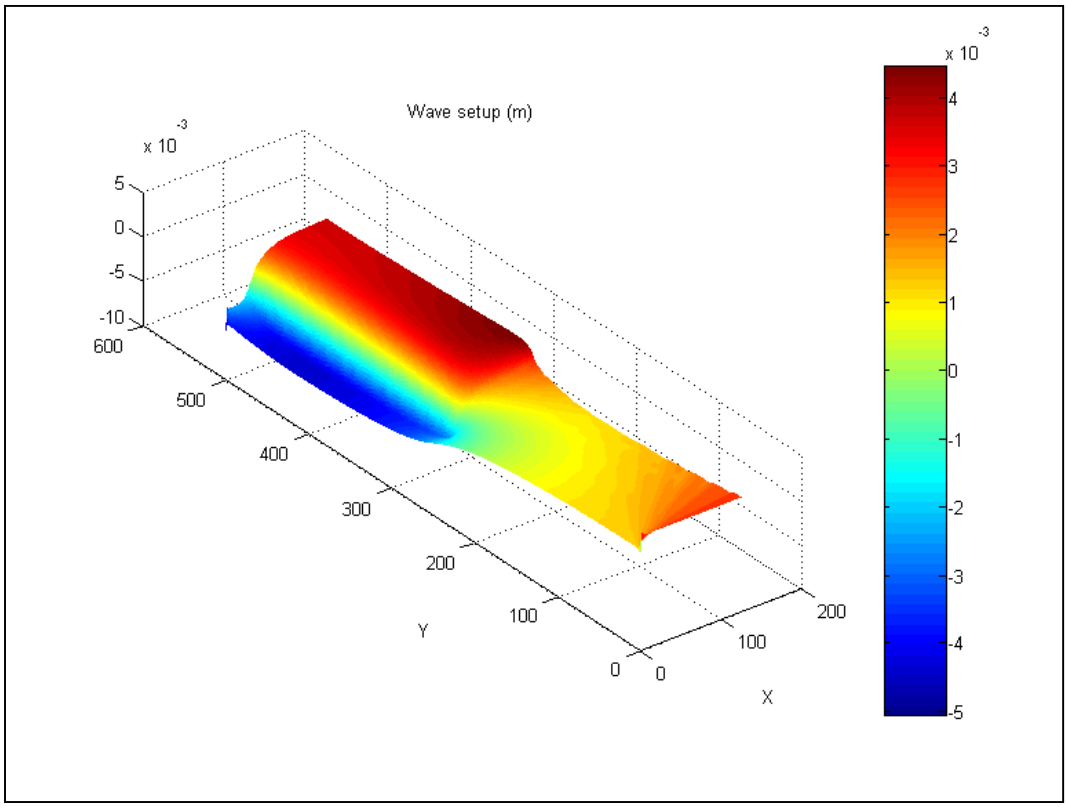
Top view significant wave height Case A



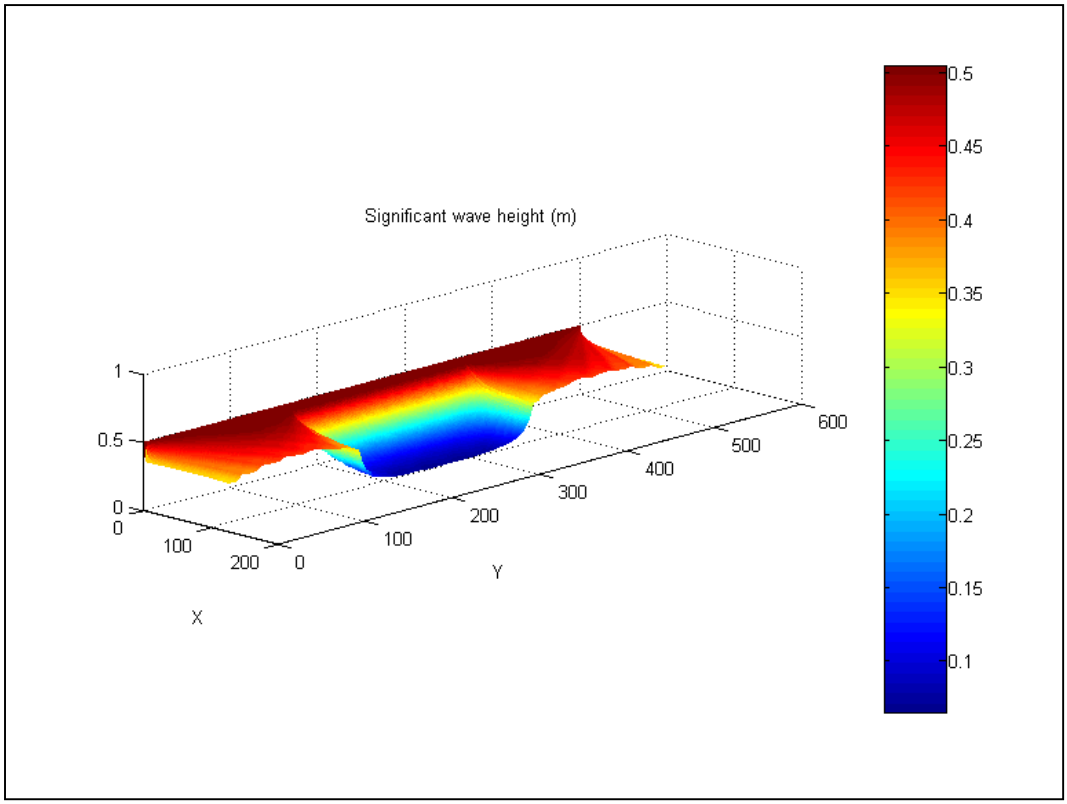
Top view wave setup Case A



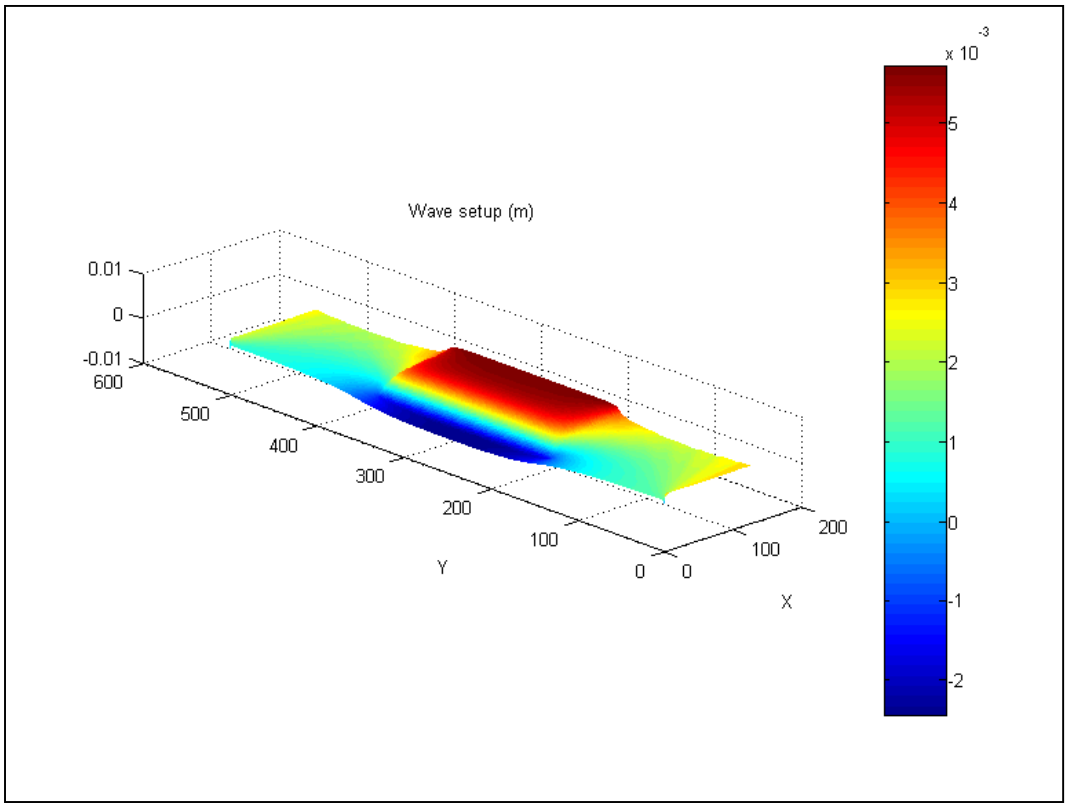
Significant wave height Case A



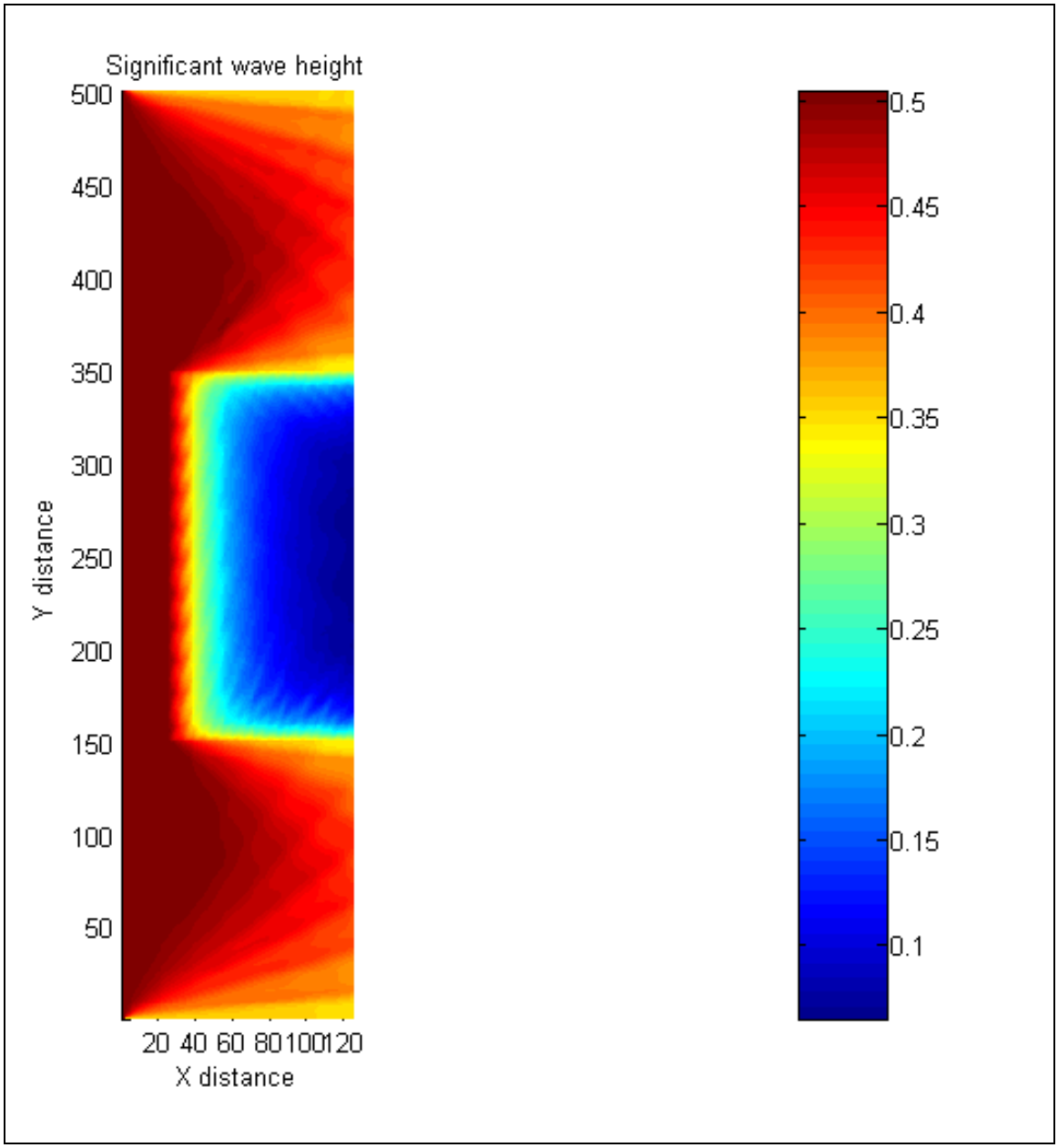
Wave setup Case A



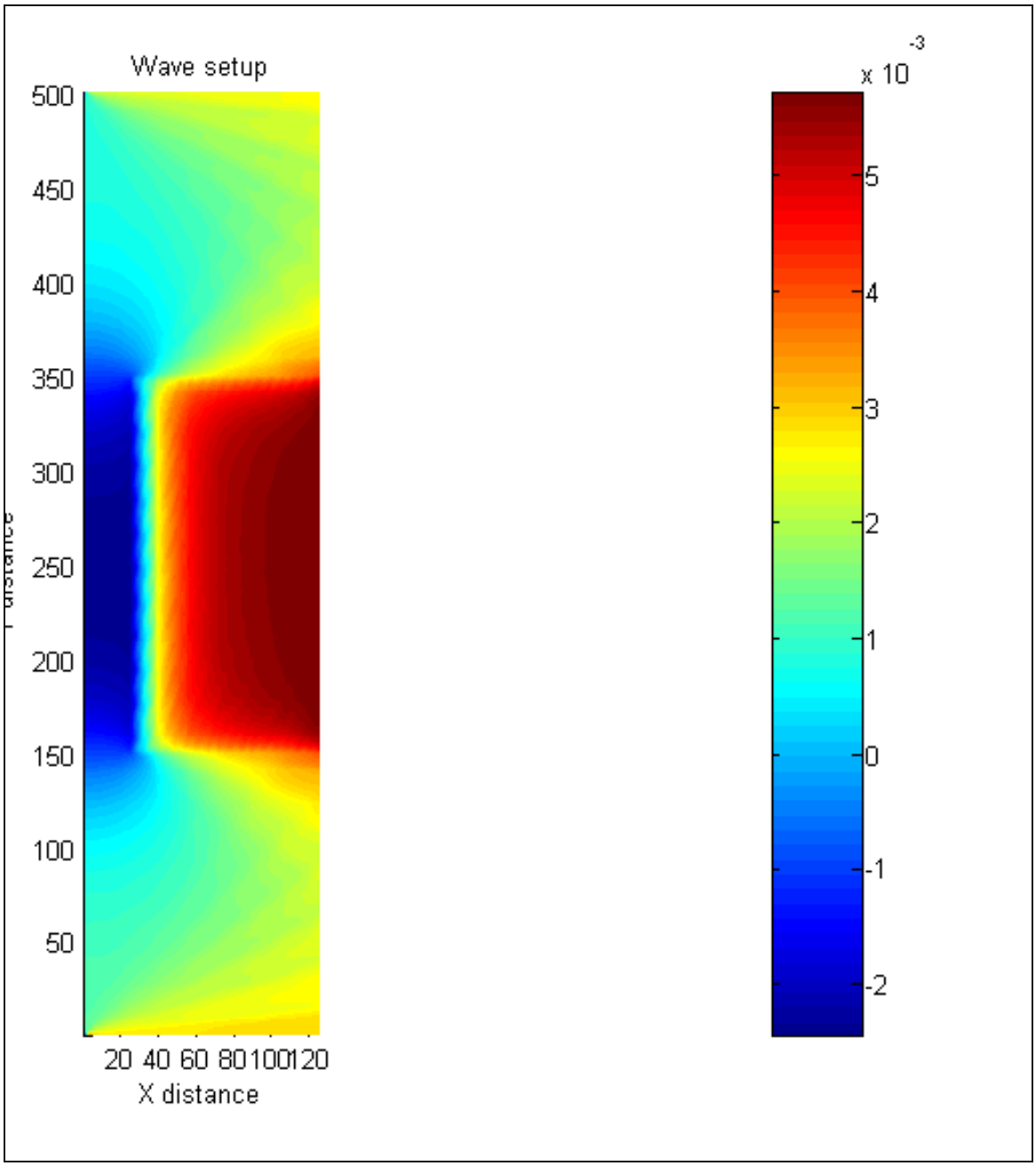
Significant wave height Case B



Wave setup Case B



Top view significant wave height Case B



Top view wave setup Case B

Appendix J List of coefficients

α	relative vegetation height	[-]
αh	vegetation height	[m]
ad	population density	[-]
b_v	plant stem diameter	[m]
C_d	drag coefficient	[-]
$\tilde{C}_D$	calibrated drag coefficient	[-]
C_m	inertia coefficient	[-]
c_V	vegetation friction factor	[-]
c_x	propagation velocities in x-direction	[ms^{-1}]
c_y	propagation velocities in y-direction	[ms^{-1}]
c_σ	propagation velocity in σ space	[ms^{-1}]
c_θ	propagation velocity in θ space	[ms^{-1}]
D	stem diameter	[m]
D_v	Dissipation of energy per unit area of vegetation	[$Nm^{-1}s^{-1}$]
dz	vegetation height	[m]
E	energy density	[Nm^{-1}]
ε_v	time-averaged rate of energy dissipation per unit horizontal area	[$Nm^{-1}s^{-1}$]
f_w^*	friction factor	[-]
$\boldsymbol{F}$	force vector per unit volume, F=(F_x, 0, F_z)	[Nm^{-3}]
g	gravitational acceleration	[ms^{-2}]
H_{rms}	root mean square wave height	[m]
H_s	significant wave height	[m]
k	wave number	[m^{-1}]
K	Keulegan-Carpenter number	[-]
K_T	Transmission coefficient	[-]
n	vegetation density (Collins)	[m^{-2}]
N	vegetation density (Dalrymple)	[m^{-2}]
N	action density (SWAN)	[$N \cdot m^{-1}$]
Re	Reynolds number	[-]
S	relative spacing	[m]
S	Energy density (SWAN)	[$Nm^{-1}s^{-1}$]
T_p	wave peak period	[s]
u	horizontal velocity	[ms^{-1}]
u_c	horizontal orbital velocity	[ms^{-1}]
U_{orb}	horizontal orbital velocity	[ms^{-1}]
$\hat{U}_\delta$	maximum orbital velocity near boundary	[ms^{-1}]
σ	wave frequency	[$rads^{-1}$]
θ	the direction normal to the wave crest of each spectral component	[rad]
ρ	water density	[kgm^{-3}]